GFZ

Helmholtz Centre
POTSDAM

HELMHOLTZ CENTRE POTSDAM
GFZ GERMAN RESEARCH CENTRE
FOR GEOSCIENCES

Evgeniia Martuganova

Imaging of an enhanced geothermal reservoir in Groß Schönebeck with vertical seismic profiling using the distributed acoustic sensing technology

Scientific Technical Report STR23/08

www.gfz-potsdam.de

HELMHOLTZ
RESEARCH FOR GRAND CHALLENGES

Recommended citation of the publication

Martuganova, E. (2023): Imaging of an enhanced geothermal reservoir in Groß Schönebeck with vertical seismic profiling using the distributed acoustic sensing technology, (Scientific Technical Report STR; 23/08), Potsdam: GFZ German Research Centre for Geosciences.
https://doi.org/10.48440/gfz.b103-23087

Originally published as

Martuganova, E. (2022). Imaging of an enhanced geothermal reservoir in Groß Schönebeck with vertical seismic profiling using the distributed acoustic sensing technology, PhD Thesis, Berlin: Technische Universität.
https://doi.org/10.14279/depositonce-16639

Imprint

Helmholtz Centre Potsdam
GFZ German Research Centre for Geosciences
Telegrafenberg
D-14473 Potsdam

Published in Potsdam, Germany
2023

DOI: https://doi.org/10.48440/gfz.b103-23087
URN: urn:nbn:de:kobv:b103-23087

This work is published in the GFZ series Scientific Technical Report STR and electronically available via our repository GFZpublic: https://tinyurl.com/GFZ-ST-Reports

Imaging of an enhanced geothermal reservoir in Groß Schönebeck with vertical seismic profiling using the distributed acoustic sensing technology

vorgelegt von
M. Sc.
Evgeniia Martuganova
ORCID: 0000-0003-4261-074X

an der Fakultät VI - Planen Bauen Umwelt
der Technischen Universität Berlin
zur Erlangung des akademischen Grades

Doktorin der Naturwissenschaften
- Dr. rer. nat. -

genehmigte Dissertation

Promotionsausschuss:
Vorsitzender: Prof. Dr. Tomás Fernandez-Steeger
Gutachterin: Prof. Dr. Charlotte Krawczyk
Gutachter: Dr. Jan Henninges (BASE)
Gutachter: Dr. Stefan Lüth (GFZ Potsdam)
Gutachter: Prof. Dr. Michael Weber (Universität Potsdam)
Tag der wissenschaftlichen Aussprache: 04. Juli 2022

Berlin 2022

Zusammenfassung

Ein detailliertes Verständnis der geologischen Strukturelemente ist für die Erkundung geothermischer Reservoire unerlässlich. Unter den bekannten geophysikalischen Methoden werden vor allem seismische Untersuchungen zur Abbildung des Untergrunds aufgrund der vergleichsweise hohen Auflösung bis in große Tiefen genutzt. Seismikkampagnen sind jedoch verhältnismäßig teuer. Die hohen Anfangsinvestitionskosten bilden eine erhebliche Hürde für die Wärme- und Stromproduktion aus geothermischen Ressourcen. Daher ist die Entwicklung neuer Techniken zur Reduktion von Exploarations- und Bohrkosten für die notwendige Förderung geothermischer Projekte essenziell.

Im Rahmen des Verbundforschungsprojekts RissDom-A, der Untergrunderkundung des 40 km nördlich von Berlin gelegenen Groß Schönebeck in-situ Geothermielabors, wurden seismische Messungen durchgeführt, bestehend aus einer 3D-Oberflächen- und einer 3D-Bohrlochseismik. Die VSP-Daten (Vertical Seismic Profiling) wurden mittels kabelgebundenem DAS (Wireline Distributed Acoustic Sensing) aufgezeichnet, was die Umwandlung eines frei im Bohrloch hängenden faseroptischen Kabels in ein dichtes Array seismischer Sensoren zur Registrierung von Strain oder Strain-Rate erlaubt. In dieser Doktorarbeit wird die Anwendbarkeit dieser Methodik für die seismische Abbildung von EGS-Reservoiren (Enhanced Geothermal System) eingehend ausgewertet.

Die Messkonfiguration bestand aus 61 Vibrator-Quellpositionen, die in einem spiralförmigen Pattern um die beiden Bohrlöcher E GrSk 3/90 und Gt GrSk 4/05 derart verteilt wurden, dass eine optimale Durchschallung des Reservoirs gegeben war. Die DAS-Aufzeichnungen zeigen ein exzellentes Signal/Rausch-Verhältnis (40-50 dB bei ca. 1000 m, 4-10 dB bei ca. 4200 m). Diese Datenqualität konnte aufgrund der durchschnittlich 16-fachen vertikalen Stapelrate erzielt werden. Zu Vergleichswecken zusätzlich vorgenommene konventionelle Beschleunigungsaufnehmer-Messungen zeigen eine sehr gute Übereinstimmung der Wellenformen. Die Messkampagne umfasste vier Tage, was die Attraktivität von Wireline-DAS unter sowohl qualitativen als auch ökonomischen Aspekten überzeugend demonstriert.

Eine 3D-VSP Bearbeitungssequenz wurde an die Besonderheiten der Groß Schönebeck Messungen angepasst und auf die Daten angewendet. Einzelne Tiefenbereiche der Aufzeichnungen enthalten starke kohärente Störsignale, die ein ausgeprägtes Muster sowohl im Zeit- als auch im Frequenzbereich aufweisen. Diese Art Noise ist auf eine ungenügende Ankopplung des Kabels im Bohrloch zurückzuführen. Zur Verbesserung des Signal/Rausch-Verhältnisses wurden verschiedene gebräuchliche Unterdrückungsmethoden untersucht. Nach Analyse der Kopplungsnoise-Filterfunktion konnte eine neuartige Methode zur Rauschunterdrückung etabliert werden, welche auf einer Matching-Pursuit Dekompositionstechnik mit Gabor-Atomen basiert. Der auf diese Weise entwickelte Prozessierungsansatz wurde gleichmäßig auf den

gesamten Datensatz angewendet, was die Datenqualität signifikant erhöhte, so dass in der Folge Migrationsabbilder unter Verwendung eines Kirchhoff-Tiefenmigrationsverfahrens mit beschränkter Apertur erzeugt werden konnten.

Nach erfolgter Datenbearbeitung wurde anhand der DAS/VSP 3D-Daten eine detaillierte Untergrundanalyse im Bereich der Groß Schönebeck Bohrlöcher durchgeführt. Das resultierende Bohrlochaten-Volumen löst viele neue Details auf, die mit dem 3D-Volumen der Oberflächenseismik aufgrund des vergleichsweise geringeren Auflösungsvermögens nicht abgebildet wurden. So konnten in der geothermischen Reservoirsektion komplexe dünnschichtige Einlagerungen im Oberen Rotliegend nachgewiesen werden, die erstmalig die Ansprache und Charakterisierung sogenannter „Phantom-Horizonte“ ermöglichen, wie sie typisch für das Gebiet Brandenburg, Deutschland sind. Weiterhin liefert der Bohrlochdaten-Kubus neue Einblicke auf zwei Hauptziele zukünftiger Explorationen. Das DAS/VSP 3D-Datenvolumen zeigt eine Intra-Reservoir Strukur innerhalb der Elbe-Sandstein Schicht, die poröse Anteile eines gestapelten fluvialen Sandsteinkörpers repräsentieren könnte. Die geschätzte Mächtigkeit dieser Struktur variiert zwischen 25 und 40 m, was dünner ist, als zuvor angenommen. Des weiteren konnte im Untersuchungsgebiet eine Diskordanz im Unteren Rotliegend (in einer Tiefe von ca 4.2 km) kartiert werden. Dies erlaubt es, die mögliche Mächtigkeit der Vulkanite darunter abzuschätzen. Somit helfen die VSP-Daten dabei, die Unklarheiten und das Explorationsrisiko zu reduzieren, indem sie wertvolle Informationen zur geologischen Charakterisierung des Groß Schönebeck Standorts liefern.

Mit dieser Fallstudie konnte ich erfolgreich demonstrieren, dass mithilfe faseroptischen Kabels gewonnene Messdaten zur Charakterisierung geothermischer Reservoire maßgeblich beitragen können. In der Konsequenz fördern die präsentierten Ergebnisse die Bedeutung von Wireline Distributed Acoustic Sensing im Hinblick auf eine moderne, verlässliche und ökonomische Explorationsmethode für geothermische Energiekonzepte.

Abstract

A detailed understanding of the geological structural elements is vital for geothermal reservoir exploration. Among existing geophysical methods, seismic methods are most commonly used for subsurface imaging due to the relatively high resolution at significant depths. However, seismic campaigns are rather expensive. The high upfront investment cost represent a substantial barrier for heat/electricity production from geothermal resources. Thus, developing new techniques is vital for further reduction in exploration and drilling costs, which is necessary for geothermal project advancements.

Within the framework of the joint research project RissDom-A, the subsurface exploration of the Groß Schönebeck in-situ geothermal laboratory, situated 40 km north of Berlin, a seismic survey was carried out using 3D surface seismic and 3D vertical seismic profiling methods. VSP was acquired with wireline distributed acoustic sensing (DAS), which allows converting a freely suspended fibre optic cable inside a borehole into a dense array of seismic sensors to record strain or strain rate. In this thesis, the applicability of this method is evaluated for seismic imaging of an enhanced geothermal reservoir.

The survey design consisted of 61 vibrator source positions organised in a spiral pattern around the boreholes E GrSk 3/90 and Gt GrSk 4/05 in such a way to optimise the illumination of the reservoir. The DAS recordings have an excellent signal-to-noise ratio (40-50 dB around 1000 m, 4-10 dB at around 4200 m). This data quality was reached with 16 vertical stacking rates on average. In addition, a comparison with a conventional accelerometer measurement showed excellent waveforms agreement. The acquisition campaign was conducted within four days, illustrating that wireline DAS is very attractive both from a data quality point of view and economically.

A 3D VSP processing workflow was adapted to the Groß Schönebeck specifics and applied to the data. Particular depth ranges of the recorded data are subjected to strong coherent noise, which has a distinct pattern both in the time and the frequency domain. This type of noise is related to the poor coupling conditions of the cable in the borehole. For signal-to-noise ratio improvement, several existing denoising methods have been analysed. After coupling noise filter function assessment, a new noise elimination method was proposed based on the matching pursuit decomposition technique with Gabor atoms. The developed processing routine was uniformly applied to the whole dataset, which significantly improved the data quality, and as a result, migration images created using the Kirchhoff depth migration algorithm with restricted aperture.

After data processing, a detailed subsurface analysis in the vicinity of the boreholes at the Groß Schönebeck was carried out using the 3D DAS VSP image. The resulting borehole cube data resolve new features that could not be imaged with the 3D surface seismic cube

due to the lower resolution of the 3D surface seismic cube, with respect to the 3D VSP cube. Complex thin interlaying of the Upper Rotliegend horizons has been revealed in the geothermal reservoir section, allowing for the first time to access and characterise so-called “phantom horizons” which are typical for the Brandenburg area, Germany. Furthermore, the borehole cube provided new insights on two main targets for future exploration. The 3D DAS VSP cube revealed an intra-reservoir structure inside the Elbe reservoir sandstone layer, which could represent porous parts of a stacked fluvial sandstone body. The estimated thickness of this structure varies between 25 to 40 m, which is thinner than previous estimations. Additionally, a lower Rotliegend unconformity (at around 4.2 km depth) was mapped in the study area. This allowed to estimate the possible thickness of the vulcanite sections below this boundary. VSP data thus helped to reduce the uncertainty and exploration risks by providing valuable information for the geological characterisation of the Groß Schönebeck site.

With this successful case study I demonstrated that fibre optic data could significantly contribute to the characterisation of deep geothermal reservoirs. Consequently, presented results contribute to the wireline distributed acoustic sensing method promotion to develop modern, reliable and economically affordable exploration methods for geothermal energy assessments.

"I have no special talent. I am only passionately curious." - Albert Einstein

Acknowledgements

During the past 4 years of my PhD, I walked a winding road with few peaks and valleys. I wouldn't be able to finish this challenging journey alone without my supervisors, GFZ colleagues, friends, and family support. Without **you**, this would not have been possible.

To *Charlotte Krawczyk*: I appreciate your skilful guidance throughout this PhD. Thank you for believing in me and giving me academic freedom. I am grateful that you always had time for me in your busy schedule to discuss my ideas. Thank you for teaching me to focus not only on the general context but also on being meticulous about smaller details. Thank you for being an inspiring STEM role model. Your example taught me the importance of perseverance, dedication, and creativity in the academic world. Last, but not least I feel a lot of gratitude that you pushed me to be more active at the international level conferences. Thank you for helping me to grow within these past 4 years.

To *Manfred Stiller*: Thank you for helping me in rediscovering my passion for seismic data processing. I value a lot that you always took your time to draw little sketches, explain basic principles and make me always think about what lies behind the nice software interface buttons. It was always my pleasure to discuss my ideas and sometimes argue with you about them.

To *Michael Weber*: I am endlessly thankful for your support throughout this PhD. You always helped me subdivide the enormous and often scary chank of work into manageable smaller tasks, setting the right priorities. Thanks to your wise advice, sometimes cups of coffee or pieces of tissue in moments of need, when I felt really overwhelmed with everything, I didn't give up and continued pursuing my goals. Every time you said "Poehali" (Let's go) at the end of our meetings, I had a thought that in the end, everything will be alright.

To *Klaus Bauer*: Thank you for providing prompt feedback on my research and supporting me in my PhD crisis moments.

To *Stefan Lüth*: Thank you very much for your support at the final stages of this PhD journey and for making this thesis better with your comments and suggestions.

To *Jan Henninges*: Thank you for bringing me into exciting world of fibre optics and sharing your extensive experience in this field. Additionally, I would like to acknowledge your advice and guidance throughout this research.

To *urban DAS team members*: I will always remember our meetings on Tuesdays with great warmth in my heart. I believe this informal exchange of ideas between students and senior scientists played an essential role in developing of my scientific skills.

To *GFZ colleagues*: Dear gesos and rockers, I was lucky to be a part of two sections at the GFZ, and I spent these 4 years surrounded by cherishing and supportive atmosphere. I am grateful for the time we spend together during company outings events, GFZ race running

experience, endless lunch breaks, small parties in the kitchen and amphitheatre next to A69 together. All of you showed me how to be a passionate scientist and have a lot of fun meanwhile.

To *other PhD's at GFZ*: (Tania, Anna, Chaojie, Christian K., Christian W., Florian, Hector, Martin, Marton (in alphabet order). Thank you for our small chats in the kitchen after the Dienstagsrunde on Tuesday's morning, unforgettable experience of organizing the European Geothermal PhD Days (EGPD 2019) together, GFZ PhD days and all the time which we spent together.

To *the Welcome Center team (Lydia Bauer and Pia Sojka)*: I am endlessly thankful for your help in my battles with German bureaucracy.

To *my friends*:

To *Lydia*, I would like to thank you for your endless support. It was reassuring to know that although we are living thousands of kilometres away from each other, you will always cover my back. I especially cherish these moments when you took your time to help me with my Python scripts. Your telegram stickers reactions to my coding attempts always cheered me up even on the gloomiest day.

To *girls from the girly chat*: Dasha, Galia, Nelia, Sasha and Tania (in alphabet order), my dear MSU friend's team, I am utterly happy that we are still in touch after all these years. Thank you for your support and for the countless laughs we shared together.

To *Menno*: Thank you for listening to me talking about everything on my mind and for being there for me no matter what. Thank you for supporting me. Always.

To *my parents*: Thank you for always investing in my education, your kindness and support.

Table of Contents

List of Figures

List of Tables

1

Introduction

1.1 The objective for further development of geophysical methods for geothermal exploration

Geothermal power plants provide a clean and reliable energy source for producing electricity and heat. Energy production can be done within a wide range of geological conditions. Efficient extraction of the Earth's natural heat requires fluids, heat, and a reservoir with sufficient permeability. These parameters make up the hydrothermal system (Barbier, 2002). Places where all these factors occur naturally are referred to as conventional hydrothermal systems. In case of a lack of naturally occurring fluid or an insufficient natural permeability of the geothermal reservoir, creation of the enhanced geothermal system (EGS) is required, also known as engineered geothermal systems (Chamorro et al., 2014). Depending on the geological conditions two types of EGS's are distinguished. Hot sedimentary aquifers (HSA), where heat is distributed by conduction, since convection of the heat does not occur naturally inside the sedimentary formation, and petrothermal EGS, where a hot crystalline rock formation requires to be stimulated to increase insufficient permeability or fluid saturation to allow fluid exchanger movement (Carrara et al., 2020). For either type of EGS fluid is pumped into the reservoir to heat up. These heated fluids then resurface where the heat can be extracted to drive steam engines for the production of electricity, or where it is extracted for heat production. After the heat extraction, the fluids are reinjected to start another cycle. Examples of such EGS include SHEGS Demonstration Project in the Battonya - Mezőkovácsháza - Kunágota area (Hungary, Garrison et al., 2016), Soultz-sous-Forêts (France; Genter et al., 2010), Cooper Basin (Australia; Hogarth and Holl, 2017), Brady field in Nevada (USA, Siler and Pepin, 2021), Reykjanes (Iceland, Friðleifsson et al., 2017, 2019) EGS system in Acoculco, Pue., and a superheated system at Los Humeros (Mexico, Gutiérrez-Negrín et al., 2021; Hernández-Ochoa et al., 2021.

Currently, geothermal sources in the EU produce 7 TWhel (terawatt-hours of electric power), which accounts for only 0.2% of the total electricity consumption (IEA Geothermal, 2020). The majority of geothermal energy in the EU is generated from hydrothermal resources,

a technology that is considered to be relatively mature, though there is still some room for further development (Carrara et al., 2020). To further increase the production of electricity from the geothermal sources, it is required to shift the focus from relatively well studied high temperature to the lower temperature resources. For economically efficient geothermal electricity production, temperatures should exceed about 130 °C (Konietzky, 2020). Deep drilling is often needed to reach depths with sufficient temperature for economically feasible electricity production.

The economic potential of geothermal power in the EU by 2050 is expected to reach 2570 TWh (The European Commission, 2021). In general, the EU has restricted hydrothermal resources, therefore, the expected increase in geothermal power should come from the development of EGS projects (Carrara et al., 2020). So far, EGS plants have very limited applications within the EU (IEA Geothermal, 2020). This is caused by high development costs, the high risks associated with the drilling of deep wells, and the possible requirement of well stimulation (Carrara et al., 2020). Development of state-of-the-art technological solutions is essential to reduce high costs and risks related to the deep geothermal wells drilling and EGS plants installations. These challenges are discussed in geothermal energy technology development report 2020 (Carrara et al., 2020). Among other measures, such as research of enhancement methods of conventional reservoirs, development of unconventional reservoirs, there is a suggestion to optimise geothermal exploration through the development of techniques for improved seismic measurements.

1.2 Surface seismic methods in geothermal exploration

Exploration and assessment of natural heat energy require the application of the geophysical exploration methods. A common method applied for this purpose is seismic reflection imaging, which allows to image larger depths with reasonable resolution compared to other methods (Barbier, 2002). The high resolution for large depths is one of the reasons why seismic methods are vastly applied for oil and gas exploration. However, seismic surveying is rarely used for geothermal investigations (Schmelzbach et al., 2016).

Due to the similarities between petroleum systems and hot sedimentary aquifer geothermal systems, analogous seismic exploration approaches can be used to characterise the latter. Thus, reprocessed legacy 2D and 3D surveys obtained for hydrocarbon exploration are commonly utilised for geothermal exploration. Examples of successful hydrothermal system exploration in sedimentary basins using old data include an exploration campaign in Southern Germany in the Molasse Basin (Von Hartmann et al., 2012). In this case, successful reprocessing of seismic data acquired in 1985 for hydrocarbon exploration with a target in upper Jurassic carbonate platform allowed to resolve studied reservoir, gave a characterisation of the distribution of different carbonate facies, which in combination with information about faults served as an input for realistic reservoir simulation. Analysis of the 3D seismic dataset from the Polish Basin (Pussak et al., 2014), provided valuable information for identifying regions with decreased RMS amplitudes, interpreted as fractured fluid-bearing compartments within the sandstone reservoir. This was used to identify favourable conditions for geothermal exploration. A case study from Łódź Trough in the Central Part of Poland (Maćkowski et al., 2019) demonstrated how the

network of seismic profiles from the 1970s allowed to guide selection of future geothermal targets and determination of the geometry of the geothermal aquifer. Ballesteros (2018) showed benefits of combining existing petroleum exploration data and borehole image logs can help in identifying geothermal targets in the North Perth Basin, Australia. Dutch SCAN (Seismische Campagne Aardwarmte Nederland) program aims to lower the uncertainty related to geothermal exploration programs for Lower Carboniferous (Dinantian) carbonates, Permian Rotliegend sandstones as well as Triassic sandstones (Rehling et al., 2021). For this purpose, old 2D seismic lines from Haarlem to Nijmegen area, acquired between 1984 and 1988, are reprocessed, and test lines for the Utrecht to Almere area are collected to test different state-of-the-art acquisition and processing schemes.

Reprocessed data has limitations related to different horizons/depths targeting due to oil and gas exploration goals. Therefore, it is beneficial to adjust survey planning for a specific target to get an optimal dataset for geothermal exploration. One of the first experiments of the 3D surface seismic measurements explicitly acquired for the geothermal exploration was a seismic cube recorded in the Larderello-Travale area in Tuscany, Italy (Casini et al., 2010). Geological and structural models were developed based on the 3D seismic survey acquired at the Travale test site, which helped to map and characterise fractured zones inside the deep geothermal reservoir. Later, another 3D seismic data set in Unterhaching, Munich (Lüschen et al., 2014), was collected to characterise Malm formation for geothermal district heating and electricity production.

In all the cases mentioned above, the surface seismic method provided a subsurface structural image that included essential information for geothermal well placement and production.

Geothermal projects are not limit to only sedimentary basins and often require studies of the crystalline structures. A 3D seismic experiment conducted in the Upper Rhine Graben region near the city of Schneeberg, Germany (Buness et al., 2014; Ahmed et al., 2015; Hloušek et al., 2015) demonstrated that surface seismic can be used to characterise steeply-dipping faults and fractures in crystalline rock reservoir at a depth of about 4–5 km, which could serve as a geothermal reservoir. High-resolution 3D seismic imaging acquired in Northern Alsace in 2018 (Salaun et al., 2020) allowed to improve structural information of the studied reservoir dramatically. Despite difficulties associated with a deep target and very low-velocity layer at the shallow subsurface, the granitic basement and the important fault network inside the granite basement were mapped using the seismic data.

Seismic data is also successfully used to image complex subsurface structures in mountain regions, for instance, at Pirouette Mountain and Eleven-Mile Canyon in Nevada (Huang et al., 2021). The authors successfully suppressed the strong and coherent ground-roll noise in the seismic data. They then produced high-resolution subsurface images of Pirouette Mountain and Eleven-Mile Canyon, facilitating accurate fault interpretation for geothermal exploration. Most recently, Tsuru et al. (2017) suggested using seismic attenuation profiling (SAP) calculated from the seismic reflection data to access information on deep structures in Miyakejima volcanic island despite poor reflectivity of the volcanic areas. Nevertheless, these results are quite restricted due to limited reflections.

Seismic surveys allow to create a detailed image of the reservoir, which is needed to reduce exploration risks and therefore provide vital information for geothermal feasibility studies.

One drawback of this method is weak amplitudes for reservoir reflections overlaid by a thick salt layer (Krawczyk et al., 2019) or within crystalline rocks. Furthermore, it is hard to image challenging reflectors due to complex morphology lithology and deformation regimes. In addition, there are challenges related to obtaining a reliable velocity model in complex geology and anisotropy related to fractures or layering, which lead to more complex wave propagation (Salisbury et al., 2012). In addition, 3D surface seismic surveying is costly. Geothermal projects generally have a lower budget than oil and gas exploration campaigns; therefore, expensive seismic methods are less likely to be applied.

1.3 Vertical seismic profiling in geothermal exploration

Seismic exploration can improve the exploration of geothermal sites, help with better well placement, and be used for monitoring during production. However, seismic exploration over geothermal reservoirs is challenging because geothermal fields, in general, have complicated heterogeneous geological settings. On a small scale (i.e. 50 – 1000 m), geologic and tectonic heterogeneities like fault systems, facies changes, or karstification can play a critical role in determining geothermal parameters such as flow rate. This is especially true in volcanic environments due to intense scattering and absorption of the seismic waves caused by the pronounced heterogeneity.

Borehole seismics is a promising method to image the subsurface in complex environments. With a VSP acquisition method, receivers are located in a borehole. Seismic waves pass through a highly heterogeneous attenuating near-surface layer only once, travel times are shorter, and therefore the signal is subjected to attenuation to a lesser extent. Thus, this allows preserving higher frequencies in the data, which can be used to obtain a higher resolution of the subsurface image.

Walk-above VSP survey acquired at Thônex-01 geothermal well in Switzerland (Guglielmetti et al., 2020) provided an improved subsurface image near and around the deviated well. It allowed imaging of the transition between the Tertiary Molasse siliciclastic sediments and the Mesozoic carbonates. Therefore, Guglielmetti et al. (2020) showed that the VSP method can significantly improve subsurface geology understanding at the local scale. Furthermore, imaging results can support the second well's planning and, as a result, help with creating a geothermal doublet.

Kästner et al. (2020) and Reiser et al. (2020) examined the ability of VSP to image subsurface structures in a volcanic environment. Results of zero- and far-offset VSP data from the K-18 borehole from within the Krafla caldera, Iceland, allowed to detect several reflectors related to subsurface volcanic lithology, fault zones, dykes and possibly the top of the Kraflamagma chamber. However, the resulting image has hyperbolic-shaped reflectors due to low source-receiver coverage, making data interpretation challenging. Therefore, enhanced survey design including more source positions is desirable for more detailed reservoir characterisation.

Besides benefits related to lesser influence of the near-surface weathering layer, VSP has an advantage of a relatively convenient setup for imaging steeply dipping interfaces, in particular

in multi-offset and multi-azimuth acquisition schemes. Whereas in surface seismic large offsets are necessary to be able to map steeply dipping geological features (Cosma et al., 2012).

VSP data, acquired in Soultz-sous-Forêts geothermal site in a French part of the Upper Rhine Graben (Place et al., 2011; Sausse et al., 2010), with the application of diffraction analysis, helped to improve fault location and general structural interpretation of the site. Borehole seismic data from the injection well AZ-03 in Los Azufres Geothermal Field, México (Lorenzo et al., 2015) allowed to access lower structural sections of the well and identify the fault structural system named El Chino.

The listed studies demonstrate that VSP surveys provide high-resolution imaging of lithologic interfaces, dipping features in the vicinity of the well. Thus, borehole seismic can be a valuable source of information for developing geothermal conceptual models and the proposal of locations for producers and injection wells is crucial for accurate planning of geothermal resources exploitation.

1.4 Research objectives

Although seismic campaigns provide essential information on geological site, they have a high cost in comparison to other geophysical methods. Reduction of the expenses for seismic acquisition can lower the financial barrier required for initial exploration. This can be achieved by utilising new effective methods, i.e., applying fibre optics cables to measure particle motion.

Distributed acoustic sensing (DAS) is a new acquisition method which allows recording data along the whole length of the fibre optical cable with a dense spatial sampling (Hartog, 2017). This allows to significantly reduce operational costs for data acquisition in comparison with conventional sensors. Wireline DAS surveys are relatively inexpensive and can be conducted in already drilled boreholes. Furthermore, fibre optics cables are durable and can survive in extreme conditions (elevated temperature and salinity (Reinsch et al., 2015)).

However, wireline DAS measurements have several limitations that must be considered from the survey planning stage till data processing and interpretation. Moreover, only a very limited number of publications on wireline DAS applications with active seismic sources can be found in literature. Therefore, further thorough research on the evaluation of the wireline DAS data in geothermal applications is needed.

Therefore, this thesis aims to develop a cost-effective tool for geothermal reservoir imaging based on vertical seismic profiling (VSP) acquired using the wireline distributed acoustic sensing (DAS) technology and explore how the data acquired with this method can contribute to the characterisation of the deep geothermal reservoir. Using the geothermal platform at Groß Schönebeck as a test case the scientific development of the new method consists of following objectives:

- Evaluation and quality control of the wireline DAS data.
- Comparison of recorded waveforms with conventional borehole instrument recording.
- Analysis and understanding of the coupling noise, typical for the wireline acquisition.
- Study of the existing denoising methods.

- Creation of the new efficient denoising method.
- Development of an optimal 3D DAS VSP processing flow.
- Comparison of the 3D VSP imaging results with 3D surface seismics.
- Assessment of the 3D DAS VSP imaging contribution to the geothermal exploration at Groß Schönebeck geothermal site.

1.5 Thesis structure

This document has 7 chapters. In the introduction I discuss the general context of the scientific problem and research objectives. The theoretical background of the applied reflection seismic methods (vertical seismic profiling, surface seismics), typical vertical seismic profiling processing workflow, as well as principles of distributed acoustic sensing are described in Chapter 2.

The main part of this thesis consists of three publications (Chapters 3, 4, and 5). With their results I provide solutions for deployment of wireline 3D DAS VSP surveys for future geothermal exploration projects.

Chapter 3: The evaluation of the wireline DAS VSP data and corridor stacks results (Henninges et al., 2021a). This explains the experimental setup and scientific potential of the new data type.

Chapter 4: The study of the coupling noise during wireline distributed acoustic sensing measurements. A new denoising method based on matching pursuit decomposition was developed, which was later used in the 3D processing workflow (Martuganova et al., 2021).

Chapter 5: The results of the 3D DAS VSP seismic imaging at Groß Schönebeck in-situ geothermal laboratory (Martuganova et al., In review). The interpretation of the subsurface structures reveals new reservoir characteristics.

Chapter 6 contains the discussion of obtained results and an outlook for further studies.

Finally, Chapter 7 concludes the thesis.

1.6 List of publications

This document is a cumulative thesis and consists of three articles published or under review in peer-reviewed scientific journals :

Henninges, J., **Martuganova, E.**, Stiller, M., Norden, B. and Krawczyk, C.M. 2021. Wireline distributed acoustic sensing allows 4.2 km deep vertical seismic profiling of the Rotliegend 150°C geothermal reservoir in the North German Basin. Solid Earth 12, 521–537, https://doi.org/10.5194/se-12-521-2021. Published [Chapter 3]

Martuganova, E., Stiller, M., Bauer, K., Henninges, J. and Krawczyk, C.M. 2021. Cable reverberations during wireline distributed acoustic sensing measurements: their nature and methods for elimination. Geophysical Prospecting 69, 1034-1054, https://doi.org/10.1111/1365-2478.13090. Published [Chapter 4]

Martuganova, E. Stiller, M., Norden, B., Henninges, J., and Krawczyk, C.M. In review. 3D deep geothermal reservoir imaging with wireline distributed acoustic sensing in two boreholes. Article is under review in Solid Earth [Chapter 5]

2

Methods

This chapter contains theoretical background information for the seismic reflection method, focusing on two seismic measuring techniques: surface seismic and vertical seismic profiling. Details on acquisition schemes are followed by a short introduction into main seismic wave types. Afterwards, a short introduction into vertical seismic profiling processing basics is given. Finally, a brief explanation of the distributed acoustic sensing measuring techniques, together with a description of the heterodyne distributed vibration sensing (hDVS) system operational theory is provided.

2.1 Basic principles of the seismic reflection method

Seismic acquisition is one of the main techniques used for geophysical exploration since it provides reasonable resolution at significant depths in comparison with other geophysical methods (Barbier, 2002). The basic idea of the method relies on travel time estimation, which is required for the elastic wave to travel from the seismic source, reflect from the geological boundary and be captured by the receiver. The amount of energy reflected from the geological boundary in the case when the wave has a normal angle of incidence is determined by a reflection coefficient:

$$R = \frac{Z_2 - Z_1}{Z_2 + Z_1}, \tag{2.1}$$

where Z_1 is the the acoustic impedance (the product of density and seismic wave velocity) in media 1 and Z_2 in media 2 (Figure 2.1). In general, the reflection coefficient is dependent on the angle of incidence and is determined by the Zoeppritz equations. More information about existing approximations and equations derivation can be found in Richards (1981).

Therefore, the seismic method relies on acoustic contrast, which occurs on subsurface boundaries with variations in layers density or seismic velocity. Depending on the type of energy source, seismic acquisition can be divided into two main groups of methods: passive and active. Passive seismic experiments rely on sources of natural microseismicity. A controlled energy source is used in active seismic campaigns, such as a seismic vibrator, air gun, dynamite, etc. A vibroseis source represents a hydraulic vibrator device, which sends a frequency-modulated

continuous sweep signal, usually in a range between 10 to 150 Hz. The source position, in this case, is called a vibrator point (VP). According to the convolutional model, the recorded vibroseis traces are cross-correlated with a sweep signal to retrieve the subsurface response function (Sallas, 1984).

More details on the seismic reflection method can be found in Sheriff and Geldart (1995) and Yilmaz (2001).

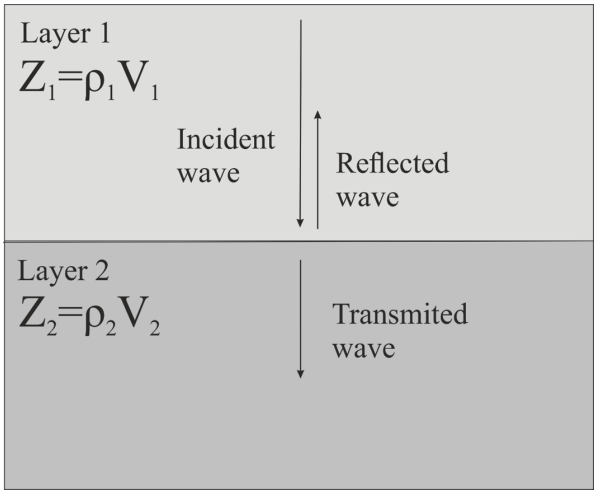

Figure 2.1: Illustration of the wave propagation. Seismic source energy travels down to an acoustic impedance boundary, where it is partially reflected and partially transmitted towards the surface.

2.2 Surface seismic

Surface seismic is a geophysical exploration method when both sensors and sources are located at the surface of the Earth. Also, seismic acquisition can be conducted in 2D or 3D depending on the geometry of the sources and receiver. In the case of active seismic source experiments, a simple typical scheme is presented in Figure (2.2).

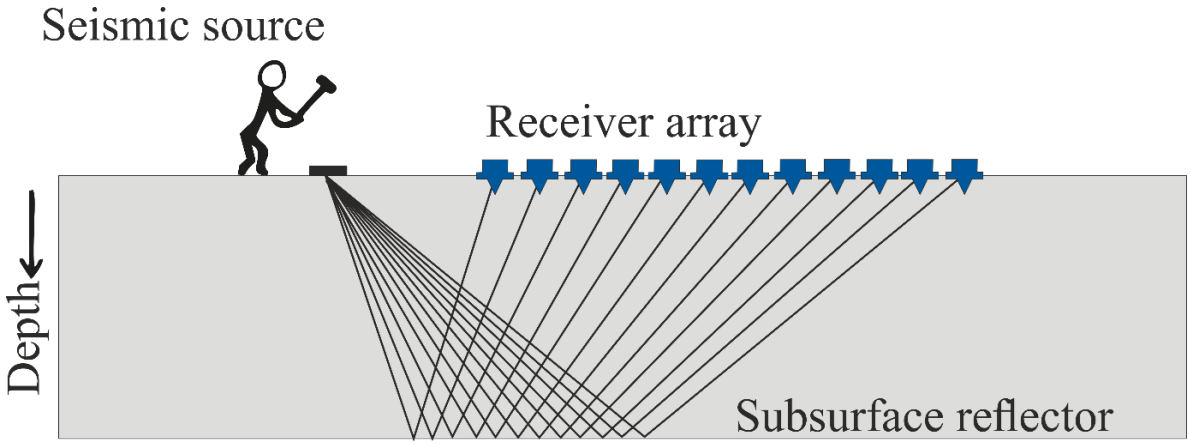

Figure 2.2: Basic principles of the surface seismic reflection method. Scheme diagram shows the travel paths of the waves emitted by the seismic source on the ground,which were reflected from the subsurface boundary and recorded by receiver array. Figure modified after Karray and Lefebvre, 2012.

2.3 Vertical seismic profiling (VSP)

VSP is an umbrella term for the seismic acquisition technique where at least one component of the observation system (either source or receiver) is located in the borehole, and another is positioned at the surface or in the same borehole or in another borehole (Galperin et al., 1985; Hardage, 2000). Depending on the well configuration, position, number and deployment method for source and receivers, there are numerous types of VSP measurements. The main well-established techniques include zero-offset, offset and walkaway/moving source profiling (Figure 2.3, Blackburn et al., 2007; Brauner et al., 1988). In zero-offset measurements, the source is positioned at the surface to achieve a vertical or nearly vertical alignment with the well. This type of survey provides a time-depth curve, which can be used to calculate velocity information and tie the surface seismic information to depth. The method when the source is positioned on a distance from the well is called offset VSP. This type of measurement is beneficial for obtaining information around the borehole. Walkaway VSP refers to the usage of several source points with increasing offset from the borehole with receivers fixed in one location (Blackburn et al., 2007). In 3D VSP acquisition, sources can be arranged in various geometries, such as, in a circle around the borehole (Radial/walkaround survey design, Blackburn et al., 2007; Tsuji et al., 2011), placed on multiple lines, which starts from the wellhead position and goes away from the well, called a walk away VSP (Spoke survey design, BJV Design Inc webpage, Vertical seismic profiles, 2022; Yu et al., 2016a), or source can be positioned on a classical parallel lines grid (Grid survey design, Blackburn et al., 2007) (Figure 2.4). A 3D VSP image is beneficial in regions where classical surface seismic methods are limited due to complex local geology (surface obstructions, thick salt layers, complex tectonics etc.).

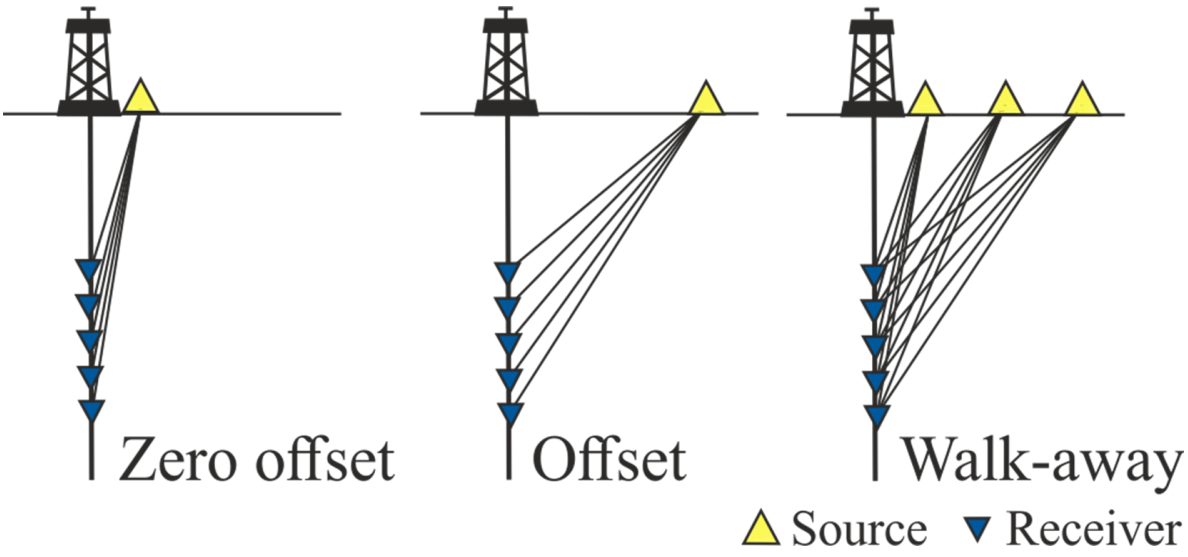

Figure 2.3: Main configurations of the 2D VSP surveys. Figure modified after BJV Design Inc webpage, Vertical seismic profiles (2022).

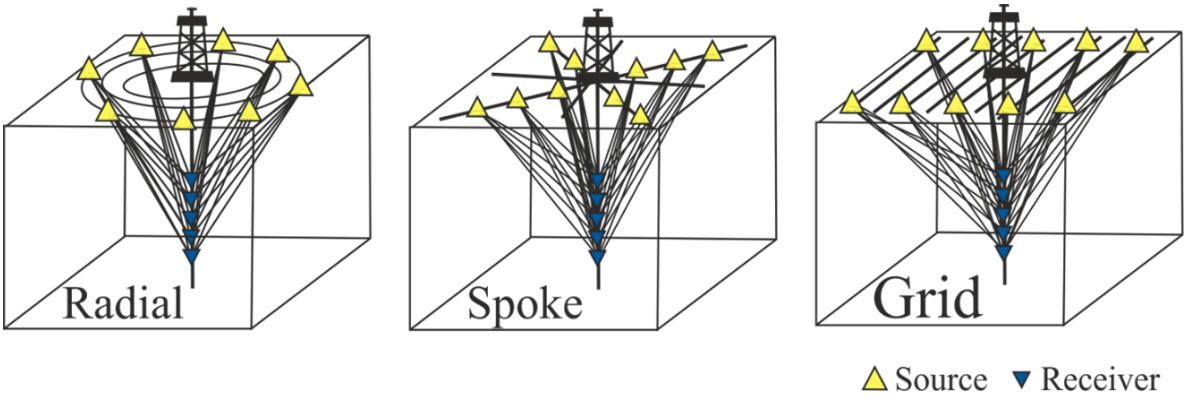

Figure 2.4: Main configurations of the 3D VSP surveys. Figure modified after BJV Design Inc webpage, Vertical seismic profiles (2022).

2.4 Types of seismic waves

With seismic methods, different types of seismic waves are recorded (Müller, 2007; Sheriff and Geldart, 1995). Seismic wave types can be classified into two groups: body waves and surface waves. Body waves propagate through the Earth's layers body. The primary (P) wave is a compressional wave where the particle motion is parallel to the wave propagation. This type of wave transmits both in liquid and solid rock. The secondary (S) or shear wave is characterised by perpendicular particle motion to the wave propagation front. Contrary to P-waves, S-waves exists only in solid medium.

Surface waves travel along the surface boundary. They propagate with a slower velocity than body waves but have much larger amplitudes. There are several types of surface waves. The main ones include the Rayleigh wave and Love waves. Love wave creates a movement of the surface from side to side perpendicular to the direction of the wave. Particles motion in Rayleigh waves is controlled by elliptical pattern movement.

Stoneley and Scholte waves are generalised Rayleigh waves and occur in solid-solid and fluid-solid boundaries respectively (Sheriff and Geldart, 1995). Another type of surface wave most typical for seismic measurements conducted in a borehole is a tube wave. Body waves or surface waves, which run into the borehole, can create disturbances in liquid along a cylindrical fluid-solid boundary (Sheriff and Geldart, 1995). Depending on the seismic method, some waves will be considered as a source and some as noise.

2.5 An introduction to vertical seismic profiling processing

This subchapter aims to provide an introduction to vertical seismic profiling (VSP) processing. The presented workflow can be applied to data acquired using conventional geophones as well as the data recorded with distributed acoustic sensing technology. The procedures and parameters given in the text below are not meant to be comprehensive guidance but are used to illustrate fundamentals used thought out this thesis. More detailed information on data processing basics can be found in Yilmaz (2001), Sheriff and Geldart (1995), more elaborate explanation related to vertical seismic profiling technique in Hardage (2000).

2.5.1 Geometry input

In order to be able to process the data, as the very first step, it is required to assign proper geometry to VSP data. Necessary headers typically include depth (Measured depth (MD), true vertical depth (TVD), true vertical depth seismic datum (TVDSD)), surface elevation at the source position, source position coordinates, receiver position coordinates, channel number. Filling of the headers is usually executed by dedicated processing modules, which use the information of the borehole trajectory to calculate proper values.

2.5.2 Stacking

Stacking is a processing step within which different seismic data records are added together to reduce noise and improve overall data quality. The number of seismic traces that have been summed together during stacking is called a fold. Various stacking algorithms include trim, median, diversity stack, and other techniques. Figure 2.5 shows an example of median stack with a stacking fold equal to five. The resulting stacked trace has significantly lower level of random noise. Depending on the type of noise, one approach can work better than another.

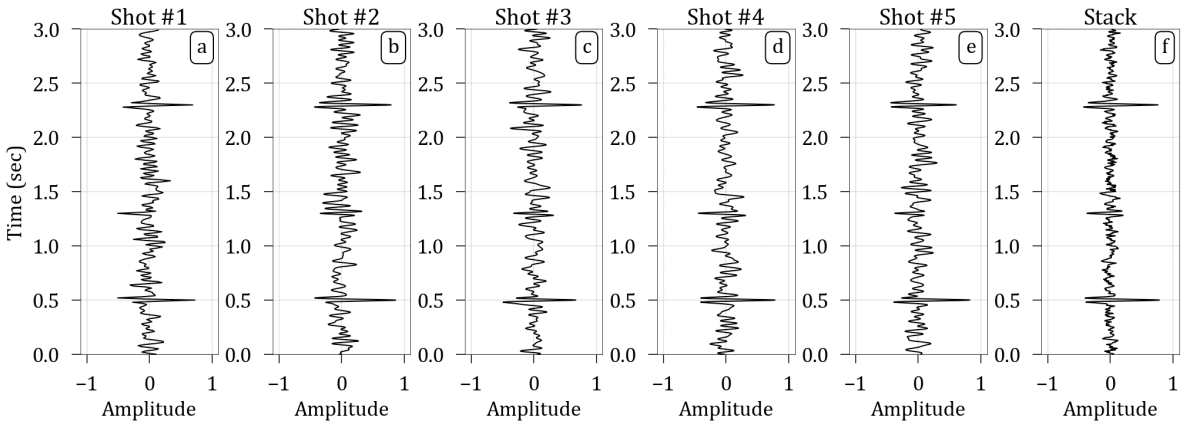

Figure 2.5: An illustration of median stacking. Plots from a to e show five different seismic trace recordings; plot f corresponds to the result of the median stack. For this example, stacking fold is equal to five.

2.5.3 Correlation

In the case of data acquisition with a vibroseis source, one of the basic processing procedures is correlation, which is based on a convolutional model assumption (Sheriff and Geldart, 1995; Yilmaz, 2001). This process aims to use the sweep signal (Figure 2.6a) characteristics to produce short duration wavelets at an acoustic impedance boundary. The series of spikes (Figure 2.6b) represents the reflection coefficients associated with the corresponding boundaries. According to the convolutional model, an uncorrelated raw seismogram (Figure 2.6f) is the sum of the convolutions ($*$) of the sweep with the reflection coefficients of each boundary (Figure 2.6 c, d, e):

$$u(t) = sw(t) * e(t), \tag{2.2}$$

where u(t) is a raw seismogram, sw(t) represents vibroseis sweep and e(t) corresponds to the Earth responce. To remove the vibroseis energy, one has to cross-correlate ($\star$) a raw

seismogram (u(t)) with a sweep signal (sw(t)):

$$s(t) = sw(t) \star u(t), \tag{2.3}$$

The resulting seismogram (Figure 2.6g) can be used for further analysis to determine subsurface properties.

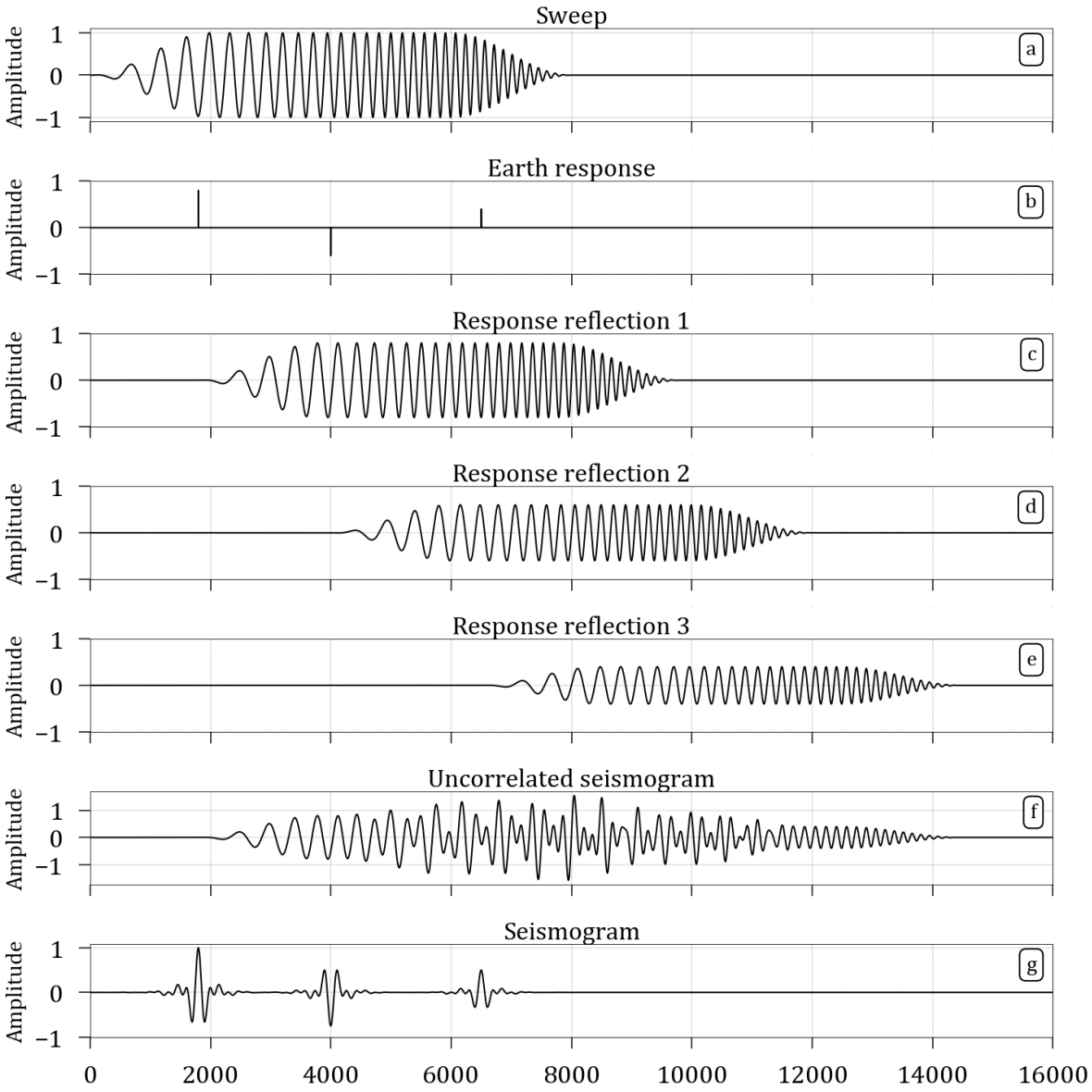

Figure 2.6: Correlation process example. (a) A 16 s synthetic vibroseis sweep signal with a frequency range from 1 to 5 Hz. (b) Reflection coefficient spike series represents earth response. (c, d, e) Response for each reflection 1, 2 and 3, respectively. (f) Summed responses produce uncorrelated raw seismograms. (g) A result of the cross-correlation of the uncorrelated seismogram with the pilot sweep. Modified after Braile (2016).

2.5.4 First Break Picking

To extract information from seismic data, it is necessary to determine the arrival time of the wave travelling from source to receiver. This processing step is called first break picking. It can be done manually or traced automatically using different techniques such as coherent methods

(Crucelis and Aldana, 2009; Gelchinsky and Shtivelman, 1983; Liang et al., 2020), attributes calculations in sliding windows (Al-Mashhor et al., 2019; Sabbione and Velis, 2010; Spagnolini, 1991), intelligent Markov optimal decision process (Luo et al., 2021), and recently used neural networks (Jia and Ma, 2017).

2.5.5 Amplitude correction

Amplitudes can be a valuable interpretation tool. Nevertheless, a few known physical processes influence the amplitude values, such as transmission losses, source-receiver directivity, spherical divergence etc. Therefore to get values most close to "true amplitudes", it is crucial to address these effects in the data by the means of the correction functions. Due to the geometrical spreading of the seismic energy, the amplitude at thr receiver points is reduced proportionally to the distance to the source. This effect has a significant impact on data. Figure 2.7 illustrates the divergences for P-wave and S-waves travelling through homogeneous media. The time-variant gain function can be applied to all traces to correct this effect. Every trace sample is multiplied by the gain function to compensate for the decay of the amplitude due to the spherical wavefront divergence. More information on this topic can be found in Hardage (2000).

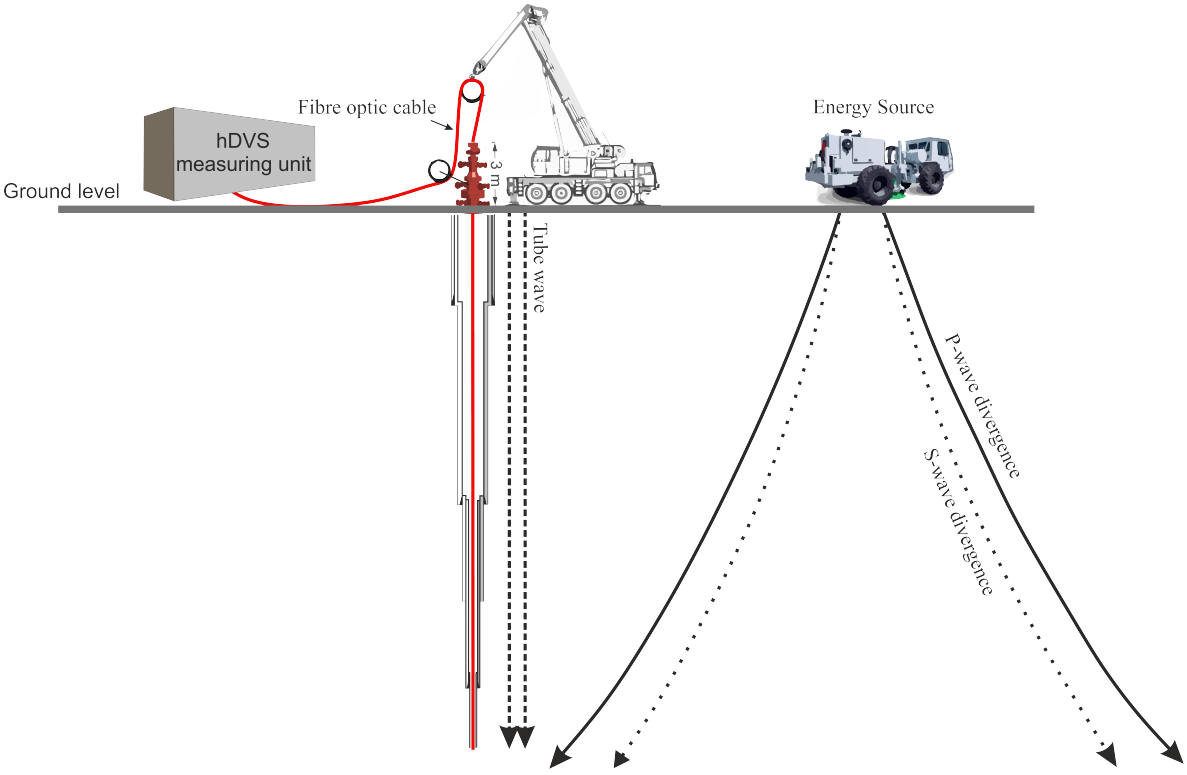

Figure 2.7: Amplitude loses due to geometrical spreading for P and S-waves. Modified after Hardage (2000).

2.5.6 Deconvolution

The basic idea behind the deconvolution process is to improve the temporal resolution of the seismic trace by compressing the source wavelet contained in a seismic trace to a spike (spike deconvolution). Another commonly used method, predictive deconvolution, is typically

used to eliminate reverberation and to attenuate short-period multiples. The construction of the deconvolution operators is based on the optimum Wiener filtering. Existing conventional processing modules usually use either one operator for the whole seismic gather or operators constructed/applied on a trace-by-trace basis. More theoretical explanations on deconvolution techniques can be found in Sheriff and Geldart (1995); Yilmaz (2001).

2.5.7 Wavefield separation

The downgoing wavefield (direct arrivals) should be separated to get an image using reflected waves. This procedure is called a wavefield separation. The most commonly used methods include f-k(frequency/wavenumber) transform, f-p (frequency/slowness) transform, median separation. The process of median reflected wave separation is illustrated in Figure 2.8 and consists of:

- picking a travel time curve for a noise wave (any wave other than the reflected one),
- alignment of the data using static correction calculated from picked arrival times of the noise wave,
- subtraction of this wave from the wavefield using a two-dimensional spatial filter,
- inverse static corrections.

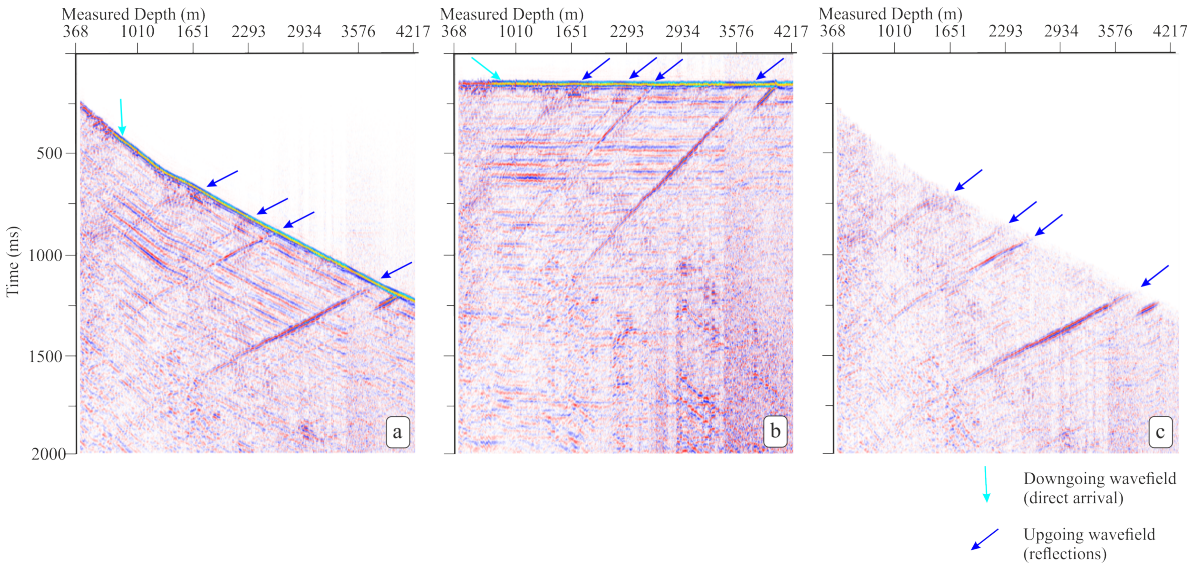

Figure 2.8: An illustration of the median wavefield separation process. (a) An input seismogram contains direct P-wave arrival (downgoing wavefields shown with light blue arrow) and P-wave reflections (upgoing wavefield shown with dark blue arrows). (b) Aligned seismogram using static corrections calculated from the direct P-wave arrival to which a median filter is applied to extract downgoing energy. (c) The resulting seismogram with only upgoing wavefield.

2.5.8 Velocity model building

In seismic data imaging, velocity model building plays a crucial role. Any migration method requires knowledge of the propagation velocity field. The velocity model is usually constructed using all available information such as geological formations boundaries, surface seismic stacking velocities, sonic log values, arrival times from the VSP. Depending on the type of imaging, 2D

or 3D model construction is required. Figure 2.9 shows an example of a 3D velocity model, where values are set using a 3D grid. The correctness of the imaging results depends directly on the accuracy of the velocity model.

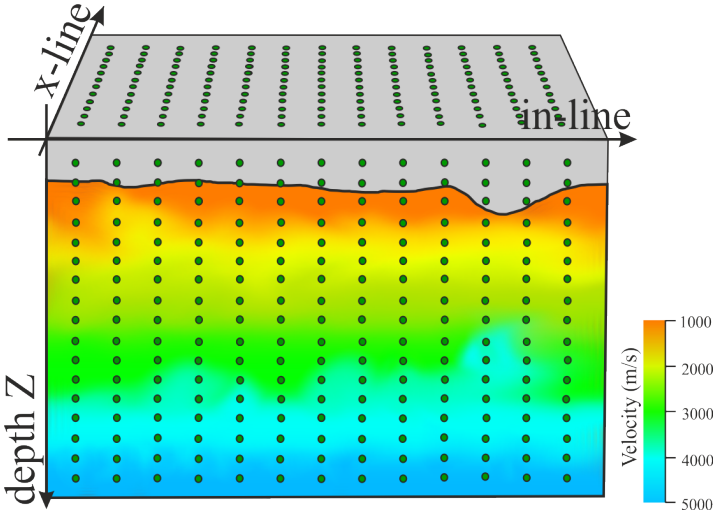

Figure 2.9: An example of a 3D velocity model. Modified after Robein (2010).

2.5.9 Kirchhoff migration

There are a few well-known migration schemes. Depending on the geology of the site, available computational power, a particular method might be more suitable for the specific target. One of the most commonly used migration schemes is Kirchhoff migration, which employs the wave equation's integral form (Kirchhoff equation). A weighted superposition of waves propagating from adjacent points and times is estimated by the Kirchhoff integral representation of a field at a given point. In practice, the implementation scheme is based on stacking the data along the curves that tracing the arrival time of energy scattered by image points in the medium (Figure 2.10). More information can be found in Dillon (1990); Yilmaz (2001). A commercial 3D Kirchhoff migration algorithm (VSProwess Ltd.) was used to acquire the 3D imaging results shown in Chapter 5.

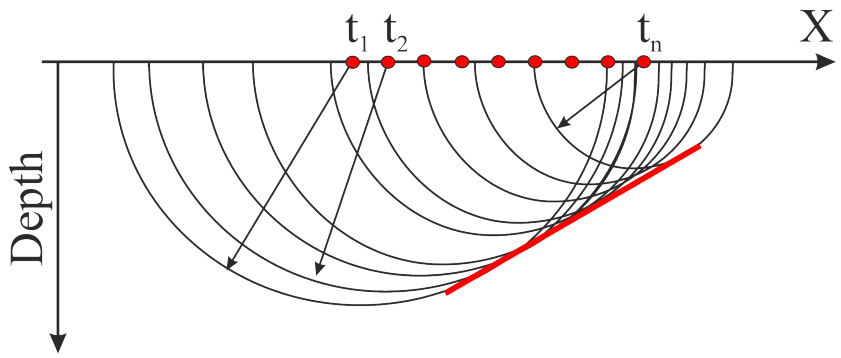

Figure 2.10: An illustration of the stacking nature of the Kirchhoff migration algorithm. Modified after Robein (2010).

2.5.10 Zero offset specific processing steps

Time verticalization This step should be considered for zero offset data processing after the geometry input. Zero offset measurements assume placement of the source right above the receiver. Due to different reasons, this is frequently not possible. Time verticalization aims to correct recorded times for this effect. Time corrections can be calculated using a velocity model and sophisticated ray-tracing algorithms or by a direct geometrical approach (Figure 2.11). Vertical time is calculated using the following formula:

$$T_v = T_s \frac{D_{hg}}{h} = T_s cos(\theta), \tag{2.4}$$

where T_v – vertical time, T_s – measured time, and θ is equal to $\arccos(D_{hg}/h)$. More explanations can be found in Hu et al. (2015).

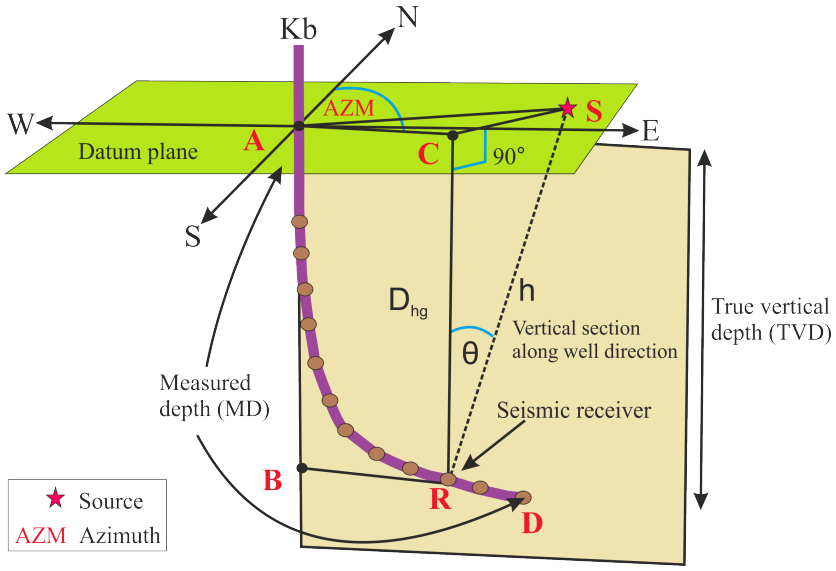

Figure 2.11: A sketch explains the geometrical approach of the calculation for the vertical time calculation.

2.5.11 Corridor stacking

Aim of this step is to build a so-called corridor stack containing mainly primary reflection events. After the main data processing block, the upgoing wavefield is shifted to two-way travel time (TWT). In the example shown in Figure 2.12, 72 traces were transposed from the deconvolved PP-up wavefield. Then first 20 traces, closest samples to the time-depth curve, were selected, stacked, and duplicated x 10 times for display to get a corridor stack. This kind of data provides a robust time-depth relationship and seismic response along a wellbore. Corridor stack is used for correlation with surface seismic (well tie), the direct comparison with synthetic data calculated using well logs. More theoretical background can be found in Hardage (2000); Hinds et al. (1996).

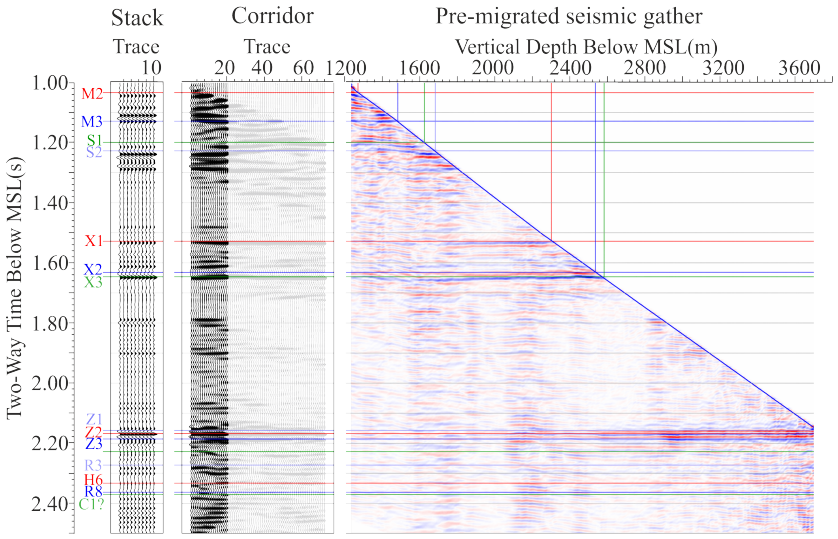

Figure 2.12: An example of pre-migrated seismic gather shifted to two-way travel time with selected traces for a corridor and resulting corridor stack. Modified after VSProwess Ltd Final report (2018).

2.6 Distributed acoustic sensing (DAS)

Distributed acoustic sensing is a data acquisition technique, which enables the usage of fibre optic cables as dense seismic arrays to measure strain variation along the cable (Hartog, 2017). A typical acquisition scheme consists of an interrogator unit that sends coherent light pulses and receives a backscattered light signal from an optical fibre attached. Currently, in commercial use, there are several DAS instruments. Many of them operate on the principles of Rayleigh scattering but have significant differences in measuring systems such as the usage of a single or dual pulse input signal, evaluation of backscattered signal based on phase or amplitude information, measuring principles of optical phase information etc.

At the Groß Schönebeck geothermal site, a Schlumberger hDVS optical interrogator unit was used. Therefore in the following subchapter, I will focus on this particular instrument specifications.

2.6.1 hDVS system operational theory

The hDVS measuring principle is based on optical time-domain reflectometry (OTDR). A series of short light pulses are injected into an optical fibre. During the propagation of the light along the fibre, it scatters. Some backscattered light (about 0.25% for the fibres typically used for hDVS) is gathered back by the waveguide. The returned light represents an exponential decay function as the probe pulse travels to the scattering point and back. Variations in backscattered light are used for the characterisation of the optical fibre. Using the known velocity of the light in the fibre and the recorded time of the returned light, it is possible to determine the location along the fibre where scattering occurred.

The Schlumberger hDVS system uses a phase-based approach for data acquisition. This principle is derived from the assumption that the phase of the backscattered signal of all subsequent fibre sections alters in a linear manner with respect to the strain. Therefore subtraction of the signals from two closely spaced separate regions of the fibre can provide a

quasi-linear signal, which can be used to calculate local strain applied to the fibre (Hartog et al., 2013).

A typical hDVS system scheme is presented in Figure 2.13.

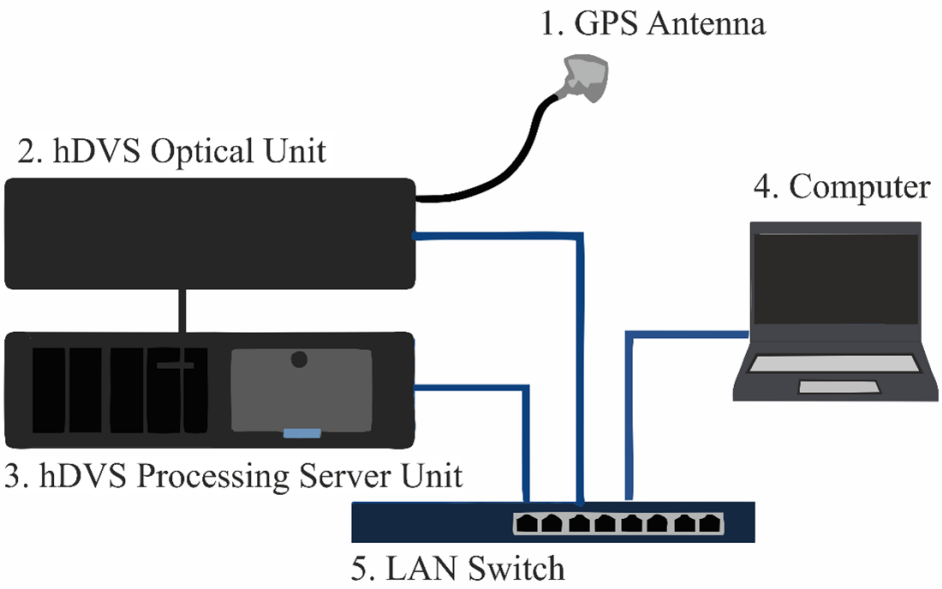

Figure 2.13: A typical scheme of the hDVS System.

The hDVS system consists of 5 major components:

1. GPS Antenna – used for receiving satellite signals to provide an accurate timestamp.
2. hDVS Optical Unit – used for acquiring hDVS data.
3. hDVS Processing Server Unit – used for sending commands to the hDVS Optical Unit, processing and storing the data.
4. Computer – used to communicate to the hDVS Processing Server Unit to start/stop acquisition and playback the data and edit parameters. The seismic source controller is also connected to the computer for allowing Fire Order and Time Break communication.
5. LAN Switch – used to allow all the instruments to communicate with each other.

For more detailed information on fibre optics sensing the following resourses are recommended for further reading Hartog (2017), Zhan (2019), Lindsey, Rademacher, and Ajo-Franklin (2020), Jousset, Reinsch, Ryberg, Blanck, Clarke, Aghayev, Hersir, Henninges, Weber, and Krawczyk (2018), Krawczyk (2021).

3

Experiment & Survey design

The feasibility of this study for the 3D DAS VSP measurements for the geothermal exploration started with a careful experiment design. This chapter explains the details of the survey planning, provides an overview of the main DAS-VSP acquisition parameters and data quality estimations. Afterwards, data processing and resulting zero offset dataset products which include interval velocities profiles, time-depth relationship curves, and corridor stacks for two boreholes, E GrSk 3/90 and Gt GrSk 4/05 situated in the geothermal well, are presented and discussed. Finally, the chapter is finished by geological interpretation of produced 1D reflectivity traces.

Wireline distributed acoustic sensing allows 4.2km deep vertical seismic profiling of the Rotliegend 150 °C geothermal reservoir in the North German Basin

Jan Henninges[1], **Evgeniia Martuganova**[1,2], Manfred Stiller[1], Ben Norden[1] and Charlotte M. Krawczyk[1,2]

[1]Helmholtz Centre Potsdam, GFZ German Research Centre for Geosciences, 14473 Potsdam, Germany

[2]Department of Applied Geophysics, Technische Universität Berlin, 10587 Berlin, Germany

Article published in Solid Earth, 12, 521–537, 2021

https://doi.org/10.5194/se-12-521-2021 [accepted manuscript]

3.1 Abstract

We performed so-far-unprecedented deep wireline vertical seismic profiling at the Groß Schönebeck site with the novel method of distributed acoustic sensing (DAS) to gain more detailed information on the structural setting and geometry of the geothermal reservoir, which is comprised of volcanic rocks and sediments of Lower Permian age. During the survey of 4 d only, we acquired data for 61 source positions using hybrid wireline fiber-optic sensor cables deployed in two 4.3 km deep, already existing wells. While most of the recorded data have a very good signal-to-noise ratio, individual sections of the profiles are affected by characteristic coherent noise patterns. This ringing noise results from incomplete coupling of the sensor cable

to the borehole wall, and it can be suppressed to a large extent using suitable filtering methods. After conversion to strain rate, the DAS data exhibit a high similarity to the vertical component data of a conventional borehole geophone. We derived accurate time–depth relationships, interval velocities, and corridor stacks from the recorded data. Based on integration with other well data and geological information, we show that the top of a porous and permeable sandstone interval of the geothermal reservoir can be identified by a positive reflection event. Overall, the sequence of reflection events shows a different character for both wells explained by lateral changes in lithology. The top of the volcanic rocks has a somewhat different seismic response in both wells, and no clear reflection event is obvious at the postulated base of the volcanic rocks, so that their thickness cannot be inferred from individual reflection events in the seismic data alone. The DAS method enabled measurements at elevated temperatures up to 150 °C over extended periods and led to significant time and cost savings compared to deployment of a conventional borehole geophone string. This wireline approach finally suggests significant implications for observation options in old wells for a variety of purposes.

3.2 Introduction

Borehole seismic array measurements benefit from deploying fiber-optic cables and using the novel distributed acoustic sensing (DAS) method. This technique allows for rapid seismic data acquisition, because DAS provides continuous measurements along the cable and therefore does not require vertical repositioning of the cable during vertical seismic profiling (VSP) campaigns, as opposed to conventional borehole geophone strings (see proofs of concept in, e.g., Mestayer et al., 2011; Miller et al., 2012). While issues like the mechanical coupling of the sensor cable and the transfer from strain to geophone-equivalent data are still under discussion (see Hartog et al., 2014; Daley et al., 2016), we used this survey technique and further improved the processing of this new data type for geothermal applications to overcome the classical resolution problem and derive accurate time–depth relationships.

The Groß Schönebeck site is located 40 km N of Berlin in the state of Brandenburg, Germany. It is a research platform operated by the GFZ German Research Centre for Geosciences, which has been set up in order to test if production of geothermal energy from deep-seated reservoirs in the North German Basin is feasible. An enhanced geothermal system (EGS) has been created by hydraulic stimulation of low-permeability sedimentary and volcanic rocks of Lower Permian (Rotliegend) age (Huenges et al., 2006; Zimmermann et al., 2010). So far, two deep research boreholes, the former E GrSk 3/90 hydrocarbon exploration well and the Gt GrSk 4/05 geothermal well (referred to as GrSk3 and GrSk4 in the following), exist at the site. For further development of the site, the implementation of a new stimulation concept and drilling of a new well have been proposed (Blöcher et al., 2015).

In order to gain more detailed information on the structural setting and geometry of the reservoir, a 3-D seismic survey within an 8 km x 8 km permit area has been carried out in February and March 2017 (Krawczyk et al., 2019). In addition, VSP has been performed within the GrSk3 and GrSk4 wells. The primary aims of the VSP survey were to establish precise time–depth and velocity profiles, and to image structural elements within the reservoir interval of the Rotliegend at 4200 m depth in the vicinity of the boreholes with higher resolution

in three dimensions. The imaging of structures in the target reservoir interval is a special challenge, as it is overlain by the 1400 m thick Upper Permian Zechstein salt complex.

The VSP measurement was performed using the novel DAS method. This method is based on optical time-domain reflectometry and enables us to register strain changes along optical sensor cables with high spatial and temporal resolution (Parker et al., 2014). Within recent years, a growing number of VSP surveys have been reported, where the DAS method has successfully been applied using sensor cables permanently installed behind casing or along tubing (e.g., Mestayer et al., 2011; Daley et al., 2013; Götz et al., 2018). This deployment method is very convenient as it allows for data acquisition without well intervention. There is also a growing number of studies reporting on successful application of DAS for microseismic monitoring during hydraulic stimulation (e.g., Karrenbach et al., 2017; Molteni et al., 2017), also including EGS reservoirs (Lellouch et al., 2020). In cases where such a permanent installation is not possible or has not been performed during construction of the well, a sensor cable can be lowered downhole temporarily, similar to conventional wireline logging. For this wireline deployment method, nevertheless, only very few experiences have existed until now. First tests using an experimental optical wireline logging cable deployed in a 625m well were described by Hartog et al. (2014), while a more extensive DAS walkaway VSP survey has been performed by Yu et al. (2016a) in a vertical well to a depth of 4004 m. Within the current study, we report on the results of a DAS-VSP acquisition on wireline cable to a depth of 4256 m, which to the authors' knowledge represents the deepest survey currently documented in literature worldwide. In the following, the survey design and data acquisition, the overall characteristics of the acquired data, and the data processing and evaluation for a zero-offset source position are described. The processing and interpretation of a 3-D VSP seismic cube will be the subject of a separate publication.

3.3 Survey design and data acquisition

The target area was defined by the positions of the existing wells, the expected extent of the hydraulic fractures, and the trajectory of the proposed new well. It has a horizontal extent of approximately 700 m x 500 m and a vertical thickness of approximately 300 m. A spiral pattern of 61 source-points with offsets between 180 and 2000 m from the wellheads was chosen, in order to achieve a good 3-D coverage of the target area with a uniform distribution of azimuths Figure (3.1). Survey planning was based on well trajectories and geometry of the major geologic units (Moeck et al., 2009), taking into account DAS-specific acquisition characteristics like directivity and signal-to-noise ratio. The source-point positions were optimized based on ray tracing, using average acoustic properties of the major geologic units from a previous regional seismic survey (Bauer et al., 2010). Based on the ray tracing, reflection-point fold maps for representative layers at target depth and incidence angles of upgoing reflected waves at the sensor cables were calculated and compared for different source-point distributions. The most suitable source-point distribution was then selected, and individual source-point locations were further adjusted according to the conditions within the survey area, i.e., location of roads and agricultural areas, as well as required distances to sensible infrastructures like gas lines or buildings.

A listing of the acquisition parameters is shown in Table 3.1. Energy excitation was performed with four heavy vibrator trucks operating simultaneously at each source position. For acquisition of the DAS data in well E GrSk 3/90, the GFZ hybrid borehole measurement system was used, which allows for deployment of fiber-optic sensors and electric downhole tools in parallel (Henninges et al., 2011). The GrSk3 well is near vertical (maximum inclination 7.2°), and the fiber-optic data were acquired to a measured depth (MD) of 4256m below ground level, which corresponds to a true vertical depth (TVD) of 4245.8 m below ground level (note that all depths in this study are given in MD, if not stated otherwise). Within the well Gt GrSk 4/05, which is deviated up to 49° in the reservoir interval, a second wireline cable containing optical fibers was deployed (maximum DAS acquisition depth 4196m MD/4126.1m TVD). This is an experimental optical wireline cable developed by Schlumberger, referred to as an optical heptacable (Hartog et al., 2014). This cable was also used to deploy a conventional three-component borehole geophone with acceleration characteristics (Versatile Seismic Imager (VSI) tool; Schlumberger), in order to record several check shots at specific depths within the GrSk4 well. DAS data were acquired on both cables using two separate Schlumberger hDVS (heterodyne distributed vibration sensing) optical interrogator units.

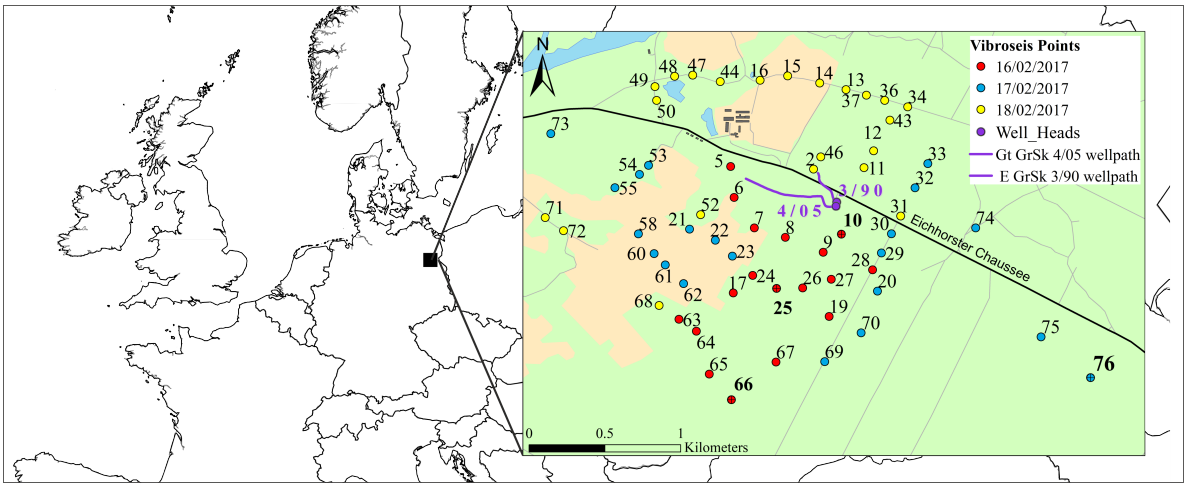

Figure 3.1: Overview map of central Europe with location of survey area in NE Germany. Inset shows detail of survey area with VSP source point positions and borehole trajectories of wells E GrSk 3/90 and Gt GrSk 4/05. Selected source-point positions for which common-source gathers are displayed in Figures 3.3 and 3.4 are marked with crosses and printed with bold type.

Fieldwork was carried out within 4 d from 15 to 18 February 2017. At the beginning, we performed a start-up test (referred to as day 0 in the following), where suitable source and recording parameters were determined. As a result, we selected a sweep with 10–112 Hz (linear) and 36 s duration for acquisition. For some of the larger offsets, a sweep with reduced frequency range of 10–96 Hz was used. After testing of several different gauge length values (see Henninges et al., 2021b), which can be varied with the hDVS interrogator, a gauge length value of 20 m was selected for online DAS data processing during recording. This value was later adjusted to 40 m during post-processing as a result of an optimization procedure (see Sect. 3.4.1). The DAS measurements were recorded with a temporal sampling of 2 ms and a spatial sampling of 5m spacing across the entire length of the wells.

During the start-up test, we recorded several shots with variation of the wireline cable tension in the GrSk3 well, in order to test the influence on the mechanical coupling of the

cable and the quality of the recorded signals (cf. Frignet and Hartog, 2014; Constantinou et al., 2016). After the bottom of the drivable depth in well GrSk3 had been reached at 4259 m MD, recordings with increasing amounts of cable slack of 1, 5, 11, and 20 m were performed. Based on the results, it was decided to keep the wireline cable under almost full tension for recording, as the best overall data quality was found to be achieved under these conditions (see Sect. 3.5.2).

Within the following 3 d (days 1–3), acquisition was performed with a nominal number of 16 repeats for the 61 source positions distributed around the wells (see Figure 3.1). Nevertheless, due to a technical problem with acquisition in well GrSk4 during day 1, mainly only data for well GrSk3 could be recorded during this time. Therefore, in order to improve the reduced coverage around the GrSk4 well caused hereby, we relocated some of the original source positions from the northern to the southwestern part of the survey area.

Table 3.1: DAS-VSP acquisition parameters.

Parameter	**Value**
Seismic source	Four vibrator trucks; Mertz M12 Hemi 48, peak force 200 kN (45 100 lbf) each
Number of source points	61
Offset	188–2036 m
Sweep (near offsets)	10–112 Hz, linear up, 36 s, 360 ms taper
Sweep (far offsets)	10–96 Hz, linear up, 36 s, 360 ms taper
Vertical stacking rate	16 repetitions (nominal)
Signal recording	Two Schlumberger hDVS units, two hybrid wireline cables
Depth interval receiver channels E GrSk 3/90	Ground level – 4256 m MD/4245.8 m TVD
Depth interval receiver channels Gt GrSk 4/05	Ground level – 4196 m MD/4126.1 m TVD
Receiver channel distance (spatial sampling along borehole)	5 m
Gauge length	20 m
Sampling interval	2 ms
Trace length (after correlation)	4 s
Polarity convention	European/EAGE normal

3.4 Seismic data processing

As one of the first processing steps, the DAS data recorded along the length of the sensor cables were correlated to the measured depth along the boreholes. This depth correlation was

performed using the gamma-ray logs recorded during running in hole with the sensor cables, as well as travel-time data from check shots recorded at 1200, 2400, 3600, and 4207 m depths in the GrSk4 well. During further processing, the depths were transferred to vertical depths below the seismic reference datum, which is mean sea level (true vertical depth below mean sea level; TVDSS), using the geometries of the borehole trajectories.

3.4.1 Gauge length optimization

The choice of an optimized gauge length value is an essential part of the DAS data acquisition and processing. This parameter has a significant effect on the signal-to-noise ratio of the data and on resolution in the frequency domain. Dean et al. (2017) presented an approach which helps to maximize the signal-to-noise ratio while keeping interfering influences on the frequency content below a desired threshold value. By selecting an optimum gauge length $\mathrm{GL_{opt}}$ (m), a favorable compromise between these two factors can be achieved, using

$$GL_{opt} = \frac{Rv}{f_p}, \tag{3.1}$$

with R the gauge length / spatial wavelength ratio (–), v (apparent) acoustic velocity (m/s), and fp peak frequency (Hz).

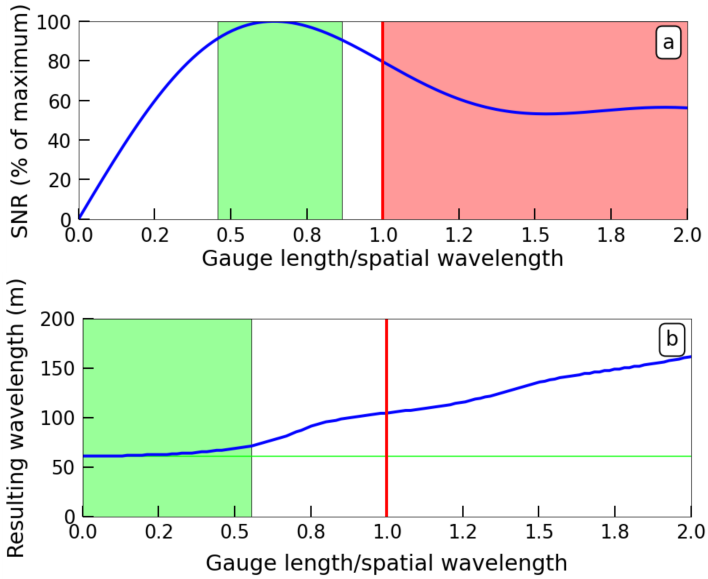

Figure 3.2: The signal-to-noise ratio (SNR) (a) and resulting wavelength (b) for different ratios of gauge length to spatial wavelength for a 10–112 Hz Klauder wavelet with a velocity of 4800 m/s. The green boxes indicate the range of ratios where SNR> 90% of the maximum, and the resulting wavelength is within 3m of the actual wavelength (indicated by green line). If the gauge length is larger than the spatial wavelength (red box, ratio of 1 indicated by the red line), the wavelet shape is distorted. The optimum conditions satisfying both constraints are found in the region where the two green boxes in panels (a) and (b) overlap.

The graphs presented in Figure 3.2 show the dependence of signal-to-noise ratio and resulting wavelength on R for the conditions of the current survey. According to this, optimum conditions within the desired limits are found for R values between 0.46 and 0.56. For an intermediate R value of 0.5, an optimum gauge length of 39 m is calculated using Equation 3.1, for a velocity of 4800 m/s, which has been extracted from the interval velocities derived

for the Rotliegend reservoir interval (see Sect. 3.5.3), and a middle frequency of 61 Hz for the 10–112 Hz sweep. Therefore, the acquired DAS-VSP data were reprocessed accordingly using the derived optimum gauge length value. It would also be possible to apply a depth-dependent gauge length optimization, as suggested by Dean et al. (2017), by taking local variations of velocity and frequency content into account. This was nevertheless not performed in the current study, because the focus here is predominantly on the deeper Rotliegend reservoir section only.

3.4.2 Pre-processing

An overview of the further seismic data processing steps is shown in Table 3.2. Seismic pre-processing included stacking and correlation with the pilot sweep. The hDVS output strain data were then transformed to strain rate by differentiation in time, resulting in a 90° phase shift. The strain-rate data are proportional to acceleration (Daley et al., 2016), and acceleration is in phase with the pilot sweep (Sallas, 1984).

Table 3.2: Sequence of processing steps for zero-offset DAS-VSP data sets.

Processing step	**Methods, parameters, and description**
Pre-processing	Diversity stack of shots (suppression of impulsive noise). Correlation with pilot sweep. Conversion to strain rate (time derivative).
First arrival time picking	Peak of direct downgoing wave.
Interval velocities	Correct times to vertical. Velocity inversion of travel-time data.
Data preconditioning	Amplitude corrections (spherical divergence compensation and lateral balancing). Coherent (ringing) noise suppression (Burg adaptive deconvolution).
Wavefield separation	Subtraction of downgoing P wavefield (median filter).
Wave shaping/zero phasing of upgoing wavefield, removal of multiples	Deterministic deconvolution using operator derived from downgoing wavefield.
Polarity reversal	180° phase shift to match polarity convention of conventional geophone data.
Corridor stack	Shift to two-way time (horizontal alignment of upgoing reflections); stacking of 0.2 s window after first arrival.

3.4.3 Common-source gathers and coherent noise suppression

Common-source gathers for zero-offset, intermediate, and far-offset source positions are displayed in Figures 3.3 and 3.4. The common-source gathers are dominated by downgoing P-wave arrivals and arrivals of upgoing waves originating from several reflectors at different depths. For several shots, a strong tube wave arriving at later times is clearly visible as well.

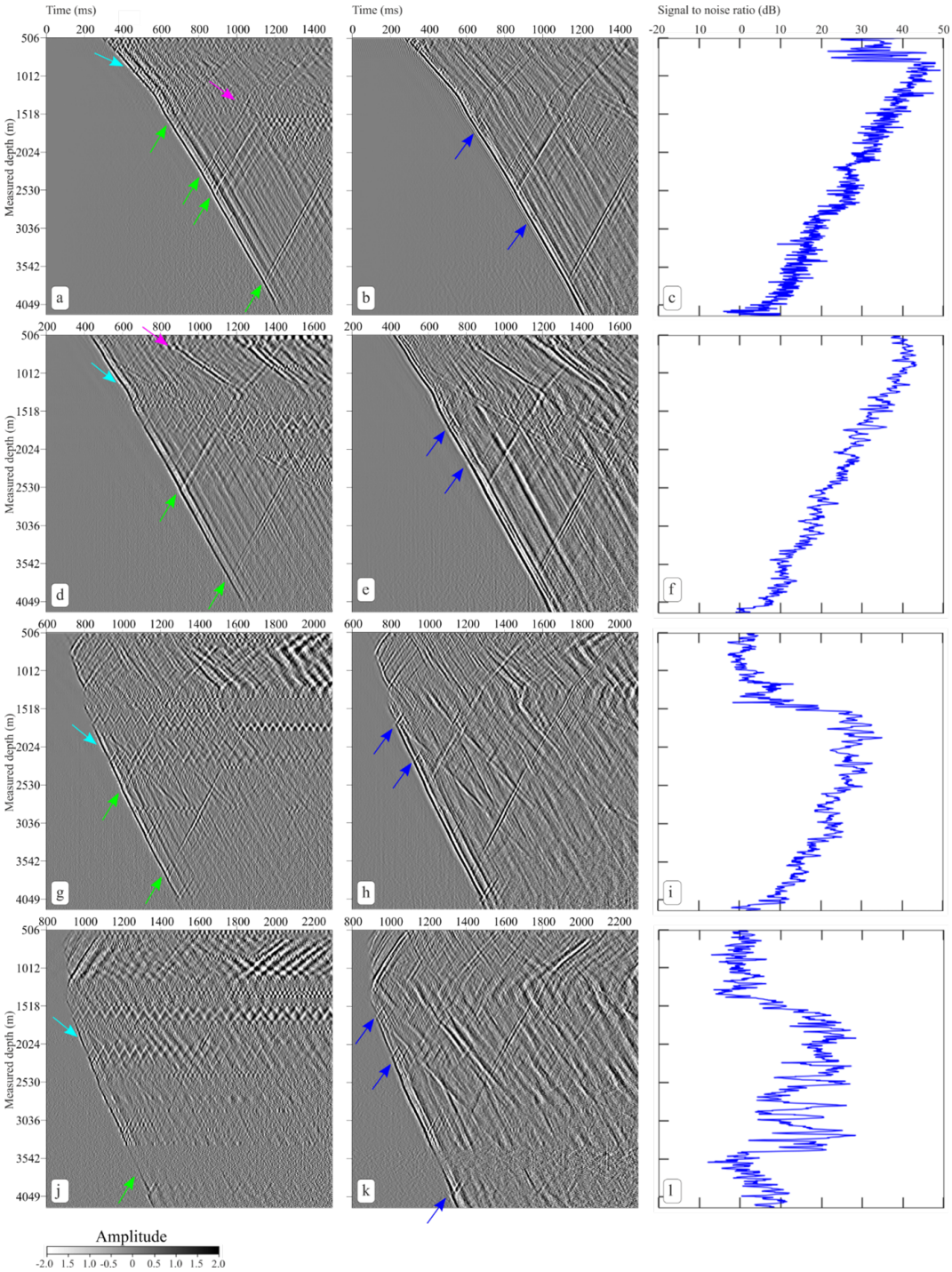

Figure 3.3: Selected common-source gathers for well GrSk3 for zero-offset, intermediate, and far-offset source positions. First column of panels shows data after pre-processing for source positions 10 (a), 25 (d), 66 (g), and 76 (j). Second column (panels b, e, h, and k) shows the data for the same source positions after ringing-noise suppression (Burg adaptive deconvolution) and moderate coherency enhancement. For display, we applied a windowed trace equalization. The third column (panels c, f, i, and l) shows the signal-to-noise ratio of the data after pre-processing. Colored arrows (exemplary): direct downgoing P wave (light blue), upgoing reflected P–P waves (green), tube wave (magenta), residual noise after application of ringing-noise filter (dark blue).

Over several intervals along the wells, a coherent noise with a particular zigzag pattern can be recognized in the DAS data. Similar noise in DAS data recorded using cables suspended in boreholes has also been described in some earlier studies, e.g., by Miller et al. (2012), Yu

et al. (2016a), Cai et al. (2016), and Willis et al. (2019). It has also been found to occur for tubing-deployed cables, e.g., in the studies of Barberan et al. (2012) and Didraga (2015).

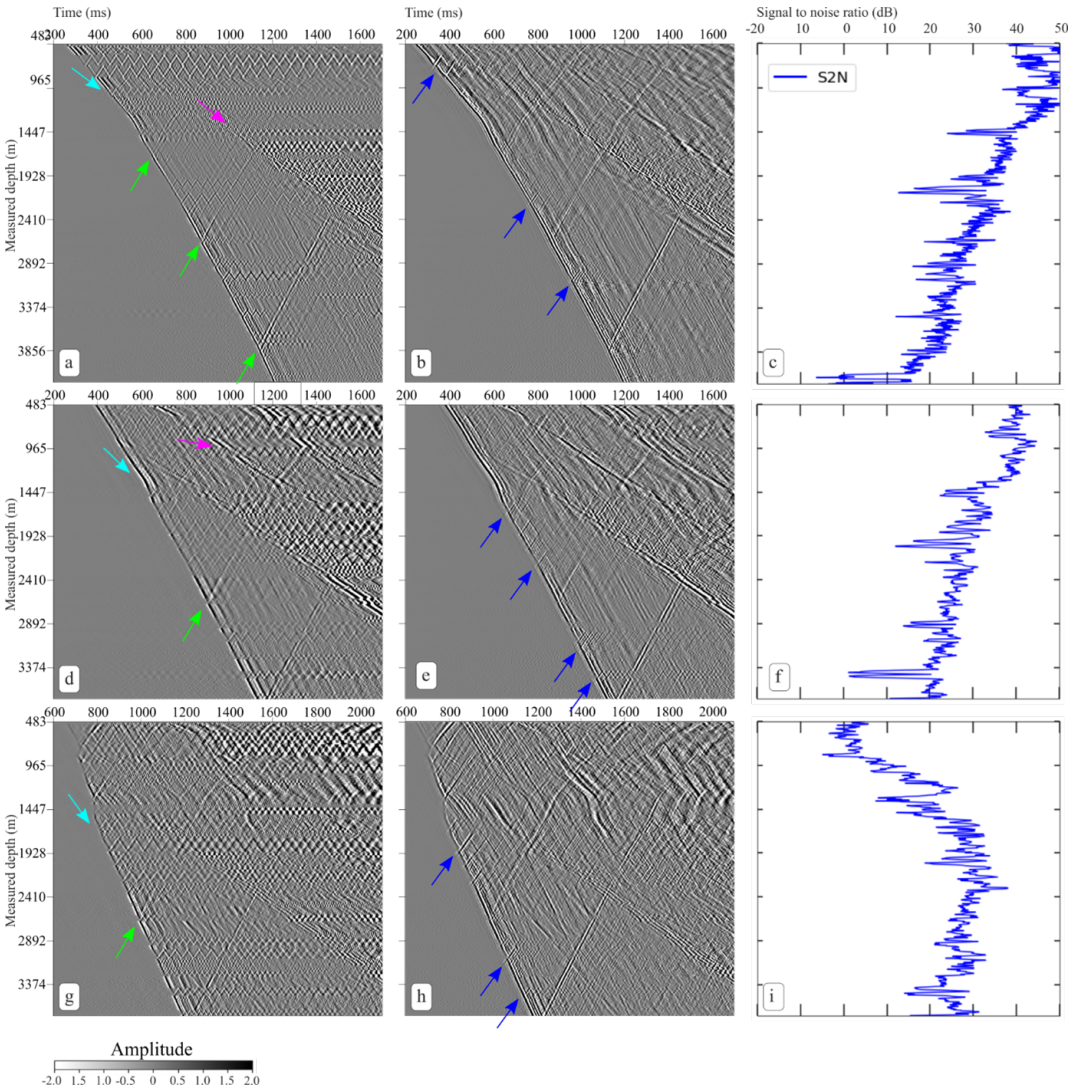

Figure 3.4: Selected common-source gathers for well GrSk4 for zero-offset, intermediate, and far-offset source positions. First column of panels shows data after pre-processing for source positions 10 (a), 25 (d), and 66 (g). Second column (panels b, e, and h) shows the data for the same source positions after ringing-noise suppression (Burg adaptive deconvolution) and moderate coherency enhancement. For display, we applied a windowed trace equalization. The third column (panels c, f, and i) shows the signal-to-noise ratio of the data after pre-processing. Colored arrows (exemplary): direct downgoing P wave (light blue), upgoing reflected P–P waves (green), tube wave (magenta), residual noise after application of ringing-noise filter (dark blue).

Several methods for elimination of this "ringing" noise, like spectral balancing, deconvolution, and time–frequency domain filtering (Elboth et al., 2008), were tested. For zero-offset data processing, we selected the Burg adaptive deconvolution (Griffiths et al., 1977). This method is a good compromise between computational effort, robustness, and application simplicity. A more thorough description of this ringing noise and further methods of noise suppression can be found in Martuganova et al. (2021). The filtered data sets are displayed in Figures 3.3 and 3.4, together with the unfiltered data sets for comparison.

Usage of self-updating linear prediction operators is the foundation of the Burg adaptive deconvolution method. The designed filter operator is different at each trace sample. A set of

filter coefficients is convolved with the data in order to predict the future data values at some prediction distance. Coefficient values are recomputed for each data sample in the seismic record with the criterion of minimizing the root-mean-square error. The computations are performed in forward and reverse directions in the time domain.

The application of Burg adaptive deconvolution resulted in a significant reduction of the coherent ringing noise (Figures 3.3 and 3.4). After filtering, reflections are better visible and sharpened. Nevertheless, not all parts of the noise can be suppressed, especially in a short time window after the first-break arrivals. This residual noise is difficult to distinguish from upgoing reflected waves, as the velocity of the noise traveling along the cable is similar to the compressional velocity of the formation (Martuganova et al., 2021).

3.5 Results and discussion

3.5.1 Comparison of DAS and borehole geophone data

A comparison between the DAS strain-rate data and the vertical component of the borehole geophone acceleration data recorded at specific depths in the GrSk4 well is displayed in Figure 3.5. Note that during recording of the check-shot data a sweep with 10–88 Hz was used, which is different from the recording of most of the other data during the survey.

The traces recorded at 1200 and 3600 m depth both contain direct P-wave arrivals, at 520 and 1090 ms, respectively. The DAS trace for 1200 m depth is strongly influenced by the ringing noise described above, which is confined to a narrow frequency band between 40 and 50 Hz (Figure 3.5b) at this location. Similar noise characteristics have been observed, e.g., in the study of Chen et al. (2019). This noise is however not evident in the geophone data recorded at the same depth, which suggests that the ringing noise in the DAS data is related to the deployment method of the DAS sensor cable. While the DAS sensor cable is freely suspended inside the borehole, the geophone tool is clamped to the borehole wall. Closer analysis of the ringing noise shows that the sensor cable acts like a vibrating string within the affected intervals, with resonances occurring at a fundamental frequency and higher overtones (Didraga, 2015; Martuganova et al., 2021).

The traces recorded at 3600 m depth (Figure 3.5e) also contain strong reflected waves, which arrive at around 1190 ms and originate from the base of Zechstein reflectors, at around 3850 m depth (see Figure 3.4). Overall, the DAS strain-rate data exhibit a high similarity to the geophone measurements, except for the upgoing reflections. Here, the DAS strain-rate data display the opposite polarity as the geophone data. This polarity reversal for reflected upgoing waves has also been observed in previous studies, e.g., by Hartog et al. (2014), Mateeva et al. (2014), or Willis et al. (2019). Frignet and Hartog (2014) note that such a polarity flip compared to geophone data is similar to the characteristics of hydrophone sensors.

As a test, we have also converted the DAS data to geophone-equivalent acceleration data using the method described by Egorov et al. (2018). For this, we performed a transformation of the original DAS strain data into acceleration via filter application in the vertical wavenumber domain (k_z) and further double differentiation in the time domain. The results for the check-shot traces recorded at 2400 and 3600 m depth are shown in Figure 3.6. After conversion

to acceleration, the DAS data display the same polarity as the geophone data, also for the upgoing reflections. This is in line with previous results obtained by Correa et al. (2017).

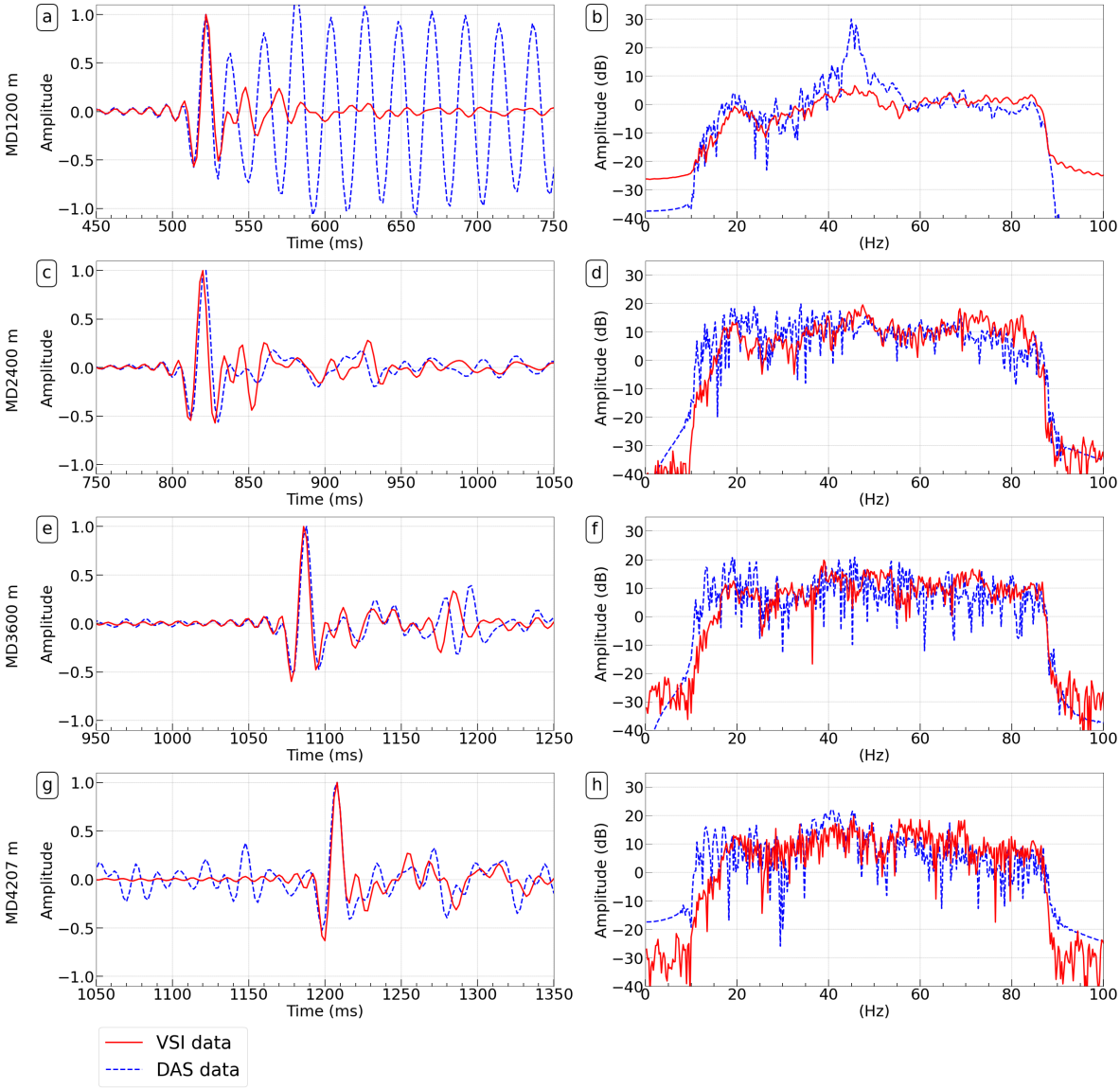

Figure 3.5: VSP traces and frequency spectra for borehole geophone data (VSI, solid red line) and DAS strain-rate data (dashed blue line) recorded in well GrSk4 at measured depths of 1200 (a, b), 2400 (c, d), 3600 (e, f), and 4207 m (g, h). The borehole geophone is a threecomponent accelerometer, and the vertical component parallel to the tool/borehole axis is displayed. The recorded amplitudes have been normalized to the absolute maximum first-break amplitude of the individual traces.

3.5.2 Signal quality

Common-source gathers recorded with different amounts of cable slack in well GrSk3 are displayed in Figure 3.7. There is a zone with decreased amplitude of the first-break signal at the bottom of the well, which increases in length with increasing amount of cable slack. While the random noise is similar, leading to an overall signal-to-noise ratio (SNR) drop within the affected zone, the coherent noise is changing. For the recordings with 1, 5, and 11 m cable slack, a zone with ringing noise is visible at a depth of approximately 2890 m MD. This zone almost disappears in the 20 m cable slack data set, where the zone of decreased first-break

amplitudes is approximately approaching the same depth. So ringing noise seems to be reduced within the affected zone, likely because of improved mechanical coupling of the cable to the borehole wall. But at the same time, the signal amplitude is significantly reduced within the affected zone as well.

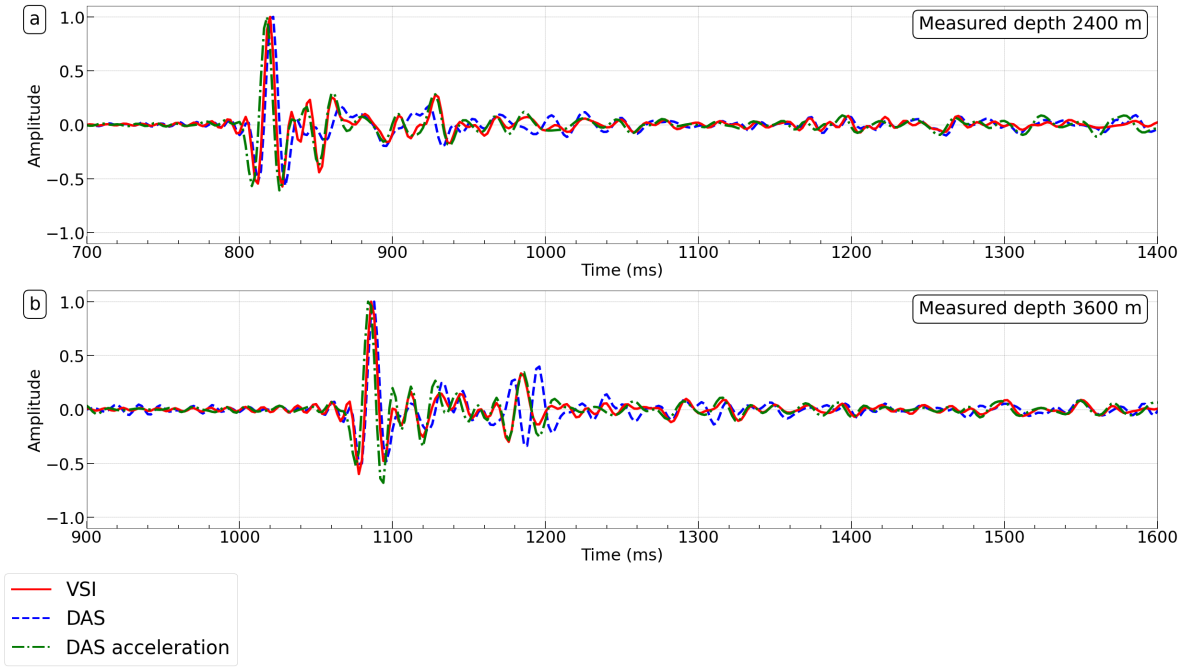

Figure 3.6: Comparison of data from the borehole geophone (VSI, red, acceleration), DAS converted to strain rate (blue) and DAS converted to acceleration (green), recorded at measured depths of 2400 (a) and 3600 m (b) in well GrSk4. The recorded amplitudes have been normalized to the absolute maximum first-break amplitude of the individual traces.

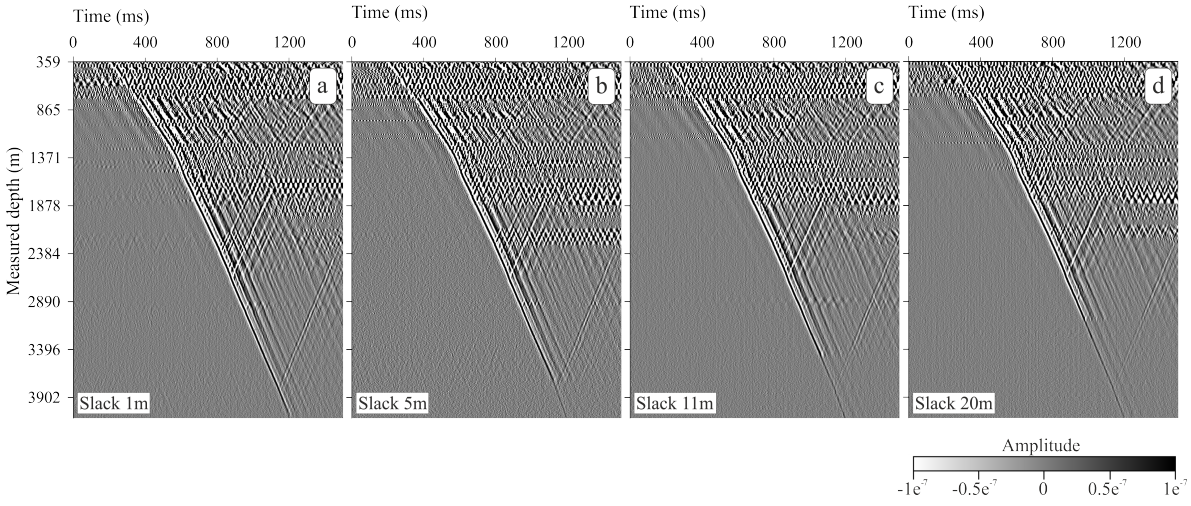

Figure 3.7: Comparison of common-source gathers recorded with cable slack of 1 (a), 5 (b), 11 (c), and 20 m (d) for VP10 in well GrSk3. No additional amplitude normalization was applied.

Due to the higher first-break amplitudes, the best signal quality overall was assigned to the data set recorded with 1m cable slack, i.e., under almost full cable tension, and further recording was performed like this. Notably, the best seismic record had been found to be recorded under the opposite conditions with released cable tension during the field trial reported by Frignet and Hartog (2014). Nevertheless, in their study, the optical wireline cable

had been deployed in a relatively shallow well of 625 m depth, and the borehole conditions might not be representative of deep wells as in the current study for the Groß Schönebeck case. Constantinou et al. (2016) observed a behavior similar to the current study during a field trial in a well of 2580 m depth at the Rittershoffen site in France. Here, the zone of reduced signal amplitudes was found to coincide with a region where the cable was interpreted to form a spiral, gradually building up from the bottom of the well when additional cable slack had been introduced. Schilke et al. (2016) investigated the effect of cable slack on the mechanical coupling of a sensor cable deployed in a vertical well using numerical simulations.

For data quality evaluation, the SNR for each trace of the data set was calculated. The energies of signal and noise were computed as the root mean square (rms) amplitude (in arbitrary units) within time windows of -10 to +30 ms around the first arrival and 150 ms at the beginning of the trace before the first arrival, respectively. The signal-to-noise ratio was then calculated in dB using the following formula:

$$SNR = 20 \log_{10} \frac{rms_{signal}}{rms_{noise}}. \tag{3.2}$$

The calculated SNRs are displayed in Figures 3.8 and 3.9. The data are sorted for the different acquisition days and with increasing source offset. Each vertical column represents a source location, and the calculated SNR for each trace is color coded. Altogether, the data have a good SNR, with average values of approximately 40 to 50 dB at a depth region around 1000 m for the smaller offset source locations, decreasing to approximately 4 to 10 dB at around 4200 m close to the final depth. There is an overall decrease of the SNR with increasing channel depth and source offset, which corresponds to the decay of signal amplitudes to be expected due to spherical divergence of the acoustic waves. The data for the first acquisition day have similar characteristics for both wells, with slightly larger SNRs for well GrSk4.

From the start of the second acquisition day, a sharp drop of the SNR is evident in the data recorded in GrSk3 at a depth of approximately 3400 m. In addition, there are further intervals with decreased SNR at depths of approximately 3100 and 2600–2800 m. Curiously, the SNR for the channels below 3400 m gradually recovers again with increasing depth, until even improved SNRs in comparison to the first acquisition day are reached in the bottom interval.

The observed signal drop at 3400 m after day 1 seems to be similar to the effect of reduced signal amplitudes observed during the slack test. Nevertheless, the configuration of the wireline cable remained unchanged between day 1 and day 2. Accidental introduction of additional cable slack during this time, e.g., by slipping of the wireline winch, or movement of the crane arm holding the cable sheave, can be excluded, as the position of the cables was carefully monitored by placing marks on them after running into the hole. Furthermore, no significant change of the wireline cable tension at surface has been registered between day 1 and day 2. Other causes must therefore be responsible for the observed effect.

Combined with the remaining coherent noise after filtering, there is a significant heterogeneity in the data, which requires to carefully select the data to be considered during evaluation and interpretation.

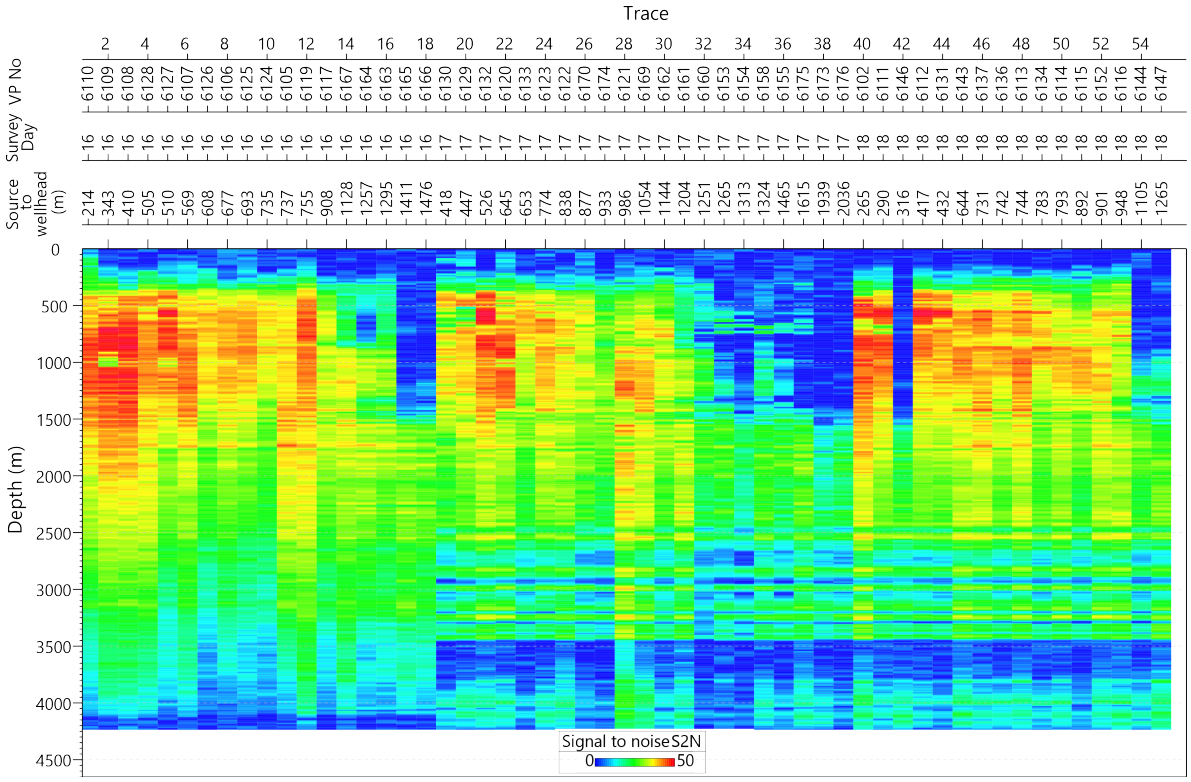

Figure 3.8: Signal-to-noise ratio (dB) for DAS-VSP data from well GrSk3.

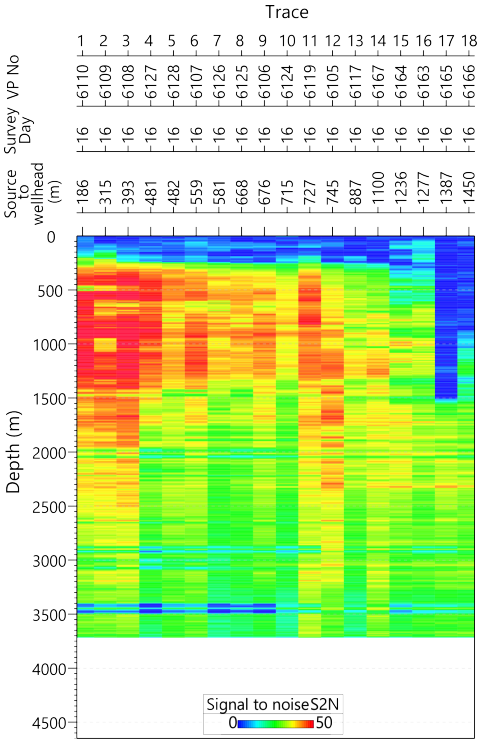

Figure 3.9: Signal-to-noise ratio (dB) for DAS-VSP data from well GrSk4.

3.5.3 Time–depth relationships and interval velocities

For every source point, the travel times of the direct downgoing waves were determined by picking of the first-break times (Table 3.2). A velocity model has been set up based on the

geometry of the existing geological model from Moeck et al. (2009) and by calibrating the model velocities with the picked travel times. Vertical travel times have then been determined by ray tracing through the calibrated model. For the VP 10 zero-offset position, VSP interval velocities along the wells have been calculated from the travel times using the method of smooth inversion after Lizarralde and Swift (1999). Here, a damped least-squares inversion of VSP travel times is applied, which reduces the influence of arrival-time picking errors for closely spaced sampling points and seeks to result in a smooth velocity/depth profile. In our study, a 1.1 ms residual of the travel times has been allowed for. The calculated VSP interval velocities vary between about 2.8 and 5 km s^{-1} (Figure 3.10). Variations within the VSP interval velocity profile show a good correlation to stratigraphy and the dominant lithologies. Taking into account the desired smoothing of the profiles resulting from the applied computation method, the VSP interval velocities agree well with the compressional velocities from the sonic log only recorded in the lower part of the GrSk3 well.

3.5.4 Corridor stacks

Further processing steps applied to the data from the VP 10 zero-offset position included separation of up- and downgoing wavefields, deconvolution, and transformation to two-way travel time (Table 3.2). After this, reflections are aligned horizontally, and vertical reflection profiles were generated by stacking of the separated upgoing wavefield data over a defined time window after the first arrival (corridor stack). Because of the recording characteristics of the DAS data (see Section 3.5), the polarity of the upgoing wavefield data has been reversed (see Table 3.2) in order to match the polarity convention of conventional geophone data. The polarity convention of the data is European or European Association of Geoscientists and Engineers (EAGE) normal; i.e., a negative amplitude value (trough) corresponds to an increase in acoustic impedance downwards (Simm and White, 2002).

Corridor stacks for GrSk3 and GrSk4 are displayed in Figure 3.10. The recorded reflections are accurately correlated to depth and can therefore directly be assigned to lithology and other borehole data. The most prominent reflection events within the corridor stacks occur at the base (reflectors Z_1, Z_2, Z_3) and top (reflectors X_1, X_2, X_3) of the Upper Permian (Zechstein) and within the Middle Triassic (Buntsandstein; reflectors S_1, S_2).

Larger differences between the corridor stacks are mostly related to intervals where the reflection data are disturbed by residual ringing noise. The slope of this residual noise in the common-source gathers is similar to the slope of reflected upgoing waves, leading to positive superpositions and enhancements in the corridor stack which cannot be distinguished from real reflection events.

In the eastern part of the North German Basin, the deepest seismic reflections that can be readily recognized and correlated are at or close to the base of the Zechstein. The reflecting interface Z_1 is at the boundary between the Stassfurt salt and the underlying Stassfurt anhydrite ("Basalanhydrit"). This "base Zechstein" reflector is used as a marker horizon over the entire Southern Permian Basin area (Doornenbal et al., 2010).

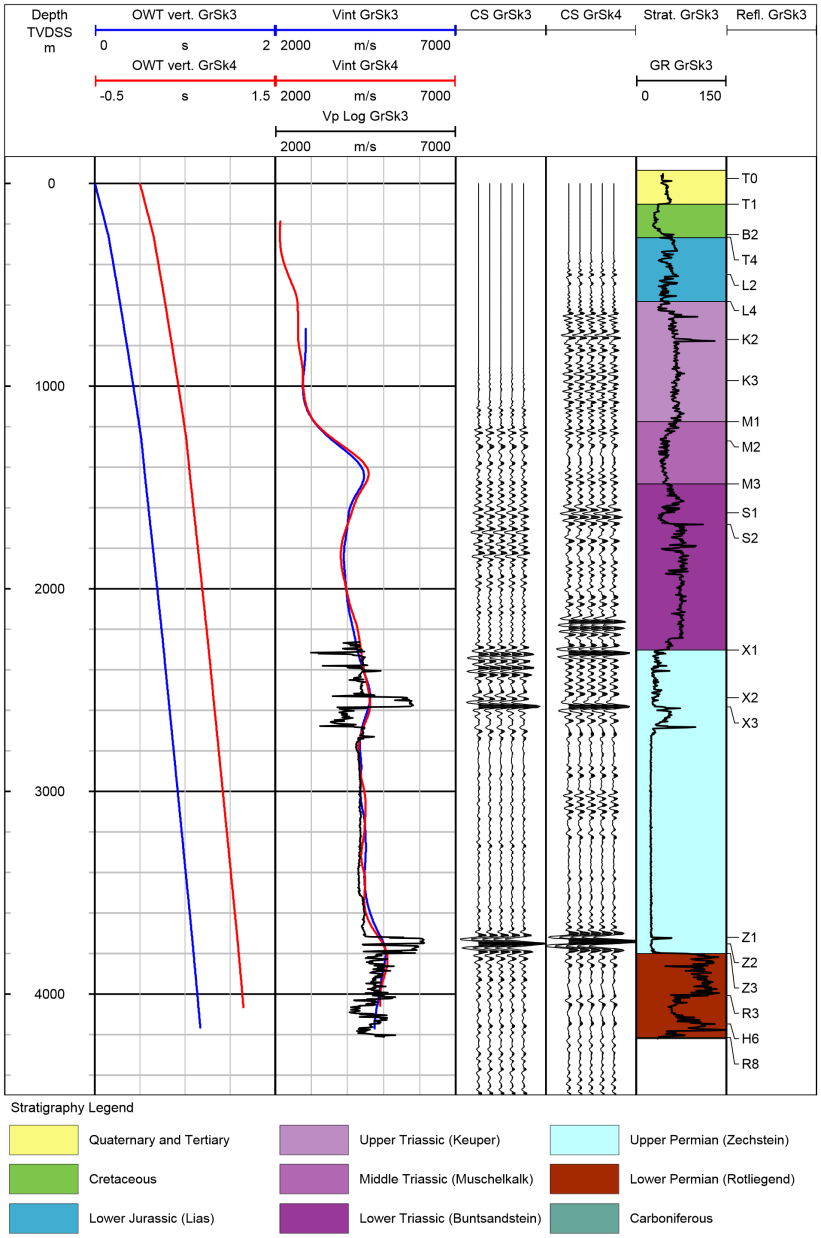

Figure 3.10: Vertical one-way travel times (OWT vert), VSP interval velocities (Vint), acoustic log sonic velocities (Vp Log), and corridor stacks (CS), together with stratigraphic units, gamma-ray (GR) log, and seismic reflectors. TVDSS: true vertical depth below mean sea level.

At Groß Schönebeck, the base of the Zechstein is comprised of an 80–90 m thick sequence of anhydrite, salt, and carbonate layers, which is underlain by the sediments of the Rotliegend. This interlayered sequence of strata with high impedance contrasts gives rise to several strong and closely spaced reflection bands, which mark the base of the Zechstein in the corridor stacks (see Figures 3.10 and 3.11).

Reflections within the underlying Rotliegend interval are evident as well, which can now be assigned to individual sections of the reservoir. The corridor stacks for the Rotliegend reservoir interval are shown in Figure 3.11, together with well logs and lithology data for both wells. Some of the well logs are unfortunately not available for the lower parts of the wells, especially for GrSk4. Acoustic impedance has been calculated as the product of bulk density and sonic velocity.

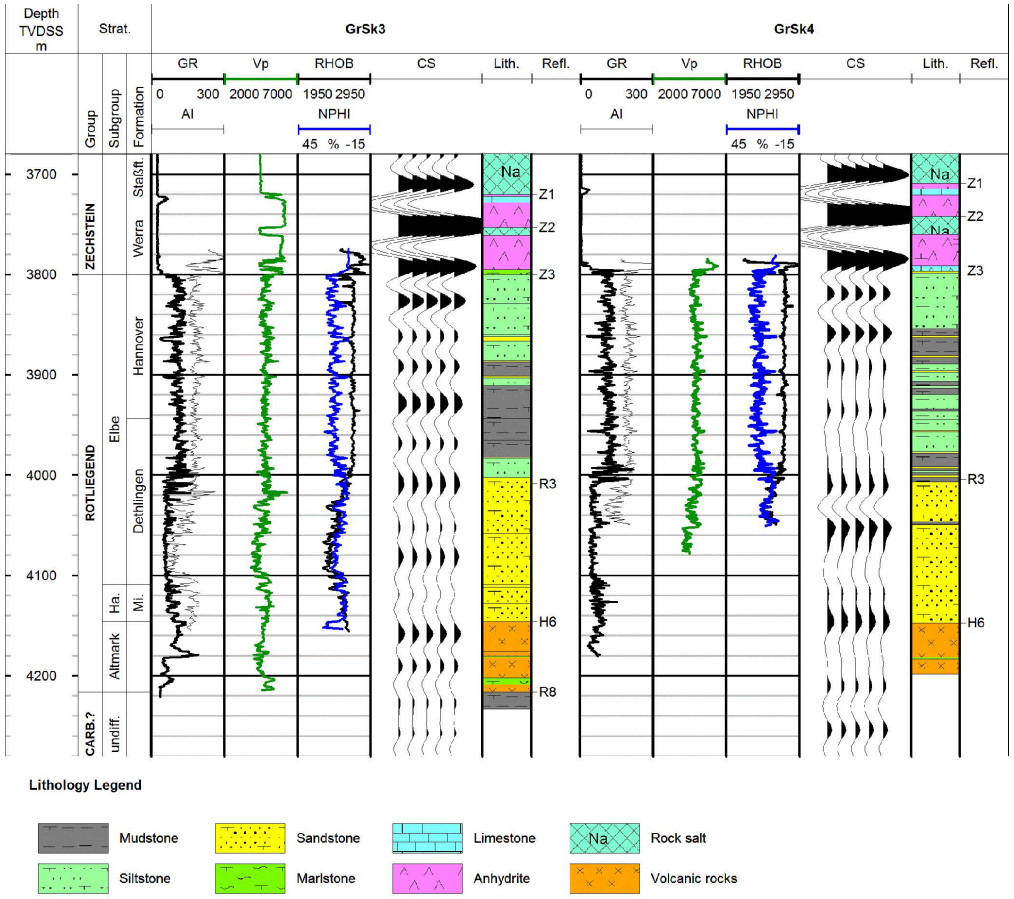

Figure 3.11: Corridor stacks (CS) for reservoir interval of the GrSk3 and GrSk4 wells, together with well logs (GR: gamma ray, Vp: sonic velocity, RHOB: bulk density, NPHI: neutron porosity), lithology (Lith.), stratigraphy (Strat.), and seismic reflectors (Refl.). Acoustic impedance (AI) was calculated from bulk density and sonic velocity. TVDSS: true vertical depth below mean sea level.

The Lower Rotliegend is formed by andesitic volcanic rocks of the Altmark Formation. At the depth of the possible top of the Carboniferous (reflector R_8), which was postulated at 4216 m TVDSS for the GrSk3 well, no distinct reflection event is evident in both wells. This is consistent with other regions in the North German Basin, where the base of the Rotliegend series is essentially non-reflective (Gutercch et al., 2010). The transition to the overlying Upper Rotliegend sediments occurs at a depth of 4146 m TVDSS. The corridor stacks show a positive reflection around this depth (reflector H_6), which nevertheless has a somewhat different character and a slight offset in depth of several meters for both wells.

The succession of the Upper Rotliegend sediments starts with the Mirow Formation, in which conglomerates are the dominant lithology. The clasts of the rock matrix are lithic fragments of the underlying volcanic rocks. The sediments of the overlying Elbe subgroup are of fluvial and eolian facies (Gast et al., 1998). Within the lower part, sandstones with good reservoir properties, i.e., high porosities and permeabilities, are occurring within the Dethlingen Formation. Within the wells, the Dethlingen sandstones, which are also known as the Elbe base sandstone, occur as a continuous interval with a thickness of about 100 m, approximately between a depth of about 4000 and 4100 m TVDSS. This interval is characterized by low gamma-ray values, bulk densities, and sonic velocities, which correspond to a low shale content and increased porosity. It is furthermore marked by a crossover of the bulk density and

neutron porosity curves. Bauer et al. (2020) presented an approach to map the distribution and properties of this sandstone layer based on analysis of seismic attributes of the 3-D surface seismic volume.

Above the Dethlingen sandstones, a succession of siltstones and mudstones follows. The transition is marked by a change in the log response, with higher values for the gamma-ray, density, and sonic velocity readings, and a separation of the bulk density and neutron porosity curves. This change in density and velocity corresponds to an overall increase of acoustic impedance. The top of the sandstone interval correlates with a positive amplitude event at a depth of 4010 m TVDSS in both profiles (reflector R_3). In GrSk4, an other reflection (peak) occurs about 40 m below at a depth of 4051 m TVDSS, which correlates with a step-like decrease of both gamma-ray intensity and sonic velocity. This local change of the log response is not as evident in GrSk3, where only a very weak reflection event occurs at this depth.

The upper interval of the Rotliegend sediments is comprised of an interlayered sequence of siltstones and silty mudstones (Hannover Formation), with local occurrences of thin-bedded sandy layers. The succession of lithological units and interbeds differs between both wells, which is also reflected by the different character of the corridor stacks within this interval.

The different characteristics of the corridor stacks in the Upper Rotliegend are explained by lithological changes between the wells. Within the bottom part, the well trajectories have a horizontal distance of up to 475 m, and such lateral changes in lithology are typical for fluvial sediments. The observed character of the reflectors, with low reflectivity and lateral variability, is in line with other regions in the North German Basin, where deeper reflectors within the Rotliegend or Carboniferous commonly cannot be correlated over long distances, because they are of poor quality and often interrupted (Reinhardt, 1993).

3.6 Summary and conclusions

Based on this survey, several important new experiences for DAS-VSP acquisition on wireline cable have been gathered. The presented results can be used in support of planning, execution, and evaluation of future surveys of this type.

Common-source gathers of the recorded data are dominated by arrivals of downgoing P waves, upgoing reflections, and tube waves. One characteristic of the recorded DAS-VSP data is that they are affected by a coherent noise, which is correlated among neighboring traces. This ringing noise is evident in common-source gathers as a conspicuous zigzag pattern confined to distinct depth intervals and is occurring in narrow frequency bands. It is influenced by the cable tension and how the cable is aligned with the inner surface of the borehole, depending on changes of the borehole trajectory.

Several tests to determine the influence of the wireline cable tension on the mechanical coupling of the cable to the borehole wall have been performed. The highest signal amplitudes and best overall data quality were found to be achieved under almost full cable tension, and the main part of the data was acquired under these conditions. The results of these tests nevertheless also indicate that a reduction of coherent ringing noise can be achieved by adding cable slack. The interrelation between cable tension and configuration inside the

borehole, mechanical coupling to the borehole wall, and recorded signal amplitudes needs further investigation.

After conversion to strain rate, the waveforms and frequency content of the DAS data display a high similarity to vertical component data of a conventional borehole geophone. However, upgoing reflections are recorded with opposite polarity, which confirms the results of earlier studies. The polarity of the reflection data was reversed during later processing, in order to match the polarity of conventional geophone data.

Most of the data have a very good signal-to-noise ratio. Nevertheless, in the GrSk3 well, a sudden reduction of SNR along the deeper part of the profile after the first recording day has been observed. As a larger movement of the cable can be excluded during this time, the cause of this change of acquisition characteristics remains elusive. The ringing noise can be suppressed to a large extent by suitable filtering methods.

From the zero-offset data, accurate time–depth relationships and velocity profiles were derived. The reflectivity along the boreholes could be mapped with high resolution. The strongest reflections occur at the base and the top of the Zechstein salt complex and within the Buntsandstein. Nevertheless, in parts, the interpretation of the corridor stacks is hampered by residual ringing noise, which occurs within a short time window after the first-break arrivals and is difficult to be distinguished from true reflection events.

For the Rotliegend reservoir section, the sequence of reflection events in the corridor stacks shows a different character for both wells overall, which is explained by lateral changes in lithology. But it also displays local similarities: the top of the Dethlingen sandstone interval is marked by a positive reflection event in both wells. This information can be used to identify a related reflector and track the distribution of this reservoir layer in a 3-D seismic volume. Processing and interpretation of both 3-D VSP and 3-D surface seismic data are currently ongoing. The top of the volcanic rocks has a somewhat different response in both wells, and no stronger event is obvious at the postulated top of the Carboniferous. The thickness of the volcanic rocks therefore cannot be inferred from individual reflection events in the seismic data alone.

The DAS method has enabled measurements at elevated temperatures up to 150 °C and has led to significant time and cost savings compared to deployment of a conventional borehole geophone string. Such savings depend on the specific targets and conditions of an individual survey, as well as on the available technologies and performance of the equipment used. But for a VSP survey similar to this study, we would roughly estimate the operational effort to be reduced by around a factor of 5 to 10.

3.7 Acknowledgements

We gratefully acknowledge the contributions of Ernst Huenges, who led the efforts at the geothermal research platform Groß Schönebeck, and Klaus Bauer for providing major support during funding acquisition and project administration. We are thankful for the smooth cooperation with Schlumberger and DMT GmbH & Co KG during data acquisition, as well as GGL (Geophysik und Geotechnik Leipzig) GmbH during survey planning, and Schlumberger and VSProwess Ltd. during data processing. Jörg Schrötter, Christian Cunow, and Mathias

Poser of GFZ supported fieldwork and acquisition of fiber-optic data. The paper has greatly benefitted from the constructive comments of Ariel Lellouch and an anonymous reviewer, which helped us to work out several important aspects of the paper more clearly.

4

Data processing

For the wireline DAS VSP method, coupling conditions of the cable play a vital role. Loosened parts of the cable act like a vibrating string and are subjected to reverberations. In this chapter, I explain the main characteristics of the coupling noise and then compare the existing methods which can be applied to tackle this noise problem. Lastly, I present a newly developed method for noise elimination, which outperforms previously demonstrated denoising techniques.

Cable reverberations during wireline distributed acoustic sensing measurements: their nature and methods for elimination

Evgeniia Martuganova[1,2], Manfred Stiller[1], Klaus Bauer[1], Jan Henninges[1], and Charlotte M. Krawczyk[1,2]

[1]Helmholtz Centre Potsdam, GFZ German Research Centre for Geosciences, 14473 Potsdam, Germany

[2]Department of Applied Geophysics, Technische Universität Berlin, 10587 Berlin, Germany

Article published in *Geophysical Prospecting, 2021, 69, 1034–1054*
https://doi.org/10.1111/1365-2478.13090f [accepted manuscript]

4.1 Abstract

The application of distributed acoustic sensing in borehole measurements allows for the use of fibre optic cables to measure strain. This is more efficient in terms of time and costs compared with the deploying of conventional borehole seismometers. Nevertheless, one known drawback for temporary deployment is represented by the freely hanging wireline cable slapping and ringing inside the casing, which introduces additional coherent coupling noise to the data. The present study proposes an explanation for the mechanism of noise generation and draws an analogy with similar wave propagation processes and phenomena, such as ghost waves in marine seismics. This observation allows to derive a ringing noise filter function, to study its behaviour and to consider known effects of the gauge length filter. After examining existing methods aimed at eliminating ringing noise and results of their application, we propose a two-step approach: (1) developing a denoising method based on a matching pursuit decomposition with

Gabor atoms and (2) subtracting the noise model for imaging improvement. The matching pursuit method focuses on decomposing the original input signal into a weighted sum of Gabor functions. Analysing Gabor atoms properties for frequency, amplitude and position in time provides the opportunity to distinguish parts of the original signal denoting noise caused by the vibrating cable. The matching pursuit decomposition applied to the distributed acoustic sensing-vertical seismic profiling data at the geothermal test site Groß Schönebeck provides a versatile processing instrument for noise suppression.

4.2 Introduction

During the last decade, distributed acoustic sensing (DAS), a technology of seismic data acquisition using fibre optic cable as a linearly arranged array of sensors, has gained a wide range of application in geoscience (Dou et al., 2017; Henninges et al., 2017; Jousset et al., 2018; Mondanos and Coleman, 2019; Naldrett et al., 2020). In comparison with classical vertical seismic profiling (VSP), DAS technology application allows recording a continuous data set faster and more cost effectively. Currently, the majority of surveys are obtained using fibre optic cables permanently installed behind the casing or along the tubing (Mateeva et al., 2014; Correa et al., 2017; Grandi et al., 2017; Götz et al., 2018). However, there are a significant number of drilled wells in which only the use of wireline DAS technology is possible. Nevertheless, only a limited amount of data examples recorded using temporarily installed wireline cable are available (Hartog et al., 2014; Borland et al., 2016; Yu et al., 2016a; Yu et al., 2016b; Willis et al., 2019).

One of the possible explanations to this fact might be that the temporary cable installation causes problems with proper cable coupling and, as a result, it increases additional coherent noise in the data.

Miller et al. (2012) showed for the first-time data acquired using a temporarily installed fibre optic cable at Devine test site near San Antonio, Texas. The ringing signals are present in the shallow depths for all source positions and were explained as a poor coupling effect. For noise suppression a single-channel notch filter and orthogonal projection operators were applied.

Later, several authors encounter the same noise patterns during DAS data recording using wireline installation (Hartog et al., 2014; Dean et al., 2015; Yu et al., 2016a). Schilke et al. (2016) and Constantinou et al. (2016) raised the idea of providing slack to the cable during data recording to improve cable coupling to borehole walls. It was studied using numerical modelling methods and field tests from Rittershoffen, France. However, the demonstrated data set example acquired with recommended 2% slack showed a reduced amount of the noise as well as decrease of the signal-to-noise ratio in the region of cable accumulation.

Barberan et al. (2012), Didraga (2015) and Daley et al. (2016) report on ringing noise zones in the data acquired using a DAS cable clamped to the tubing. According to Didraga (2015), a noise generation mechanism is associated with vertical sections of the boreholes in which the tubing acts like a vibrating string between the contact points with an outer casing. Daley et al. (2016) explain ringing noise events as reverberation waves trapped between two depths.

Also, the above authors suggest noisy regions in the data corresponding to wave propagation in a poorly cemented steel casing.

Willis et al. (2019) further explored the properties of the ringing noise and described different velocities of up- and downgoing part of the zigzags of the noise. The noise generation is interpreted as a back-and-forth reverberation in depth regions of a loose cable.

Given this variability, the comprehension of the noise nature and the physical mechanism of its origin is essential for the subsequent imaging quality improvement. In this study, we add to the available approaches. For this purpose, we propose a physical model of so-called ringing noise and a means for its elimination based on a matching pursuit decomposition (MPD) with Gabor atoms. We evidence this by a case study at the Groß Schönebeck site, Germany.

4.3 Distributed Acoustic Sensing - Vertical Seismic Profiling Experiment

The Groß Schönebeck research platform operated by the German Research Centre for Geosciences (GFZ) is located 40 kilometres northeast of Berlin on the southern edge of the North German Basin. It serves as a reference site for geothermal energy technology development for sustainable energy production from low permeability deep geothermal reservoirs. The target geothermal reservoir zone at depths of 4000 to 4300 m is represented by siliciclastic sediments and volcanic rocks of Lower Permian (Rotliegend) age, overlaid by Zechstein salt (Zimmermann et al., 2010).

A distributed acoustic sensing (DAS) vertical seismic profiling (VSP) data set was acquired at the Groß Schönebeck in situ geothermal laboratory in February 2017 (Henninges et al., 2021a) with the additional intent to support the high-resolution 3D reflection seismic survey from the surface (Stiller et al., 2018). The 3D seismic survey, covering an area of 8 km by 8 km, has its focus on reservoir depths at 4 km. The main goal of the 3D seismic survey was to enhance the comprehension of the geological structures and to reveal the spatial configuration of fault structures (Krawczyk et al., 2019; Bauer et al., 2020).

The VSP experiment, in its turn, was designed to enable detailed imaging around the existing boreholes and especially to additionally improve 3D surface seismic interpretation in the reservoir target area.

4.3.1 Acquisition parameters

Two wireline, hybrid cables (electrical and optical; from SLB (NOVA-F) and GFZ (Rochester) (Henninges et al., 2011) were temporarily installed in the 4.3 km deep wells E GrSk 3/90 (maximum inclination 7.2°) and Gt GrSk 4/05 (maximum inclination 49°) (Figure 4.1). The DAS sensor cable was freely lowered inside the water-filled borehole until maximum measured depth in E GrSk 3/90 (4309 m measured depth (MD)), and in Gt GrSk 4/05 it was deployed until an existing restriction (4214.17 m MD). Data were recorded on single-mode fibres using hDVS (the heterodyne distributed vibration sensing, Schlumberger) technology. The spatial sampling along the borehole was set to 5 m. The recorded physical quantity of the fibre optic DAS/hDVS system is strain, distributed over a gauge length (a section of the fibre over which the strain is measured).

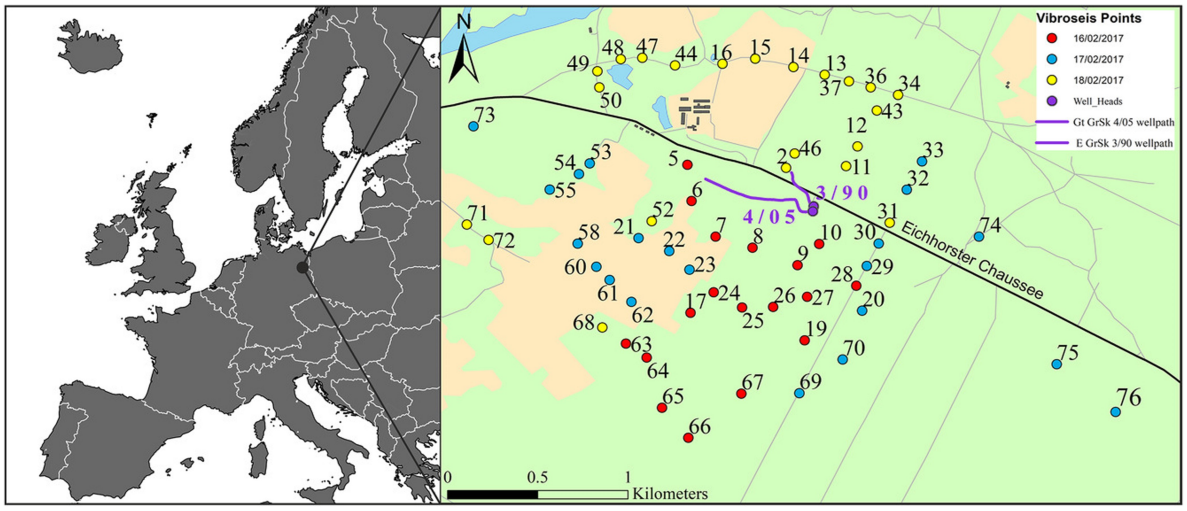

Figure 4.1: Location of the Groß Schönebeck geothermal site. Left: Position in the Northeast German basin in Europe. Right: Base map of the Groß Schönebeck geothermal site with two boreholes (violet circles) in the centre and 61 VSP source points arranged in a spiral pattern around. Borehole trajectories are shown in violet. VP locations are shown in different colours corresponding to the day of acquisition: 18 VPs on day -1 (red dots), 18 VPs on day -2 (blue dots) and 25 VPs on day -3 (yellow dots).

Data were recorded using 20-m gauge length but later adjusted to processing optimized 40 m to achieve a compromise between S/N maximization and loss of the signal frequencies (see also Dean et al., 2017, for further debate). During the experiment, we had 61 vibroseis points (VP), located at different offsets (from 200 to 2000 m) and azimuths, forming a spiral around the boreholes (Figure 4.1). Four heavy trucks vibrated simultaneously and repeatedly at each VP location, with an average stacking fold of 16 per source location. For the data acquisition, a linear sweep of 10–112 Hz and 36 s length was used. For several VPs with larger offsets, we used a sweep from 10 to 96 Hz. Overall, the VSP experiment measurements were conducted during four acquisition days (one day for detailed pre-survey start-up tests and three days of data acquisition). More experiment planning and data acquisition details can be found in Henninges et al. (2021a).

We performed different noise analysis and denoising tests on the vertically stacked raw DAS strain data set recorded at source position 10 (Figure 4.1) in well Gt GrSk 4/05 during pre-survey tests with 26 sweep repetitions with 1 m slack applied to the cable. This choice was dictated by the availability of independent measurements with the versatile seismic imager (VSI) tool string recorded in the same well with the same sweep parameters 10–88 Hz and 36 s length. A direct comparison of conventional acceleration point sensor measurements and denoising results allows to get a better understanding of DAS data and to perform additional quality control of the proposed denoising processing workflow so that these data serve as a reference for the DAS data processing. Checkshots were recorded at 1200, 2400, 3600 and 4207 m MD.

4.4 Ringing noise

Yu et al. (2016a) and Willis et al. (2019) present examples of distributed acoustic sensing (DAS) data sets recorded on a wireline cable. The authors pose that such ringing noise is most likely

caused by poor coupling of the sensor cable and the borehole casing, which is visible in certain depth intervals. During wireline acquisition, the cable is not fixed and hangs freely inside the borehole; thus, cable coupling inside the well is not well controllable. Due to a borehole's conditions, such as inclination and completion at specific depth ranges, the cable contact with the borehole wall varies; therefore, some areas are likely subjected to reverberations caused by different sources such as a vibroseis signal during data acquisition (Yu et al., 2016a; Willis et al., 2019). Cable slapping creates a specific noise pattern, elimination of which leads to considerable complication during data processing.

A typical DAS vertical seismic profiling (VSP) section from Groß Schönebeck (Figure 4.2a) presents this ringing noise phenomenon, as described above. The recorded seismic data show narrow-band noise trains with a stripe or characteristic zigzag patterns in the time domain (Fig. 2b) over at least 19 different depth regions, for instance at 594–849, 1548–1702, 2984–3282 and 3735–3807 m measured depth (Figure 4.2a). We refer to this type of noise as ringing noise. In the time domain, the noisy intervals often follow one after another, forming a larger noisy zone and even overlap like in depth interval 1755–2367 m. These zigzag patterns obscure important features such as reflections.

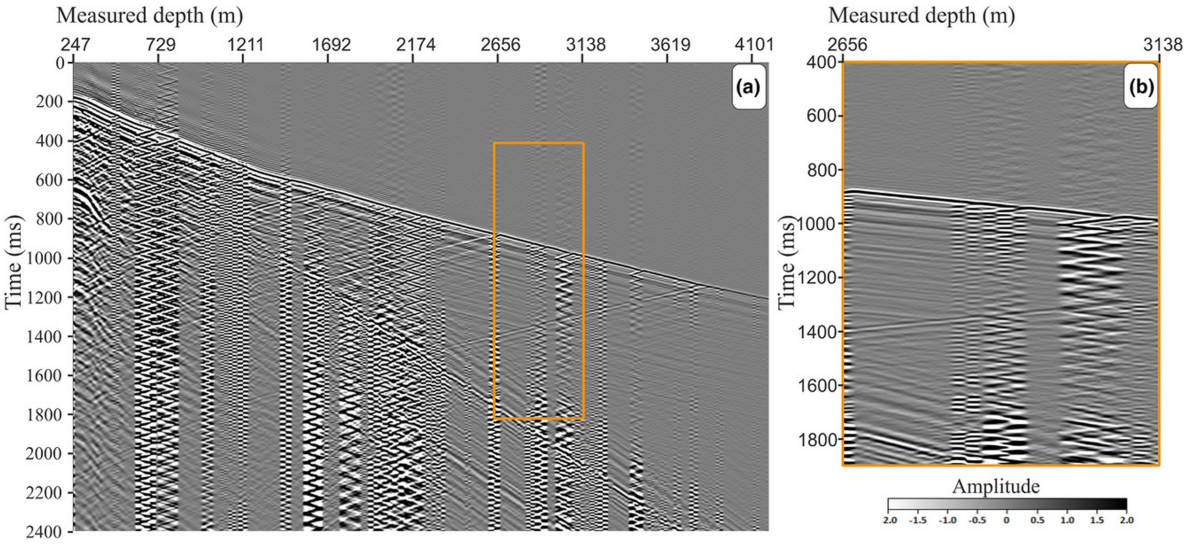

Figure 4.2: Example of a typical DAS VSP section from Groß Schönebeck. (a) Common source gather contaminated with noise, recorded for VP10 after preprocessing (vertical stacking, correlation with the pilot sweep and subsequent differentiation to achieve acceleration-like characteristics; seismic software ProMAX R5000, Halliburton). (b) The orange rectangle shows zoomed fragment of the seismic section for the depth range 2656–3138 m.

In the frequency domain (Figure 4.3), high-amplitude peaks in the amplitude spectrum can be observed. The white arrows illustrate periodic maximums corresponding to 18 Hz frequency multiples (i.e. 18, 36, 54 Hz etc.) for the seismic trace at 622.76 m MD. A similar pattern of the high-amplitude values, occurring with a certain periodicity, is also noticeable at different depth levels. The amplitude values of the peaks vary for each of the different depth levels and frequency values. Unlike in time domain displays, frequency domain displays allow for a better separation of the individual zigzag intervals and provide a better understanding of the noise. It appears that the shallow part of the record contains more noisy intervals in comparison with the deeper part (below 2000 m). From one VP record to another, these affected depth regions do not change significantly in the study presented. If we compare depth section 1418–1490 m

with depth section 1760–1909 m,we can recognize that both depth intervals contain coherent noise. However, there is a distinct difference in the level of noise contamination. Furthermore, seismic data recorded, for instance, in section 2670–2820 m, show no signs of ringing noise at all. Possibly, these differences in local amplitude and S/N ratio occur due to variable coupling conditions. Ringing noise generation mechanism will be further investigated in the next section of the paper.

4.5 Ringing noise analysis

4.5.1 Methodological background

To better understand the ringing noise, we have performed the frequency–time (FT) spectrum analysis of a single seismic trace, recorded at 622.76 m MD. We picked the data before correlation from the interval affected by ringing noise, which we already identified by examining the plot with the amplitude spectrum in the previous chapter. FT representations transform original data from the time–space domain to the time–frequency domain by performing a series of fast Fourier transforms within moving time windows. Using this type of analysis, we can study frequency–energy variations over time.

The energy of a vibrator sweep and its harmonics at VP 10 in Groß Schönebeck can be clearly visualized (Figure 4.4) with the method described above. Also, we see a repetitive pattern of horizontally elongated zones with a significant amplitude increase at frequencies 18, 36, 54, 72, 90 Hz etc., which are marked with white arrows.

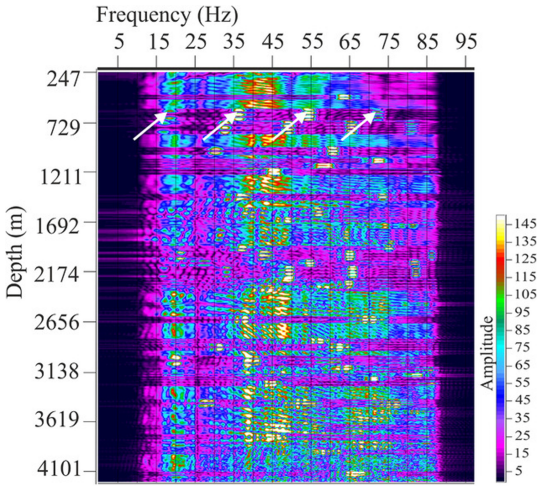

Figure 4.3: FX amplitude spectra of the VP10 seismic section after preprocessing. Irregularly occurring maximums correspond to resonances. White arrows highlight examples of the ringing noise occurrence.

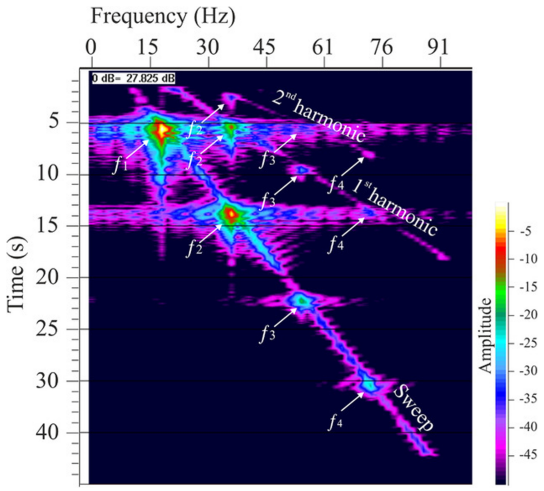

Figure 4.4: The FT amplitude spectrum, calculated for one raw uncorrelated strain seismic trace at 622.76 m MD, highlights frequency variations over time. A regular pattern of oval-shaped maxima can be observed at 18, 36, 54, 72 and 90 Hz. The fundamental labelled as f1 and overtone modes as f2–f4.

These high-energy areas at given constant frequencies may correspond to the natural frequencies of the oscillating system. When the instantaneous frequency of the sweep signal or its harmonics coincides with the string's natural frequency, the condition for resonance is met,

and the amplitude becomes strongest. Reflected waves from both ends of the vibrating cable interval will interfere with each other constructively or destructively at different points of the wire and create a standing wave, which represents an oscillation in time but does not actually move in space. Consequently, the resulting noise pattern can be interpreted as interference of two separate waves travelling opposite directions.

The harmonics of a system specify the frequency pattern of the standing waves. The lowest natural frequency is called fundamental, frequencies above it are known as overtones. The place where the waves are superimposed destructively, and which has no movement is called a node. On the contrary, the geometrical place where the waves are constructively superimposed, and the string has its maximum amplitude is called an antinode.

The freely hanging section of the cable can be approximated by a physical model of a string with fixed ends. In this case, the antinodes are located at its ends and the nodes are formed in-between. Figure 4.5(a) shows a string configuration for the first four harmonics. The fundamental harmonic contains one antinode in the middle of the string, the second harmonic will have two antinodes, the third three antinodes etc.

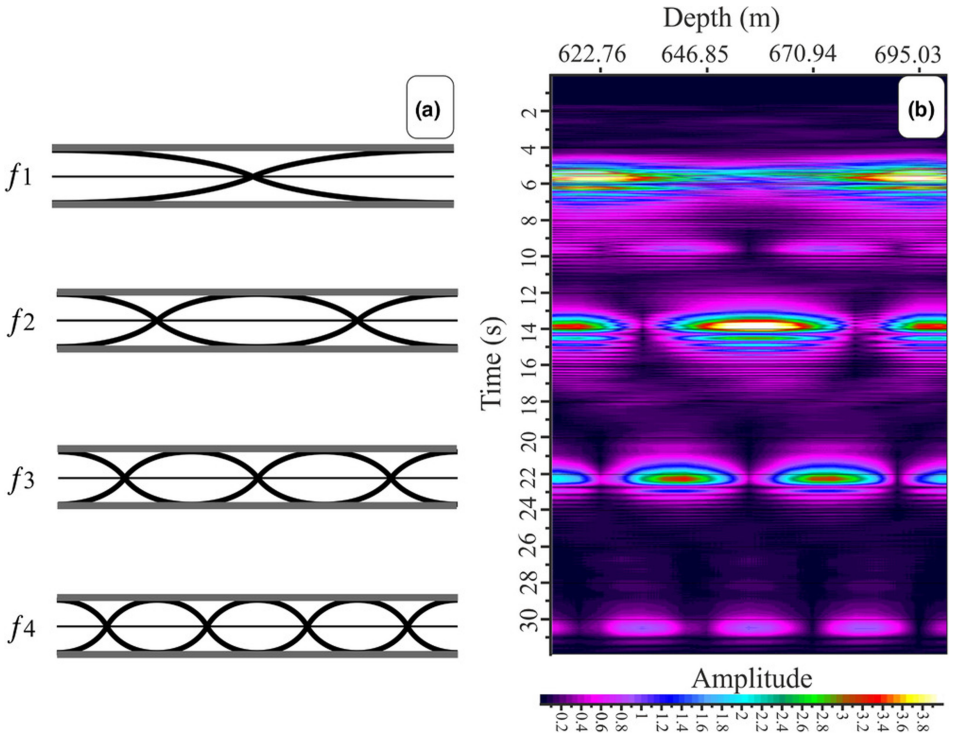

Figure 4.5: Standing wave modes for fixed-end cable vibrations for different frequencies. (a) Theoretical description of fundamental (f1) and overtone modes (f2–f4); the bold black line shows the cable strain for the corresponding frequency mode inside the borehole. (b) Reflection strength attribute calculated from raw strain data for the depth range from 611.26 to 701.30 m MD.

The harmonics (f) for the standing wave can be described via the formula:

$$fn = \frac{nV}{2L} \tag{4.1}$$

where V is the velocity of the medium, L is the length of the string, and n is an integer, harmonic number.

In case of standing waves formed on a string with free ends, there will be the same formula for harmonics. However, the position of the nodes and antinodes will be swapped.

For the fixed ends, there is a curious detail related to the phase of the strain at the left and right ends of the string for odd and even modes. In case of odd n, the motion of the string ends is out of phase, and for even n it is in-phase (Figure 4.5a).

As could be noticed from Figure 4.4 at a specific moment in time, the resulting strain of the string represents a superposition of the different modes. The highest contribution belongs to the modes generated by sweep energy. We will refer to them as the main modes of the string. Resonances created by sweeps harmonics add complexity to the resulting string motion, but in principle do not change the main mode generated by the sweep.

The transition of the main mode from odd to even will change the phase of the one end of the string. The phase alteration to the opposite will happen only for one end, which means that the string ends' resulting phases will differ. This disproportion in phases will create the zigzag pattern after correlation with different up and down velocities. Thus, the resulting dips of the noise on the correlated seismogram show phase velocities and depend on the standing wave frequency.

The reflection strength attribute (the modulus of the complex trace, or trace envelope) is calculated based on raw vertically stacked and uncorrelated distributed acoustic sensing (DAS) strain data for the depth region 611.26 to 701.30 m MD (Figure 4.5b). This interval includes the seismic trace at 622.76 m MD, which we previously inspected in Figures 4.3 and 4.4. Hot coloured areas of the plot correspond to the antinode locations, black spaces between the loops show the position of the nodes in the current mode. The length of the vibrating cable interval can be estimated by visual inspection of the noise depth range, which in our example is approximately equal to 130 m. The fundamental mode (f1) and three overtones (f_2, f_3, f_4) are clearly visible and have an identical configuration as the physical model (Figure 4.5a).

4.5.2 Cable reverberation as a linear filter

Ringing noise has frequency characteristics similar to another unwanted phenomenon – ghost waves – occurring in marine seismic data. Backus (1959) described water reverberation mathematically as a linear filtering process. Strictly speaking in the case of the acoustically soft bottom (reflection coefficient = -1, the part of the equation corresponding to the ghost wave describing the water layer filter will accurately depict the standing waves formed inside the water medium.

Based on the equations described in Backus (1959), we could write a mathematical formula for the ringing noise frequency response function, with:
L: the length of the string = the length of the reverberating part of the cable,
V: the velocity of the acoustic wave travelling along the wireline cable,
R: reflection coefficient at the end of the string,
$\tau = \frac{2L}{V}$ two-way travel time between two ends of the cable section,
n: integer index of reflection.

The resonance creates an impulse $\delta(t)$, which reverberates within a certain length of the cable. The resulting output at the receiver point $f(t)$ could be presented as bouncing reflections

between two interfaces:

$$f(t) = \delta(t) - R\delta(t-\tau) + R^2\delta(t-2\tau) - ..., \tag{4.2}$$

$$f(t) = \sum_{n=0}^{\infty}(-1)^n R^n \delta(t-n\tau). \tag{4.3}$$

The frequency response $F(\omega)$ is represented as

$$F(\omega) = \int_{-\infty}^{\infty}\sum_{n=0}^{\infty}(-1)^n R^n \delta(t-n\tau)exp(-j\omega t)dt, \tag{4.4}$$

$$F(\omega) = \sum_{n=0}^{\infty}(-1)^n R^n exp(-jn\omega\tau), \tag{4.5}$$

which is the binominal expansion for

$$F(\omega) = \frac{1}{1+Rexp(-j\omega\tau)}, \tag{4.6}$$

$$|F(\omega)| = (1+R^2+2R\cos(\omega\tau))^{-\frac{1}{2}}. \tag{4.7}$$

The phase response can be described by the following formula:

$$\phi(\omega) = \tan^{-1}\frac{R\sin(\omega\tau)}{1+R\cos(\omega\tau)}. \tag{4.8}$$

In the case of R = -1, a condition is required for standing wave existence, and equation 4.7 will become

$$|F(\omega)|_{R=-1} = |\frac{1}{2\csc(\frac{\omega\tau)}{2}}| \tag{4.9}$$

with resonating frequencies described by formula 4.1. Thereby, the resulting formula (9) corresponds to the classical equation for standing waves harmonics in the case of both free and fixed ends. Different effects of parameter variations on the ringing filter function of formula (9) can be analysed (Figure 4.6). The decrease in length of the string leads to an increase of the first resonating frequency and overall stretching of the notch areas, as well as the resonating areas (Figure 4.6a). The reduction of the velocity values has the opposite effect: the smaller the velocity, the lower the fundamental frequency (Figure 4.6b). It should be noticed that the wireline cable velocity (V) depends on the parameters string tension (T) and mass per length (μ) as follows:

$$V = \sqrt{\frac{T}{\mu}} \tag{4.10}$$

Thus, a variation of the cable tension will change the cable velocity. Similar to the guitar tuning process, additional tension will create a higher frequency of the fundamental tone.

For DAS measurements, the gauge length parameter has a significant effect on the signal-to-noise ratio of the data as well as on resolution. Basically, it acts like a spatially averaging filter. Dean et al. (2017) describe the gauge length (GL) frequency response $Rgl(k)$ with wavenumber k by the formula:

$$Rgl(k) = \frac{\sin(\pi kGL)}{\pi k} \tag{4.11}$$

Figure 4.6(c) shows frequency responses for four different gauge lengths calculated for a wireline cable velocity of 4680 m/s. It can be seen from the graph that for such a high velocity, we do not see any notches in the first 100 Hz. However, increasing of the GL value leads to decreasing of the first notch position, and the gauge length response function becomes steeper.

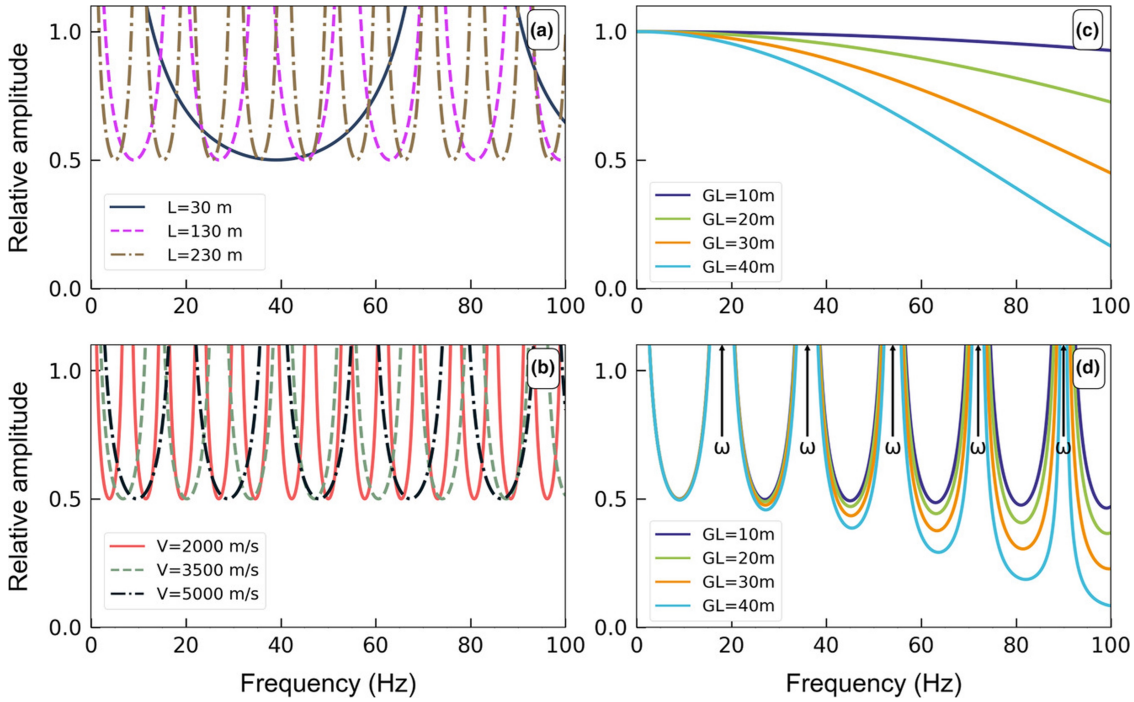

Figure 4.6: Effect of parameter variations on the ringing filter function (see text for the derivation of formula (9)). (a) Ringing noise frequency responses calculated for a string with different lengths (30, 130, 230 m; colour-coded). Wireline cable velocity is 4680 m/s. (b) Ringing noise frequency responses calculated for a string with different wireline cable velocities (2000, 3500, 5000 m/s; colour-coded). String length is 130 m. (c) Frequency responses for different gauge lengths (GL; colour-coded; velocity 4680 m/s). (d) Frequency response functions expected from the application of different gauge lengths (GL; colour-coded) to the ringing noise frequency response for a string length of 130 m and wireline cable velocity 4680 m/s; ω, resonating frequencies.

It is required to combine the frequency response of the ringing noise with the frequency response for the gauge length to estimate the influence of the ringing noise filter on the DAS data. The resulting filter frequency response function (Figure 4.6d) evidences that an increase of the gauge length leads to stronger attenuation of higher frequencies. In the example given, the effect causes a decrease of the amplitude response from 0.5 (gauge length 10 m) to 0.1 (gauge length 40 m). This is important to note because such an effect will also smear out the noise.

4.5.3 Ringing noise filter tests

To illustrate the impact of the ringing noise filter, we performed simple modelling using the raw pilot sweep from the start-up tests (10–88 Hz, linear, 36 s length), which we had used for data acquisition and correlation (Figure 4.7). The spectrum of the sweep has a rectangular shape with tapered ends. Using formula (4.9), we modelled the ringing noise response function. Notice that it has a series of narrow areas where the amplitude is approaching infinity (around 18, 36, 54 Hz etc.) alternating with notches, existing in the original spectrum (around 27,

45, 63 Hz etc.). The application of the ringing noise filter causes disturbances at the sweep spectrum and creates a series of peaks and troughs in the spectra. Additional application of the gauge length frequency response will lead to loss of energy at frequencies higher than 80 Hz. A similar amplitude spectrum behaviour we observe in the data.

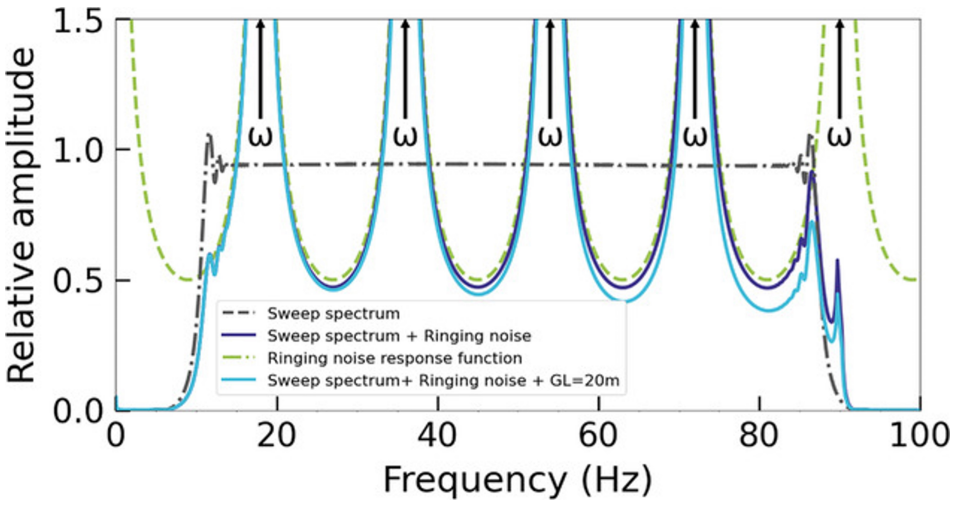

Figure 4.7: Comparison of an original sweep spectrum and colour-coded the spectra after different filter applications (parameters used: wireline cable velocity 4680 m/s; string length 130 m; gauge length 20 m).

4.6 Noise elimination with known processing methods

Cable reverberations create a sequence of distinct peaks and notches in the frequency spectrum. This decreases the useable bandwidth of the measured wavefield and, as a result, reduces the vertical resolution of the data. The existing processing methods for ringing noise elimination can be classified into three main categories: wavefield extraction methods, statistical methods and subtraction of modelled noise. We briefly summarize the first two approaches here, being accompanied by the application to the Groß Schönebeck distributed acoustic sensing VSP data.

4.6.1 Wavefield extraction methods

Wavefield extraction methods attempt to reconstruct the wavefield using information from neighbouring traces and then substitute the noise. According to the Fresnel zone theory, noisy traces should have similar characteristics as unaffected neighbour traces. We have used the time–frequency domain (TFD) filtering method (Elboth et al., 2008) that replaces anomalous amplitude values with an amplitude estimated from adjacent traces. Using a short Fourier transform algorithm, a median magnitude of each trace's spectrum is calculated within a specified filter length and frequency subband.

On the source gather before denoising (Figure 4.8a), there are many depth intervals with poor coupling. Application of the TFD to the Groß Schönebeck data shows its potential to significantly reduce the amount of ringing noise in the data (Figure 4.8b).We can see a particular reduction of the ringing noise at 1200–1933 m depth interval. Nevertheless, when the spectral amplitude values are similar, the algorithm will be unable to clean the data completely.

The residual noise can be seen Figure 8(b) at 488–970 m, 1933–2174 m and 2897–3138 m depth ranges. This is the main drawback of this method.

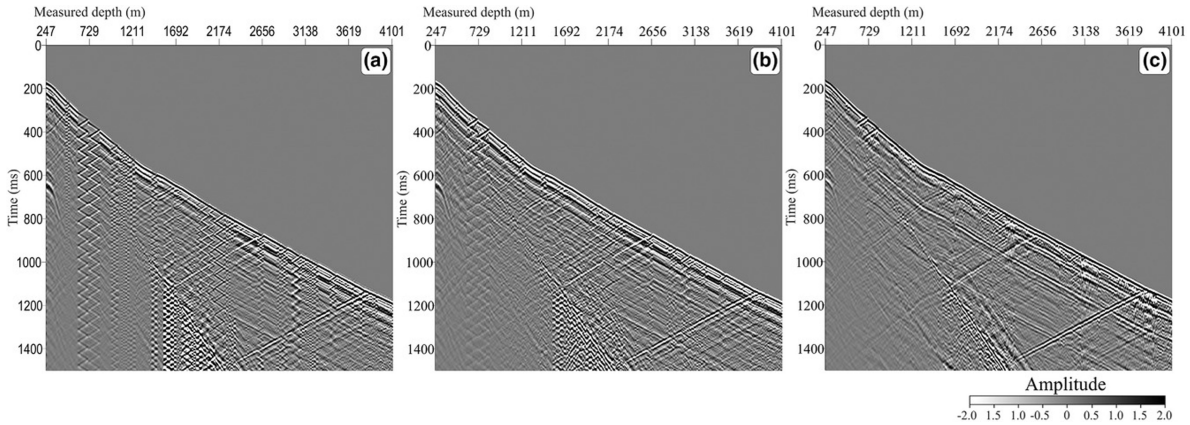

Figure 4.8: Comparison of measured and filtered common source gather: (a) before denoising, (b) after time–frequency domain noise attenuation and (c) after Burg adaptive deconvolution.

4.6.2 Statistical methods

Statistical noise estimation relies on spectrum balancing and adaptive filter construction without previous knowledge about the noise. We have evaluated several deconvolution algorithms for computing prediction error filters like Wiener-Levinson, L1 or L2 Norm and Burg's maximum entropy approach. Standard spiking or predictive deconvolution is robust under a wide variety of input conditions. However, a substantial improvement in pulse compression could be obtained by the Burg algorithm (Burg, 1972; Burg, 1975) in an adaptive formulation (Griffiths et al., 1977; Widrow and Stearns, 1985) for our type of data consisting of non-minimum phase wavelets combined with sparse reflectivity series. This method relies on the assumption that the power spectrum is an output of the hypothetical linear system, which has generated the signal. That, in turn, leads to an improved spectral estimation and minimized end-effect problems if a moderate adaption rate is chosen.

The deconvolution has a dual effect on the data: it suppresses monofrequent noise and whitens the amplitude spectrum. By the use of the Burg adaptive deconvolution to the Groß Schönebeck data, the signal of the seismic traces is clearly sharpened. The application of the Burg method (Figure 4.8c) allowed cleaning the data from the ringing noise almost completely, with small residuals around the first-break arrivals at the following depth intervals: 604–861 m, 2121–2270 m, 2969–3138 m. As a result, we were able to improve resolution and reflection continuity.

4.7 Matching Pursuit decomposition with Gabor atoms

Supplementing the application of the two known methods given above, we introduce here a new approach we termed matching pursuit decomposition (MPD). It belongs to the category of physical modelling of the noise and its subsequent subtraction from the data. Cases described in the literature mainly differ in their approach for noise modelling (e.g. Yu et al., 2016a).

The problem of signal and noise wave separation is always relevant in a seismic data processing flow. Standard approaches use frequency and velocity filters to eliminate unwanted

components from the seismic data. These filters work without considering the spatial–temporal position of the noise, and they do not allow to identify the signal patterns. In response to this problem, various time–frequency decomposition techniques were developed, for instance, decomposition of a signal with redundant dictionaries consisting out of Gabor functions. Signal decomposition methods allow splitting the wavefield into waveforms, characterizing their frequency, amplitude and duration of oscillations in time (cf. Mallat and Zhang, 1993). These algorithms are applied in various areas, including noise reduction and filtering (Wawrzyniak, 2006; Ozbek et al., 2008; Wang, 2010; Ahmed, 2012; Chen et al., 2018).Nevertheless, there are only a few examples of signal decomposition with redundant dictionary techniques applied to the ringing noise problem.

Unlike previous works on the ringing noise problem (Yu et al., 2016a; Chen et al., 2019),we advocate here (1) applying atomic trace decomposition on raw strain data, (2) modelling of the ringing noise with an overcomplete Gabor atoms dictionary and, finally, (3) subtracting it from the signal. The hypothesis to test is whether localization and elimination of the noise before correlation prevents the smearing of the noise by the correlation process and therefore leads to better denoising and thus imaging results.

The matching pursuit (MP) algorithm is the successor of the class of algorithms called 'atomic decomposition'. We have used the MP code from the MP5 and Svarog projects (Kuś et al., 2013; The Svarog developers team, 2014; Durka et al., 2015; The Svarog developers team, 2016). The code is distributed under the GNU General Public License v3.0. The MP algorithm has four main steps:

1. Set the initial signal as a current residual of the decomposition.

2. Select the basic function (atom) which provides the maximum magnitude of the scalar product of the selected atom and the current residual of the signal. The selection process also includes the mechanism of the local readjustment to the local properties of the signal.

3. Calculate the new residual of the signal by subtracting the selected atom from the current residual.

4. Check the stop condition of the signal decomposition.

In the implemented algorithm, there are two scenarios of how the computation can stop. First, if the desired accuracy of the signal approximation is achieved, i.e. when the subselected atoms explain the pre-set percent of the signal's energy, the calculation stops. A second stop criterion is based on a reasonable runtime, implemented as a check for the maximum number of iterations, i.e. if the specified number of iterations is exceeded, then the decomposition process emergently stops. Usually, the valid number of iterations is determined experimentally for a particular type of signal and specific dictionary.

The reconstruction result of the original seismic trace is a linear combination of waveforms (atoms). The result of the processing is an ordered list of basic functions called 'atoms'. It starts from the atoms with the highest magnitude, with the highest influence, and goes down to the signal's weakest parts. They are characterized by specific parameters (modulus,

amplitude, position, scale, frequency, phase), which represent time–frequency properties of the corresponding waves.

The quality of decomposition was evaluated using the formula for cross-correlation (CC) between the original seismic trace and the reconstructed trace (Semnani et al., 2019):

$$CC = \frac{\sum_{n=1}^{N}(f(n) - \mu_f)(\hat{f}(n) - \mu_{\hat{f}})}{\sqrt{\sum_{n=1}^{N}(f(n) - \mu_f)}\sqrt{\sum_{n=1}^{N}(\hat{f}(n) - \mu_{\hat{f}})}} \tag{4.12}$$

where $f(n)$ is the original signal, $\hat{f}(n)$ denotes the reconstructed signal, μ_f and $\mu_{\hat{f}}$ represent the mean values of $f(n)$ and $\hat{f}(n)$ respectively, and N is the number of signal samples.

The main property of MP algorithms is the suboptimal selection of basic functions (atoms) from the dictionary. This property allows to run the algorithm and to get the result in an acceptable time. Such algorithms are called 'greedy'. At each step (iteration), only local optimization is performed. It is assumed that the final result will be optimal for specific practical goals. Suboptimal algorithms are applied in practice when there are no exact and efficient algorithms, or the existing algorithm has such complexity that, in general, a solution to a problem cannot be obtained in acceptable computation time.

The key advantages of this decomposition are the ability to perform a sparse representation of data and adapt to a specific signal. Nonlinear methods help find the optimal representation for a particular signal on the redundant set (called a dictionary) of the basic functions. The overall procedure is somewhat similar to the visual examination of the signal.

4.7.1 Decomposition results for the Groß Schönebeck data

We calculated the MPD of the whole vertical seismic profiling section for VP 10 from the Groß Schönebeck data set. For SEG-Y file reading we used the ObsPy 1.1.0 python library (Krischer et al., 2015; The ObsPy Development Team, 2017).

The process of ringing noise model construction could be described as follows:

1. Decomposition of each original distributed acoustic sensing (DAS) seismic trace to 80 atoms with pre-set 95% recovery of the original signal. A table with parameters (modulus, amplitude, position, scale, frequency, phase) for each atom is written to a separate csv file.

2. Checking the current trace for the resonance conditions (anomalous amplitude values in the recorded seismic trace):

    a. Determining a threshold value for the trace selection process. The threshold value is determined as a product of the mean value of the standard deviations for amplitude values of the original DAS trace in 500 milliseconds moving window and a multiplier.

    b. Compare the standard deviation for amplitude values of the current atom calculated in 500 ms moving window with the threshold value estimated during step a.

        – If the standard deviation of the current atom exceeds the threshold, then this trace will be used to define atoms selection for the noise model.

        – Otherwise, the trace is marked as 'clean' and further analysis is not required.

3. Calculate kernel density estimation (KDE) for frequency values of atoms (Waskom et al., 2017).

4. Find peak on KDE. A search of the peaks could be regulated through adjusting the prominence parameter.

5. Select all atoms which have frequency parameters falling into the interval (peak frequency -2.5 Hz, peak frequency +2.5 Hz).

Computations are performed for each trace independently, and hence, computations could be easily performed parallelly, increasing the total processing speed.

After analysing the original seismic DAS traces and the atoms of decomposition results, we generated a model of the ringing noise, which we could use for data denoising (Figure 4.9). Compared with the original data (Figure 4.9a; with standard pre-processing consisting of vertical stacking, correlation with the pilot sweep and subsequent differentiation applied), we observe that amplitude and phase of the modelled ringing noise (Figure 4.9b) accurately reconstruct the noise. The created noise model was subtracted from the original raw strain data, and the same preprocessing flow was applied to the seismic section (Figure 4.9c). A closer zoom clearly shows an improvement of the seismic section after denoising (Figure 4.10). Noise has been mostly eliminated (Figure 4.10b, d, f and h). Nevertheless, in some parts of the data, we see small residuals. At a depth interval around 719 m (Figure 4.10b), the first-break arrival was already significantly corrupted, and the noise model was unable to correct for this effect. In some cases, the noise model does not include ringing signals with a lower amplitude due to the threshold parameter so that it leads to a low-amplitude residual, for instance around depth 3138 m (Figure 4.10f).

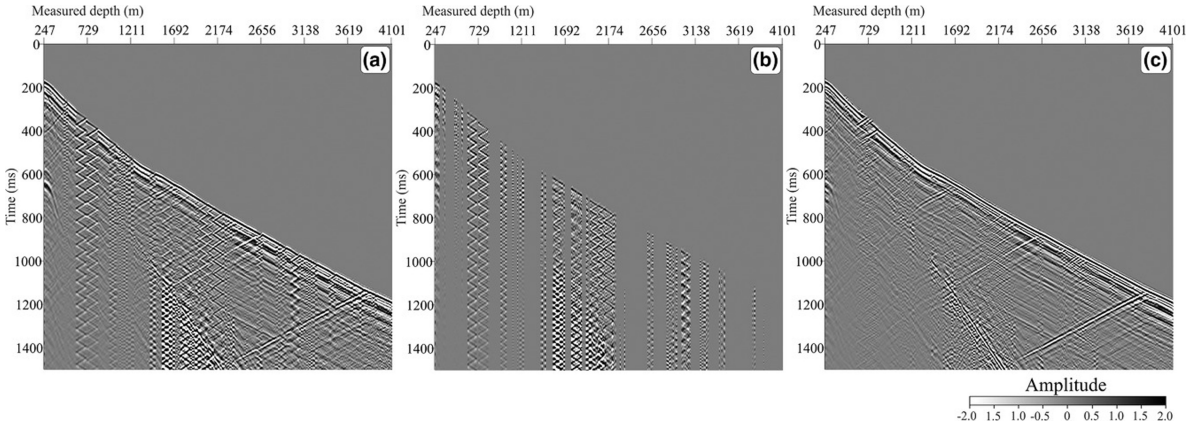

Figure 4.9: Comparison of measured and processed common source gather: (a) before denoising (same as in Fig. 8a); (b) MPD noise model; (c) after noise model subtraction.

At the depth level of 1200 m, there is a DAS strain trace, which contains a high amount of the studied high-frequent noise (Figure 4.11a). After subtraction of the noise model (Figure 4.11b), the main part of the ringing noise was eliminated. The overall shape of the cleaned DAS seismic trace revealed different characteristics (Figure 4.11c). The areas where we see the change of the seismic trace character are located at those places where we had the maximums on the ringing noise model. For instance, between 5 and 10 s and 15 and 20 s, we see a lowering of the amplitude values and a change of the envelope of the seismic signal. The

highest amplitude occurs now at 16.122 s and is 0.33, which is 3.3 times lower than the highest amplitude of the original trace. Thereby, the processed DAS trace also becomes more similar to the accelerometer trace (Figure 4.11d).

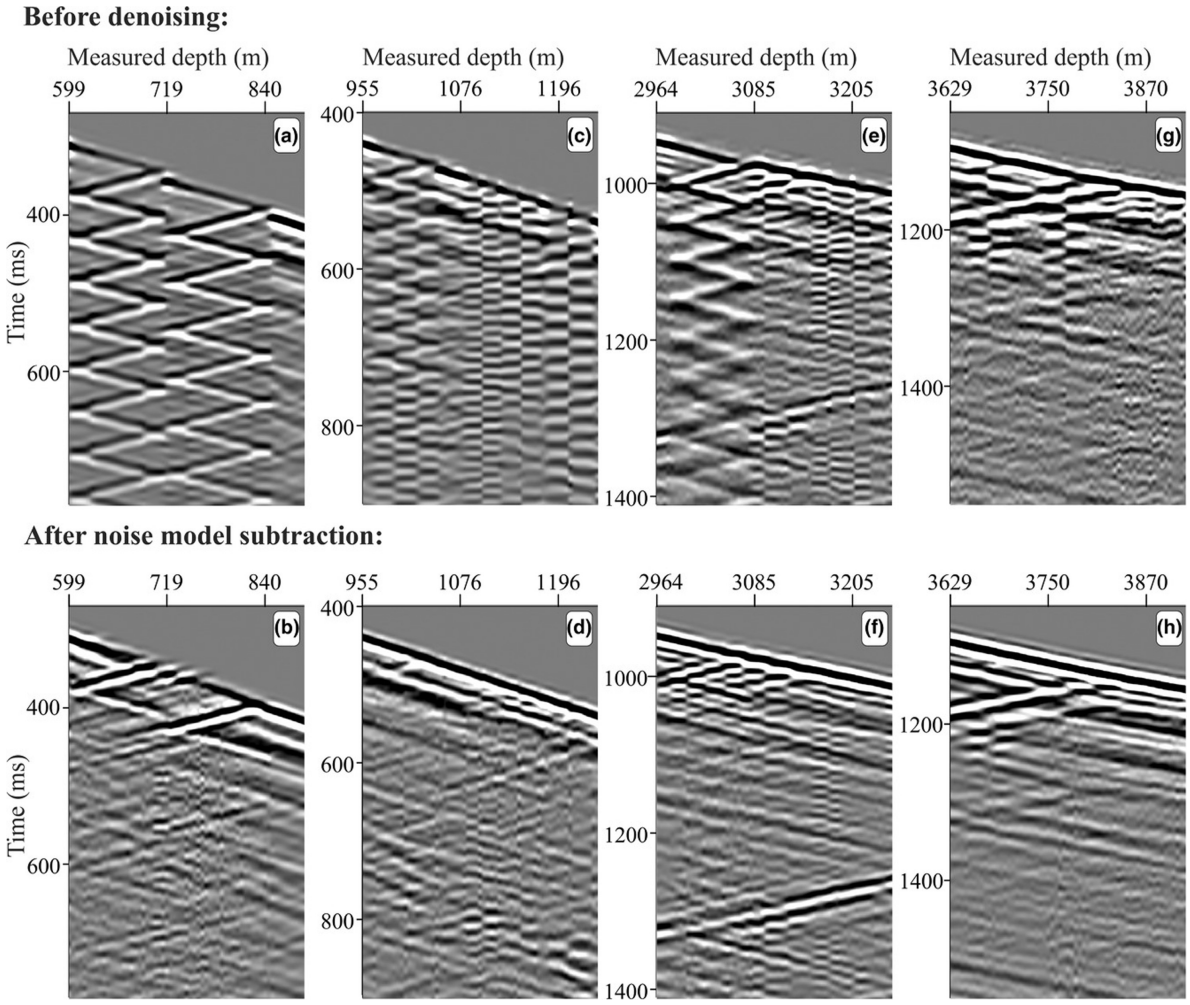

Figure 4.10: Zoom of the seismic sections shown in Figure 9(a and c). Four upper panels (a, c, e, g) show four different parts of the seismic section after preprocessing, and the four lower panels (b, d, f, h) after additional MPD denoising.

This amplitude and waveform behaviour can be further analysed by calculating FT spectra (Figure 4.12). The propagation of the sweep energy from 10 Hz up to 88 Hz at the depth level of 1200 mMD is clearly recognizable in the unprocessed DAS trace (Figure 4.12a), containing strong disturbing signals that are revealed by ringing noise modelling (Figure 4.12b). Around 45 Hz, there are distinct oval-shaped, smeared high-amplitude areas appearing at 2.3, 4.3, 7.7 and 18 s. These are resonances that were reproduced accurately. After denoising, the strong amplitudes at 45 Hz were significantly lowered down in the resulting DAS trace (Figure 4.12c). Now we see the contributions from other frequencies to the signal more prominently, even a much smaller resonance at approximately 90 Hz. These peaks do not appear in our noise model, but they lie outside of the sweep range and will be filtered out by the correlation process. The strong continuous energy band around 45 Hz corresponds to the natural frequency of the vibrating cable interval. In other words, this is a frequency at which this part of the cable tends to oscillate without the influence of an external force.

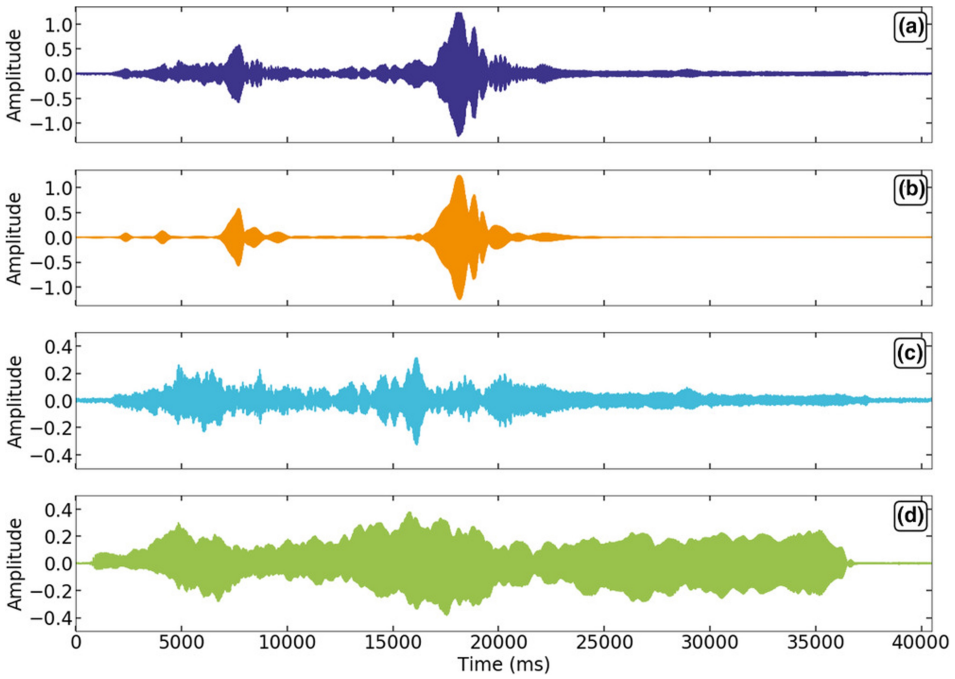

Figure 4.11: Comparison of measured and denoised DAS strain traces (depth level: 1200 m MD): (a) uncorrelated original trace, (b) modelled ringing noise, (c) trace after noise subtraction and (d) corresponding accelerometer point tool trace.

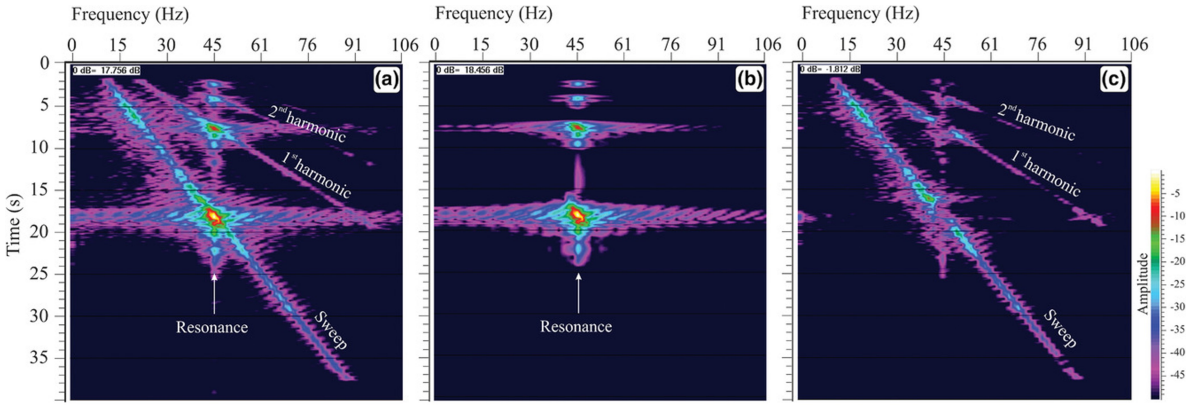

Figure 4.12: FT spectrum comparisons of DAS strain trace before and after noise subtraction (depth level: 1200 m MD). FT spectrum of (a) raw trace, (b) MPD noise model and (c) trace after noise model subtraction.

In order to get a better understanding of our denoising results, we inspected amplitude-frequency spectra of the same DAS trace after preprocessing and compared it with reference measurements. The DAS trace spectrum before noise suppression has a distinct resonance peak at around 45 Hz (Figure 4.13a). The selected Gabor atoms for the ringing noise model accurately mimic the shape of this peak. Consequently, the DAS spectrum after denoising process follows the shape of the original spectrum, except for the narrow range around the resonating frequency, which influence was lowered down. It should be noticed that the spectrum of the VSI tool measurements has greater levels for higher frequencies in comparison with the DAS trace spectrum, most likely due to the filtering effect of the GL frequency response. In the time domain (Figure 4.13b), we can also observe a significant improvement in terms of ringing noise elimination. The original DAS trace at 1200 m is strongly affected by ringing

noise. After the first-break arrival around 520 ms, we only see a sinusoidal noise pattern, but after ringing noise subtraction the DAS trace starts to resemble the VSI trace.

4.8 Cable coupling improvement methods

Processing-based solutions are always limited by quality of the initially recorded data. A certain percentage of the energy emitted by vibrators is converted into standing waves on the wireline cable, which reduces the S/N ratio. By reducing vibrations of the cable, either the problem of the ringing noise could be avoided completely or the influence of it on the data can be significantly reduced.

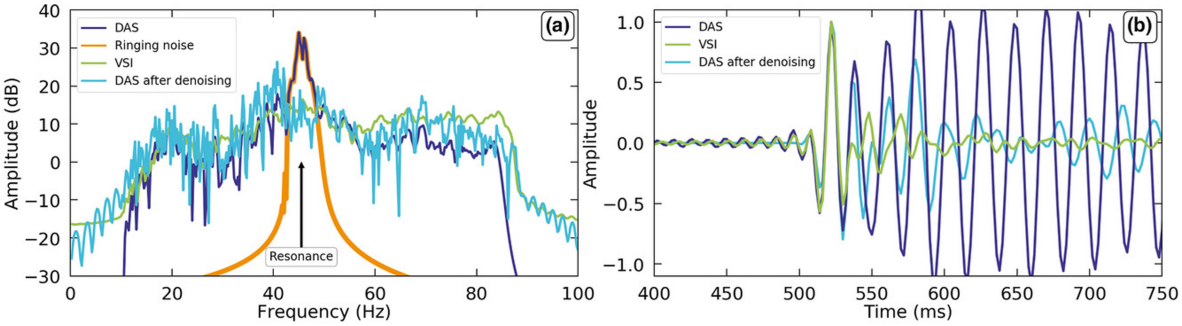

Figure 4.13: Comparison of DAS and accelerometer point tool traces (VSI). The preprocessing applied to all data sets comprised vertical stacking, correlation with the pilot sweep and subsequent differentiation; depth level is 1200mMD. (a) Amplitude spectrum for DAS trace before denoising (moderate dark blue solid curve), for DAS trace after ringing noise model subtraction (light blue solid curve), for ringing noise model (solid orange curve) and accelerometer point tool (light green solid curve). (b) Comparison of a 350 ms fragment of the DAS trace before and after denoising with accelerometer point tool measurements (same colour-coding as in a).

Noise caused by cable reverberations is common in engineering (e.g. reverberations of power lines caused by wind) and geoscience (e.g. vortex noise due to marine cable towing behind the vessel) communities. In marine seismics, the problem is settled by the usage of cable fairings (Every et al., 1982; Niedzwecki and Fang, 2013) that reduce water strumming and improve the quality of data acquisition. Munn et al. (2017) have demonstrated an enhancement of data quality in borehole surveys through an improved cable coupling. It was achieved by the application of a flexible liner, which presses the cable against the borehole wall. This installation is limited mainly to shallow boreholes with depths of 425 m or less. Constantinou et al. (2016) and Schilke et al. (2016, 2017) have described the idea that by adding slack to the wireline cable, one could create a twisting of the cable, and as a result, improve the coupling and decrease the noise amount in the data.

During the first day of acquisition in Groß Schönebeck, we conducted several start-up tests, which also included a slack test (Henninges et al., 2021a). We have collected four data sets for E GrSk 3/90 with 1, 5, 11 and 20 m slack applied to the cable. The data acquisition was performed with a 36 s long linear sweep 10–88 Hz and ten sweep repetitions. Figure 4.14 shows a comparison of these four data sets with some preprocessing applied (diversity stack, correlation with the pilot sweep, time differentiation).

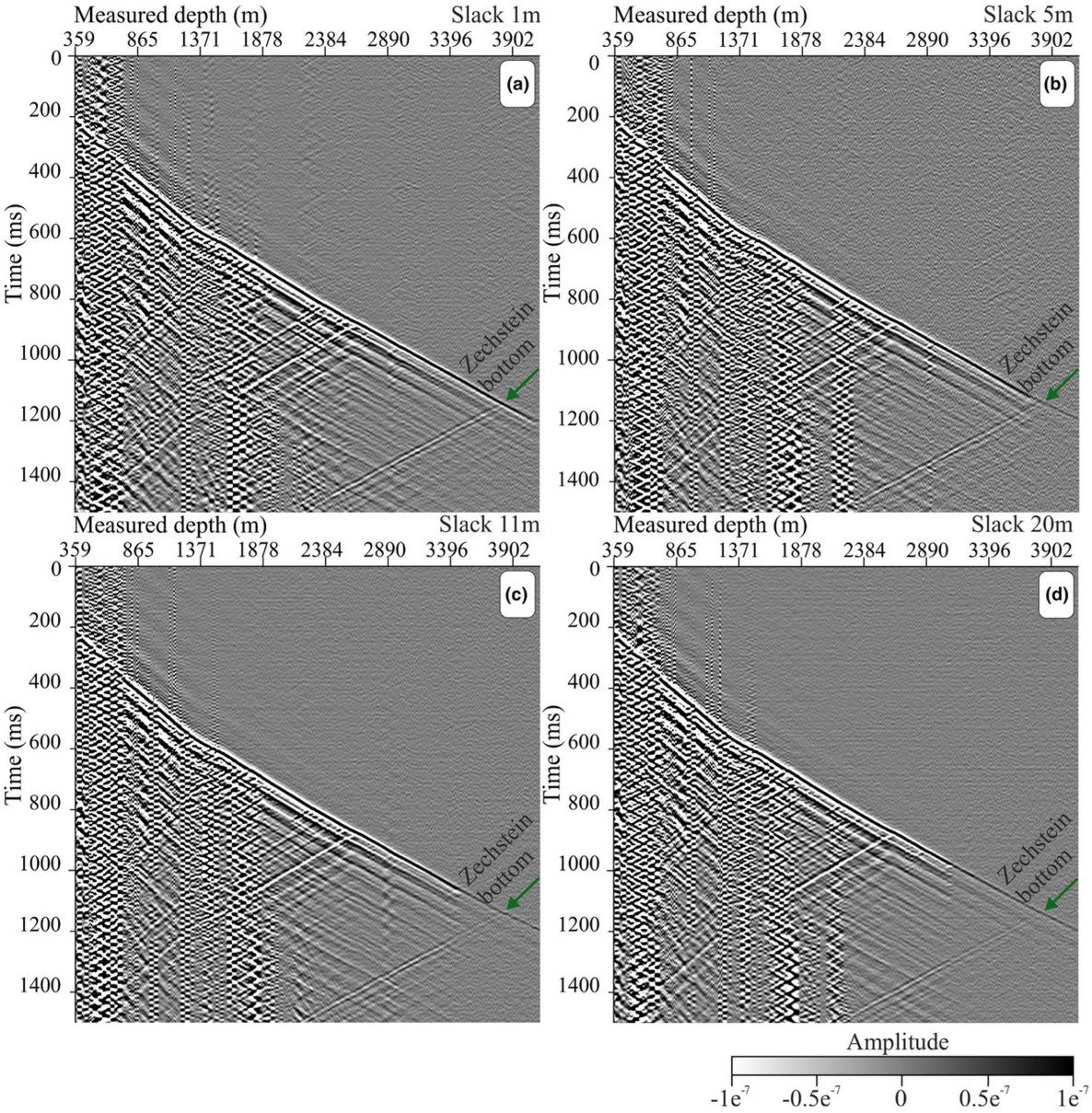

Figure 4.14: Comparison of common source gathers recorded for VP10 in E GrSk 3/90 well and acquired with different cable slacks: (a) 1 m, (b) 5 m, (c) 11 m and (d) 20 m slack. Green arrows on seismograms annotate position of Zechstein salt bottom reflection.

We cannot observe significant changes in the ringing noise distribution, although there is a certain improvement, for example at 1878–2384 m depth between the 5 m and 11 m slack tests data sets (see Figures 4.14b and c). After increasing the slack due to cable redistribution, the coupling in this area was probably improved. Nevertheless, the data set with 20 m slack shows some ringing again in the same depth range (cf. Figure 4.14d). The ringing noise between 2760 and 3016 m shows similar behaviour. However, the noise zone at approximately 2890 m MD is significantly decreased when 20 m cable slack was applied (Figure 4.14d), in comparison with the recording of the same depth interval using 1, 5 and 11 m slack (Figure 4.14a–c).

After increasing the slack, we have also noticed a dropping of the amplitude level from first arrivals close to the zone with reduced ringing signals (cf. Henninges et al., 2021a) and Zechstein bottom reflections (see Figure 4.14, green arrows) in the deeper part of the seismic section. Since the experiment was focused mainly on depths greater than 3700 m, we tuned

the best possible cable performance for this range. Therefore, after analysing the start-up test results, we continued the experiment with almost full tension applied to the cable.

4.9 Discussion

4.9.1 Comparison of processing-based methods

During the past years, there has been considerable interest in finding the appropriate approach to decrease ringing noise in wireline distributed acoustic sensing (DAS) data and clean the spectrum. A technical solution which will allow achieving a better cable coupling during the data acquisition is preferable. However, the improvement of the cable coupling during wireline acquisition remains a nontrivial process. Moreover, the results of the slack tests conducted at Groß Schönebeck showed that the suggested modifications of the current acquisition techniques such as lowering of extra cable to the borehole can lead to a decrease of the noise and the reflection signals. The observed reduction of the S/N ratio in the region of cable accumulation is consistent with the results of the experiment described by Constantinou et al. (2016) for the data set acquired at Rittershoffen, France, and should be further investigated. Therefore, taking into account the mentioned technical limitations, in the present study, we concentrate on the processing-based solutions and demonstrate several ways of tackling the ringing noise problem for the data acquired at the Groß Schönebeck geothermal site.

The comparison of the methods used for data denoising in this study is shown in Figure 4.15. A significant part of the observed noise (for example, at depth interval 1211–2656 m in Figure 4.15a) is suppressed after TFD noise rejection (Figure 4.15b). Similar noise reduction results are obtained by applying the Burg adaptive deconvolution, seen in Figure 4.15(c). Finally, yet importantly, our newly shaped and denoising method based on matching pursuit decomposition (MPD) with Gabor atoms clearly outperforms previous denoising results (Figure 4.15d). However, there are certain differences and limitations for the application of the techniques that we discuss here.

The *TFD noise rejection* is a well-known standard processing instrument, which is available in many professional software packages (e.g. Promax (Halliburton), Omega (Schlumberger), Geovation (CGG)). It is used for elimination of various noise types of different nature in seismic data such as ground roll, swell noise, wind noise etc. The process will improve a seismic record successfully, as long as the noise and the signal have different amplitude and frequency characteristics. In the case of similar characteristics, a reduction of the filter amplitude threshold will lead to noise elimination and to signal degradation at the same time. The application of the TFD is a more advanced way of data filtering in comparison with a median filter approach used by Bakku et al. (2014) for gas exploration and a simple notch filter applied in Miller et al. (2012) at the Devine test site in an active oil and gas province. In practice, accurately tuned frequency sub-bands selection criterion in TFD allows performing more accurate filtering in the frequency band of the data. Moreover, the use of the information from the adjacent traces makes the process of the ringing noise elimination more robust and minimizes the waveform distortion after filtration. Altogether, the TFD method gives a quick and reasonable result with relatively low computational cost.

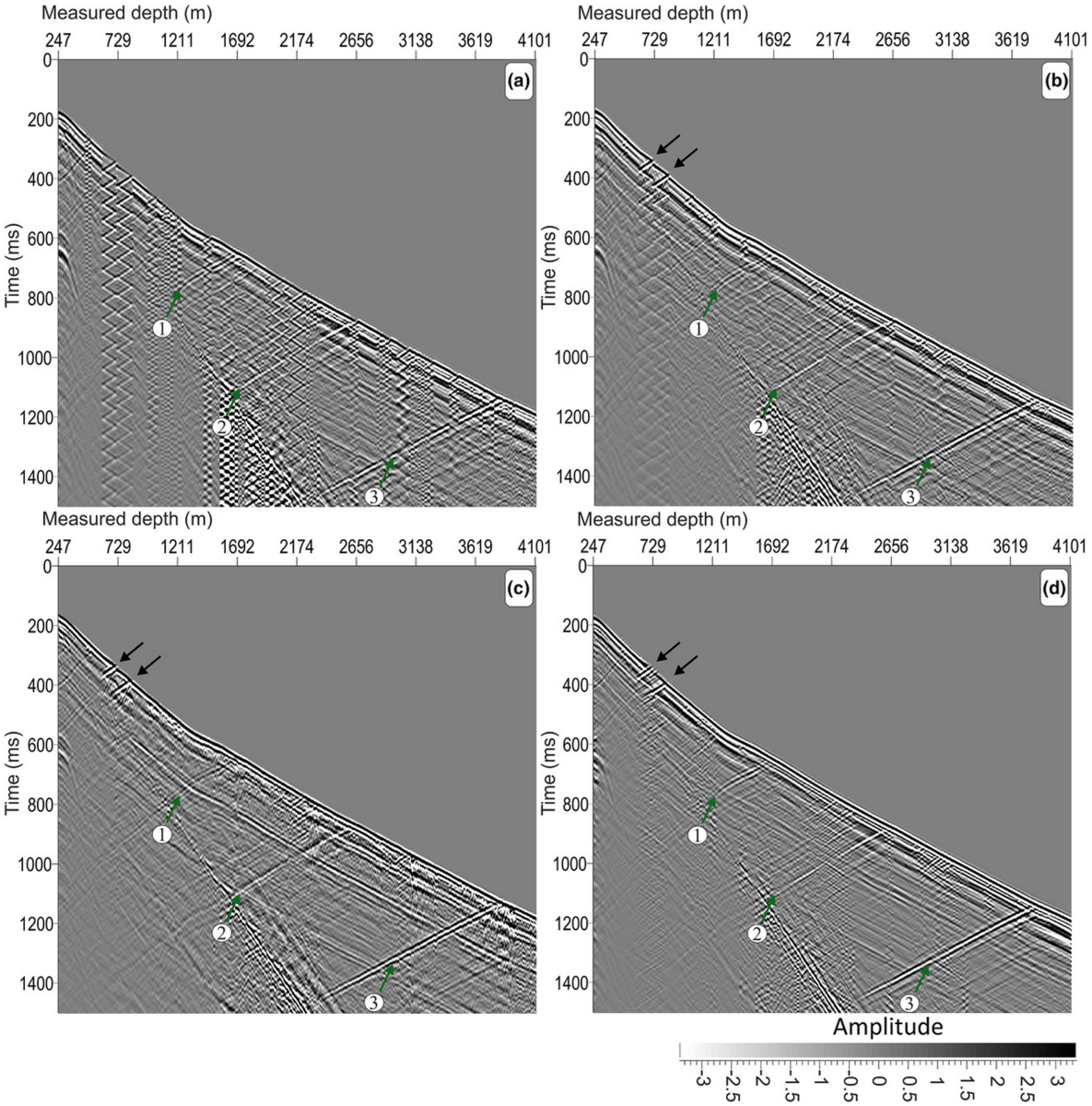

Figure 4.15: Comparison of the effect of different processing methods applied for ringing noise elimination. Common source gathers (a) before denoising, (b) after time–frequency domain noise attenuation, (c) after Burg adaptive deconvolution, d) after noise subtraction based on signal decomposition with Gabor atoms. Applied preprocessing consisted of vertical stacking, correlation with the pilot sweep and subsequent differentiation. Moderate coherency enhancement was additionally applied post-processing with methods b, c and d. In all panels, green arrows indicate reflections at different depth levels. In all panels, green arrows with numbers on seismograms mark positions of the main reflectors at different depth levels: 1, Buntsandstein; 2, Zechstein top; 3, Zechstein bottom. Black arrows mark example of depth levels with residual ringing noise.

For the Groß Schönebeck data, TFD noise rejection allowed to suppress quite a substantial part of the ringing noise. There are different depth levels with good (see 1211–1692 m; Fig. 15b) and reasonable noise suppression (for instance, 1933–2656 m; Figure 4.15b). Although the signal-to-noise ratio of the seismic section after TFD processing has been improved, there are however still some areas with residual noise with decreased amplitude (for example 2897–3379 m depth interval in Figure 4.15b) and one interval with particularly high noise residuals and distorted first-break arrivals (see black arrows in Figure 4.15b).

The application of the *Burg adaptive deconvolution* is also a quick and efficient tool for the ringing noise problem. This powerful spectral balancer has several advantages: good results can be achieved even with a general mixed-phase wavelet if the beginning of the wavelet rises sharply and the reflection coefficients are not assumed to be quite randomly distributed. The adaptive approach also takes account of wavelets that are varying with time. The main drawback of the technique is its sensitivity to high-frequency noise, which will be often amplified. Therefore, careful amplitude balancing of the data is required before application of the Burg adaptive deconvolution approach.

Most recently, Willis et al. (2020) have developed another statistical approach for ringing noise elimination based on the analysis of the noise periodicity and gap deconvolution. The identification of the ringing noise period is based on the identification of the X-like pattern on adjacent autocorrelated traces. The main difference with Burg adaptive deconvolution is that adaptive operators are replaced by prediction and adaptive subtraction. Burg adaptive deconvolution performs general equalization of the spectrum. It works without any prior information, while the application of the gap deconvolution in the approach of Willis et al. (2020) requires the knowledge of the noise period. If evaluated prediction distance is not accurate, this can lead to errors in ringing noise multiple reflections, yielding distortions and leaving the residual noise energy behind. However, since both cable reverberation inside the borehole and ghost wave generation in marine seismics represent a standing wave phenomenon, the application of classical deghosting filters for source ghost elimination (Song et al., 2015; Wang, 2010) would also be a valid option for DAS data denoising. The proposed method for the ringing noise period evaluation by Willis et al. (2020) can be used for calculations of the deghosting filters.

After application of the Burg method to the Groß-Schönebeck data, almost all ringing noise is omitted with small exceptions at some depth levels (for example, see black arrows in Figure 4.15c). Nonetheless, the Burg result has some signal distortions associated with deconvolution in the areas of ringing noise residuals, for instance, at 2318 and 3138 m depth. In general, adaptive deconvolution considerably improved the denoising results in comparison with the TFD method here.

As a new approach, we calculated a noise model based on the results of *MPD with Gabor atoms* and subtracted it to clean the DAS data (Figure 4.15d). The method of trace decomposition allows in principle to separate the noise and the signal, even for the case when they are overlapping both in time and frequency domains. Thus, this processing technique is a powerful tool, which in combination with the physical understanding behind the noise generation process, allows to perform a sophisticated data analysis and significantly improve signal quality. However, the average computation time is estimated approximately three times higher than for TFD and Burg adaptive deconvolution.

The application of MPD for coupling noise elimination can be attributed to the group of methods which attempt to use different ways of modelling for denoising purposes. The first work in this direction was published by Yu et al. (2016a). Although the authors have demonstrated the successful application of their method on the real field data, the proposed DAS coupling noise suppression requires the estimation of the noise attenuation characteristics, which might be challenging.

Algorithms based on sparse optimization decomposition can handle uncertainties such as amplitude fitting and consider changes of the coupling noise characteristics between the different zones of the well where the cable exhibits oscillation motion. Such decomposition method has been employed by Chen et al. (2019). Based on the morphological analysis of the DAS data characteristics, the authors propose using the continuous wavelet transform and the discrete cosine transform as the sparse dictionaries to represent signal and coupling noise, respectively. Arriving from a synthetic example to field data, Chen et al. (2019) emphasize that decomposition of the complex seismic response is a nontrivial process and requires a combination of the overcomplete dictionaries. To simplify this step, in our work, we came up with an idea of applying a single overcomplete dictionary based on the Gabor basic functions (atoms). The proposed dictionary is commonly used for seismic waveform representations and is easy to handle. Tests performed on the Groß Schönebeck field data demonstrate promising results. However, the application of overcomplete types of dictionaries should be further investigated in the future.

The use of MPD improves ringing noise detection and suppression and therefore increases the overall reflection coherency in the data. Thus, MPD with Gabor atoms has the best potential in terms of applicability for ringing noise elimination in wireline DAS data. The visual interpretability of the seismic reflections, marked by green arrows in Figure 15, increases gradually from Figure 4.15(a to d). Nevertheless, there are also some noise residuals after MPD at the similar depth regions as in the Burg adaptive deconvolution result (Figure 4.15c and d; black arrows). The distortion of the initially recorded strain data in these parts of the seismic record was already quite significant. Therefore, MPD, as well as Burg's method, is not able to restore it. Overall, accurate data analysis and the application of the proper denoising method allowed to increase data quality significantly. As a result, the corridor stacks (Henninges et al., 2021a) and the vertical seismic profiling imaging results at the Groß Schönebeck site were improved.

4.9.2 Effect of velocity on data acquisition

Overall, after analysis of our denoising test results, we can conclude that there is still a valid signal below the noise but depending on the number of peaks and notches (cf. Figure 4.6), the useful part of the signal might also be decreased. The efficiency of the coupling noise removal from the data depends on difference between noise and signal characteristics, in particular on the velocity values for fibre optic cables and velocity of the formation. The estimation of the standing wave velocity can be easily derived from 4.1:

$$V = \frac{f_n 2L}{n} \tag{4.13}$$

where n is the integer harmonic number, fn is the the frequency of the nth harmonic, L is the length of the theoretical string, which is equal to the length of the noisy interval in the data. However, we must keep in mind that this simple calculation can be used only for velocity estimation because it does not account for the cable tension. Also, the gauge length smears up the zone of the noise.

An average velocity of the noise for the presented data set is approximately equal 4400 m/s, which is close to values typical for fibre optic cables (ca. 5000 m/s; Raisutis et al., 2016). Chang and Nakata (2020) report similar values of the noise velocities at the Brady geothermal field.

In the Groß Schönebeck case, the local reservoir rock led to very uniform reflection dips for both the ringing noise and the seismic reflections. Consequently, the denoising method is sometimes not able to suppress ringing noise entirely in case of reflections with similar slope lying under the noise; this prevents the algorithm from distinguishing between noise and signal. Therefore, a possible overlap of reflection and ringing noise should already be considered during planning and interpretation.

4.10 Conclusion

Wireline distributed acoustic sensing still has limitations during field measurements that cannot entirely be overcome by subsequent processing. However, since fibre optic methods develop rapidly, the problem of coupling noise should be further tackled also during the development of field acquisition tools.

The presented new denoising method based on a matching pursuit decomposition with Gabor atoms adds to the approaches for the elimination of ringing noise. It especially allows the separation of signal and ringing of the cable and effectively stabilizes data interpretation even if those are superimposed. This finally increases the resolution and helps to assess small-scale effects during exploration, not only for geothermal energy.

4.11 Acknowledgements

The research project RissDom-A is funded by the German Federal Ministry of Economic Affairs and Energy (grant 0324065). We would like to thank all contractors involved in acquisition and processing and to acknowledge Ernst Huenges for the establishment of research activities at the Groß Schönebeck in-situ geothermal laboratory. Additionally, the authors thank the editor Dr Noalwenn Dubos-Sallée, the associate editor Hervé Chauris and three anonymous reviewers for their comments and suggestions that helped to improve the paper.

5

Imaging of the reservoir

This chapter describes the 3D DAS VSP workflow adapted for the Groß Schönebeck dataset and shows the imaging results. The resulting cube is compared to the 3D surface seismics. Important interpretation features are evaluated, and the application of this additional information for reservoir exploitation in terms of geothermal energy production is demonstrated. Furthermore, the acquired knowledge has potential implications for future geothermal exploration in general.

3D deep geothermal reservoir imaging with wireline distributed acoustic sensing in two boreholes.

Evgeniia Martuganova[1,2], Manfred Stiller[1], Ben Norden[1], Jan Henninges[1,3] and Charlotte M. Krawczyk[1,2]

[1]Helmholtz Centre Potsdam, GFZ German Research Centre for Geosciences, 14473 Potsdam, Germany

[2]Department of Applied Geophysics, Technische Universität Berlin, 10587 Berlin, Germany

[3]Federal Office for the Safety of Nuclear Waste Management (BASE), 10623 Berlin, Germany

Article is under review in *Solid Earth* [preprint with additional modifications]

5.1 Abstract

Geothermal exploration will help moving towards a low-carbon economy and provide a basis for green and sustainable growth. The development of new practical, reliable methods for geophysical characterisation of a reservoir has the potential to facilitate a broader application of deep geothermal energy. At the Groß Schönebeck in-situ laboratory, a unique vertical seismic profiling (VSP) dataset was recorded in two 4.3 km deep geothermal boreholes using fibre optic cables in early 2017. The experiment set-up consisted of 61 vibrator points organised in a spiral pattern around the well site to ensure a proper offset and azimuth distribution in the target reservoir section. Data were processed using a standard workflow for VSP. As a result, a detailed 3-dimensional 0.75 x 1 x 4.5 km size image around the existing boreholes was created using the Kirchhoff migration algorithm with restricted aperture. The imaging resolved

small-scale features in the reservoir essential for the future exploration of the geothermal research site. Borehole data with vertical resolution up to 16 m revealed the existing depth variations of the Elbe reservoir sandstone horizon at 4.08 - 4.10 km depth and indications of an unconformity in the area where we expect volcanic rocks. In addition, in the borehole data a complex interlaying with numerous pinch outs in the Upper Rotliegend reservoir section (3.8 to 4 km depth) was discovered. Thereby, we demonstrate that wireline fibre optic data can significantly contribute to exploration by providing an efficient and reliable method for deep geothermal reservoir imaging.

5.2 Introduction

Measurements with a fibre-optic cable installed in diverse environments are widely applied for seismic data acquisition for versatile research topics such as urban seismology (Dou et al., 2017; Spica et al., 2020b; Yuan et al., 2020), glacial studies (Booth et al., 2020; Brisbourne et al., 2021; Hudson et al., 2021), geothermal exploration (Li and Zhan, 2018; Lellouch et al., 2021), volcanology (Nishimura et al., 2021) and underwater seismology (Lior et al., 2021; Spica et al., 2020a). Perhaps, one of the most well-studied distributed acoustic sensing (DAS) applications is cable deployment for data acquisition in boreholes. Measurements with a fibre-optic cable installed along the casing or behind the tubing are widely and successfully applied for borehole seismic data acquisition. 3D vertical seismic profiling (VSP) imaging results with permanent cable installation include applications for oil and gas exploration (Jiang et al., 2016; Shultz and Simmons, 2019; Zhan and Nahm, 2020), the monitoring of CO_2 reservoirs (Humphries et al., 2015; Götz et al., 2018; Correa et al., 2019; Wilson et al., 2021), and for mineral exploration and mining (Bellefleur et al., 2020).

Nevertheless, in a vast number of already drilled boreholes, only measurements with a wireline logging cable are feasible. Surveys with wireline installation, such as the dataset collected for petroleum exploration in China, near Tangshan, Hebei (Yu et al., 2016a), are still quite unique and rarely found in the literature.

For geothermal exploration, a very limited number of wireline DAS with active seismic source was applied (Miller et al., 2018; Henninges et al., 2021a). Data acquisition in a harsh environment, such as elevated temperatures, poses additional challenges in terms of the requirements for the instrumentation. Using optical cables, a detailed image of the subsurface can be created, using, for instance, seismic imaging techniques (Krawczyk, 2021). In addition, the deployment is more efficient in terms of time and costs, in comparison with a standard installation of conventional borehole instruments. Therefore, data collection with an application of fibre optics technology can provide a reliable and efficient method for exploring and monitoring geothermal reservoirs. This paper presents results from one of the first applications of DAS VSP for deep geothermal exploration at the Groß Schönebeck geothermal research site down to 4 km depth.

5.3 The Groß Schönebeck site

The in-situ laboratory Groß Schönebeck is located in the Northern German Basin, one of Germany's main regions with deep hydrothermal resources. The joint research project RissDom-

A (RissDominierte Erschließung in German: fracture-dominated exploitation) aims to gain expertise in sustainable energy production from low permeability geothermal reservoirs by developing Enhanced Geothermal Systems (EGSs). The Buntsandstein sandstone formation and volcanic rocks of Lower Permian (Rotliegend) (Figure 5.1a) age are of interest for the direct use for the geothermal energy production (Blöcher et al., 2016). A successful geothermal exploration case study can lead to broader geothermal energy usage in the regions without hydrothermal potential. Moreover, the geological setting at the experiment site is typical for a broad part of Northern Europe. Therefore, the acquired knowledge from this case study can be applied to geothermal exploration programs in other areas with similar geological conditions.

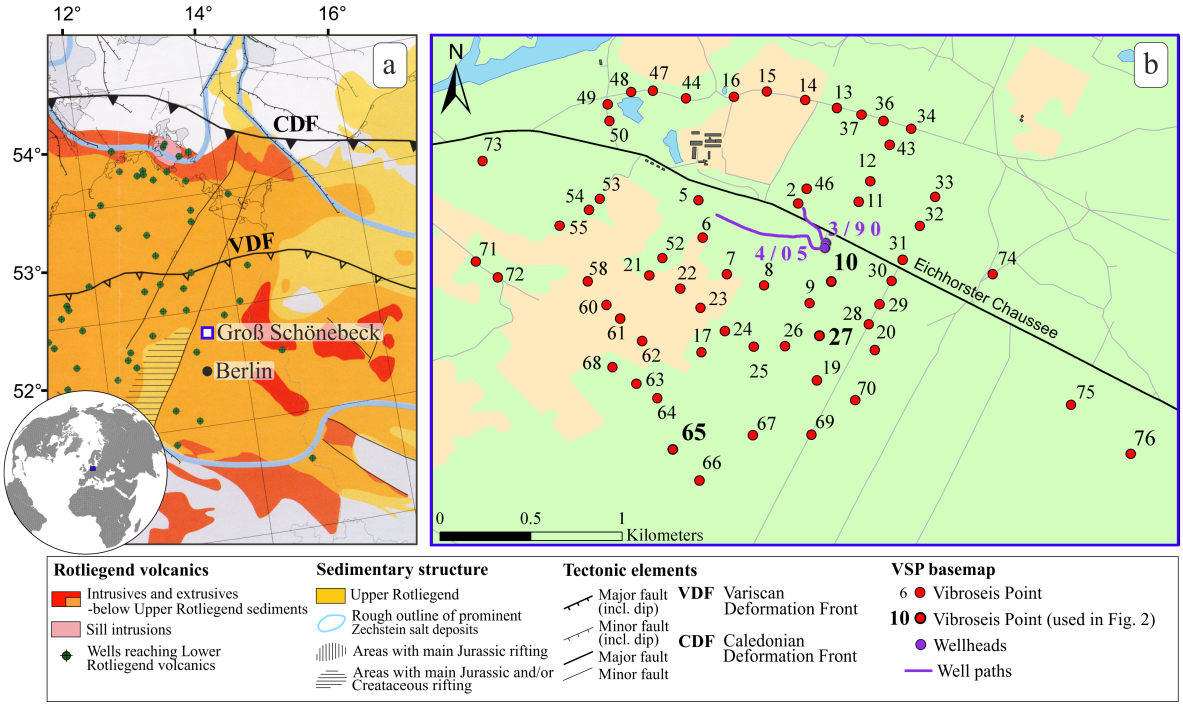

Figure 5.1: Location of the Groß Schönebeck geothermal site. (a) Rotliegend volcanics and sedimentary distribution in the Southern Permian Basin (compilation from Krawczyk et al. (2019)). (b) Base map of the Groß Schönebeck geothermal site with two boreholes (violet circles) in the centre and 61 VSP source points (red dots) arranged in a spiral pattern around.

To deepen the understanding of the geological structures interpreted on sparse vintage 2D seismic lines and locate possible faults within the area of interest, a high-resolution 3D reflection seismics acquisition campaign was carried out in February/March 2017 (Stiller et al., 2018; Krawczyk et al., 2019). The 3D surface seismic survey was designed to cover an area of 8 km by 8 km, focusing on target reservoir depth from 4 to 4.3 km. Since the studied geothermal reservoir zone is located at a depth greater than 4 km and overlaid by Zechstein salt, it is a challenging target for exploration with conventional seismic methods.

5.3.1 The distributed acoustic sensing vertical seismic profiling survey

In contrast to surface seismics, VSP has the advantage of shorter reflection travel paths. Therefore, the amplitudes are theoretically less subjected to attenuation. As a result, this provides a better signal-to-noise ratio and broader frequency content. Thus, to improve the resolution of seismic data, which is limited due to the thick salt layer (more than 1 km),

and to provide detailed imaging around the existing boreholes, an extensive VSP experiment using wireline DAS technology was conducted prior the main surface seismic experiment in February 2017. Two wireline hybrid cables (electrical and optical; from SLB (NOVA-F) and GFZ (Rochester)) (Henninges et al., 2011) were temporarily deployed inside the casing of two deep water-filled boreholes. Nearly vertical well E GrSk 3/90 (maximum inclination 7.2°), which was formerly used for oil and gas exploration, and Gt GrSk 4/05 (maximum inclination 49°) form a geothermal doublet (Figure 5.1b). Two hDVS (heterodyne distributed vibration sensing) interrogator units from Schlumberger were connected to single-mode fibres and used to record the strain along the boreholes with 5 m spatial sampling. A 20-m gauge length was used for data recordings in the field. Later, this value was adjusted to 40 m for E GrSk 3/90 according to the velocity profile in the reservoir section to get an optimal S/N ratio and preserve data resolution (Dean et al., 2017). Data recorded in Gt GrSk 4/05 were used with only 20-m gauge length due to the loss of the raw fibre optical data.

The measuring campaign consisted of 1 start-up testing and 3 data acquisition days in total. The 61 vibrator source points (VPs) had a spiral layout around the target area with varying offsets from 188 to 2036 m around the boreholes to ensure a good azimuth distribution (Figure 5.1b). As seismic source, four heavy Mertz M12 Hemi 48 vibroseis trucks were used with a peak force of 200 kN (45100 Lbf) each. All source units vibrated simultaneously at each VP location and guaranteed an average vertical stacking fold of 16 per source location. A linear sweep of 10 – 112 Hz and 36 s length was used for data acquisition. Several VPs with larger offsets, were recorded using a sweep from 10 to 96 Hz.

Due to the cable failure in Gt GrSk 4/05, the recording of the last 500 m in the reservoir section was lost, and the maximum surveyed depth is limited to 3716 m measured depth (MD). Moreover, we were only able to record 18 VPs from the originally planned 61 because the cable was retrieved from the borehole after only 1 day of acquisition. This event led to significantly reduced subsurface coverage of the survey design between the two wells. In E GrSk 3/90, we recorded the planned 61 VPs and the maximum surveyed depth is at 4251 m MD. Nevertheless, recorded datasets from this borehole have inconsistent amplitudes caused by unknown reasons, which requires further investigations (Henninges et al., 2021a).

Overall, all mentioned details make this dataset acquired at the Groß Schönebeck geothermal research site very challenging for data processing. We will focus on the processing flow in the next section of the paper, which we used to successfully identify reservoir details.

5.4 Data processing

For the 3D DAS VSP dataset a processing flow containing typical elements was adapted to the Groß Schönebeck survey specifics and then applied to the data (see Table 5.1). The major steps and parameters details are discussed in the following sub chapters.

5.4.1 Data preconditioning

As first step the proper geometry was assigned to the raw uncorrelated data, which included source and receiver coordinates, elevations and true vertical depths calculated using boreholes trajectories.

Table 5.1: 3D DAS VSP data processing flow.

Processing step	Description and parameters
Geometry input	Source and receiver coordinates, depths
Trimmed mean stack	Suppression of impulsive noise
Ringing noise suppression	Matching pursuit decomposition (MPD) with Gabor atoms
Correlation with pilot sweep	10 - 112 Hz, 10 - 96 Hz, 36 s, 360 ms taper
Conversion to strain rate	Time derivative
First arrival time picking	The peak of the direct downgoing P-wave
Amplitude corrections	Spherical divergence compensation ($t^{1.5}$) and lateral equalisation
Data enhancement	Moderate wavefield enhancement
Velocity model building	Migration velocities from 3D surface seismics and sonic log from E GrSk 3/90 as initial velocity model, checked and optimised by ray tracing
Ray tracing	Mapping of the reflectivity for all source receiver pairs
Wavefield separation	Subtraction of downgoing P-wave field (median filter) by a 9 trace median operator
Deterministic deconvolution	Waveshaping zero-phasing of the upgoing wavefield, removal of multiples
Polarity reversal	180° phase shift, to match polarity convention of conventional geophone data
3D imaging	3D Kirchhoff migration with restricted aperture of 12°

Each VP recording set contained a various number of recorded sweeps, ranging from 12 to 37. Data within each VP were sorted on increasing MD and vertically stacked using a trimmed mean stack, which helped to exclude amplitude outliers.

Wireline records are frequently suspected to ringing noise, which occurs in those depth intervals of the boreholes where the cable can move freely and creates resonances with a fundamental frequency and higher overtones in the amplitude spectrum.

Figure 5.2 shows selected VPs with variable offsets such as 214 m, 510 m and 1411 m for the borehole E GrSK 3/90 after preprocessing (vertical stacking, correlation with the pilot sweep and subsequent differentiation) and denoising. All seismograms have a distinct P wave arrival; however, they are heavily dominated by a coherent characteristic striped or zig-zag noise. For instance, depth intervals 890 - 966, 1588 - 1816 m for VPs recorded in E GrSK 3/90 are contaminated by this type of noise (Figure 5.2 panels a, b, c). It appears that the noise distribution does not change significantly from one VP to another and affects shallower depth regions more than the deeper ones. Also, it can be noted that borehole Gt GrSk 4/05 has more noisy intervals, in comparison with E GrSK 3/90, and with higher amplitudes, for example, for depth regions at 873 - 980, 2177 - 2177, 3330 - 3409 m (Figure 5.2 panels g, h, i).

Ringing noise clearly represents a challenging problem and should be tackled by means of data processing. We did a few denoising test using different denoising approaches, including Burg adaptive deconvolution and Time-Frequency domain attenuation. The optimal denoising result was achieved using a novel approach based on matching pursuit decomposition (MPD) using Gabor atoms, described in Martuganova et al. (2021). According to this method we formed an overcomplete Gabor dictionary to decompose the original signal. Then using atomic

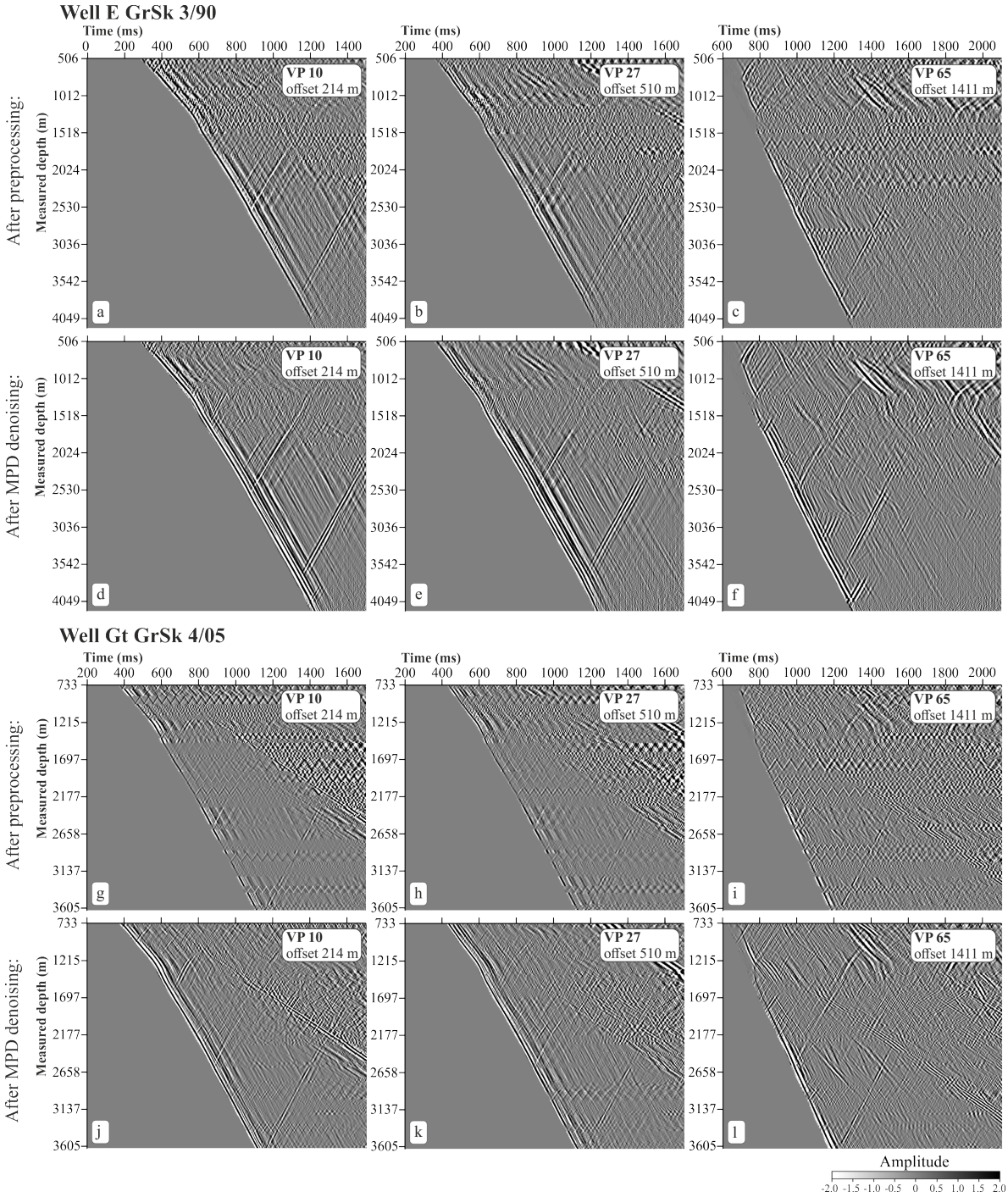

Figure 5.2: Common-source gathers displays for different source positions with offsets 214 m, 510 m and 1411 m after preprossessing (a), (b), (c) for well E GrSk3/90 and (g), (h), (i) for well Gt GrSk4/05; after noise subtraction using MPD denoising method and a moderate coherency enhancement (d), (e),(f) for well E GrSk3/90 and (j), (k), (l) for well Gt GrSk4/05.

parameters such as amplitude, frequency and position in time we determined parts of the signal representing slapping of the cable and subtracted them from the data to perform the denoising. To improve the S/N ratio of the data we applied the MPD denoising method after stacking, but before correlation to avoid smearing the noise by the correlation process. The results of denoising for two boreholes are given in Figure 5.2 on panels d, e, f and j, k, l for E GrSK 3/90 and Gt GrSk 4/05 respectively. MPD denoising eliminated almost all noise on

the seismograms and significantly improved traceability of the reflections, which are no longer obscured by the ringing noise.

After denoising, the correlation with the pilot sweep and time-differentiation to convert data to the strain-rate were applied to the data. This was followed by amplitude corrections (spherical divergence correction and lateral equalisation) and moderate wavefield enhancement. Also, measured depths were converted to true vertical depth below seismic datum elevation (TVDSD), and later in the text, we refer to it as depth.

5.4.2 Velocity model building and ray tracing

Several independent data sources were used to determine the velocity function for main stratigraphic layers of the region and assign appropriate P-wave velocities (Figure 5.3). First, velocity profiles recorded at zero offset source position were calculated with the Lizarralde smooth inversion method (Lizarralde and Swift, 1999) to get the main trend (Figure 5.3a black curve). Then, velocity values were updated according to calibrated sonic log data (Figure 5.3a thin grey curve) and the surface seismics velocity cube (Figure 5.3a, dark blue curve). The model was checked using the ray tracing results, and iteratively optimised to minimize the drift between the recorded and modelled arrival times for the rig shot at source position 10.

To improve the fit for far offset VPs a small anisotropic drift was included into the model. Thomsen's P-wave anisotropy parameters (Thomsen, 1986), namely ϵ and δ, for transversely isotropic (TI) media, 4 % δ and 16 % ϵ were selected for all layers down to the top salt. These parameters were tested and optimised, which allowed to reduce the standard deviation of drift for the longer offset VPs. Finally, all VPs were ray-traced through the constructed model, and reflection points (loci) for each source-receiver pair were extracted. The picked arrival times were compared with the ray traced times to check whether the smallest misfit for all available data was achieved. The average of the mean model drift for all VPs is 2.43 ms for the borehole E GrSk3/90 and 7.7 ms for Gt GrSk 4/05, respectively.

The layered 3D DAS VSP velocity model follows the geological model (Moeck et al., 2009) and has constant layer velocities or vertical velocity gradients indicated by the sonic log data (Figure 5.3a red curve; Figure 5.3b). Potential lateral variations are not accounted for. The values vary from 1750 m/s in the upper Quaternary and tertiary layers to 5000 m/s in the Rotliegend (Permian) reservoir section.

5.4.3 Data preparation for migration

The next processing step includes wavefield separation and deconvolution. To separate the upgoing wavefield the downgoing P-wave field was subtracted using a median filter. We tested a few different wavefield separation techniques (FK transform, FP transform), and the cleanest result was obtained by applying the median filter. This filter delivered a cleaner residual upgoing response with less smearing of the amplitude artefacts, and also preserves the resolution of data. Prior to deconvolution, the upgoing wavefields were scaled by -1 changing the polarity of DAS data to match the required European convention (increase AI = negative number on a trace.) The separated wavefield was deterministically deconvolved, using individual downgoing responses as trace-by-trace operators, followed by a bandpass filter 8, 12 – 70, 80 Hz and a front mute.

To further prepare the data for imaging, source static corrections were applied. Additionally, data were moved to pre-migration depth using a model-based stretch to map points according to reflection-point loci. Due to significant data quality variations between shots caused by unknown changes in the response of the fibre, the amplitudes across all data points were normalised using RMS amplitude values calculated in a depth window selected on the most prominent salt sequence reflection event. Each trace then was scaled by the inversed RMS trace value. The resulting pre-migrated seismograms were used as input for 3D imaging.

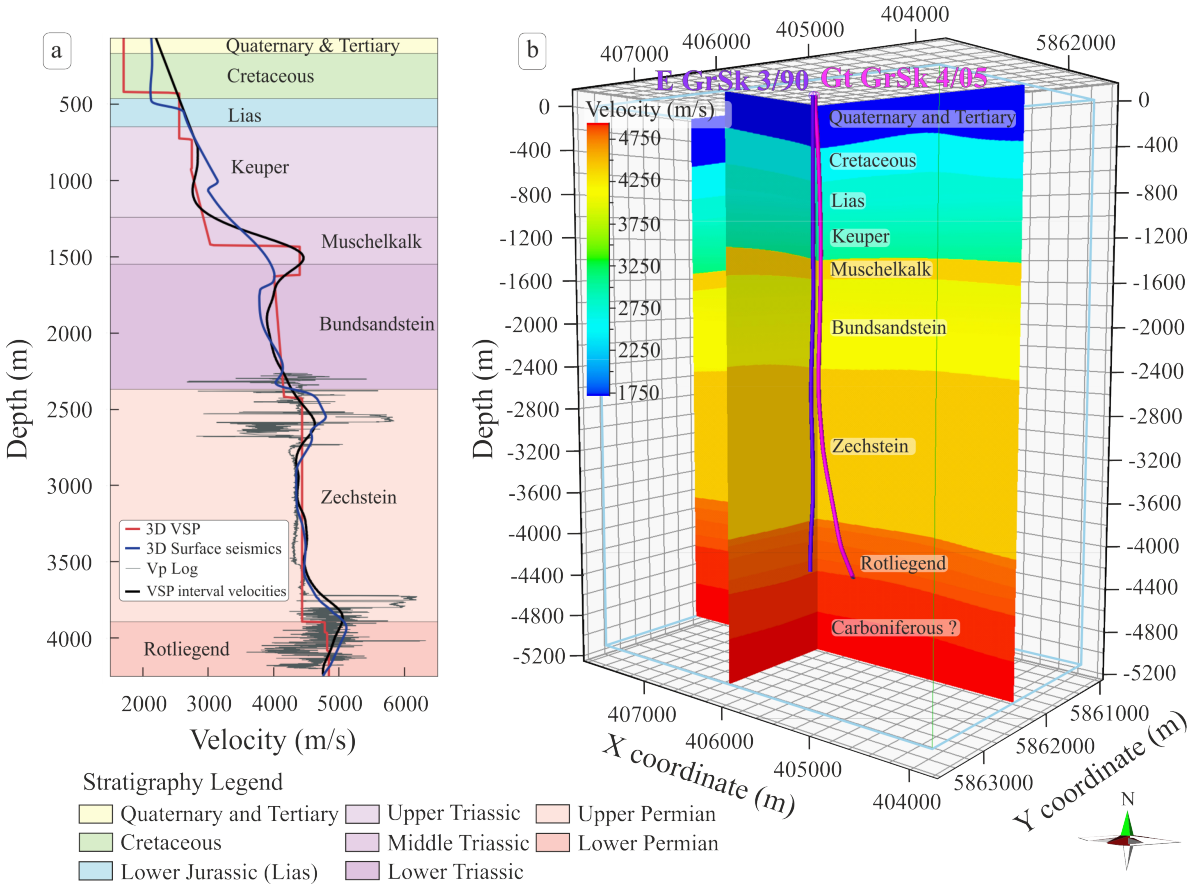

Figure 5.3: Velocity information at the Groß Schönebeck research site. (a) Velocity functions at the borehole E GrSk3/90 location. Red line - the curve extracted from the 3D DAS VSP velocity model shown in (b); dark blue line - the curve extracted from the 3D velocity model used for the 3D surface seismics prestack depth migration; thin grey line - sonic log measurement; thick black line - VSP interval velocities derived from the first break peaks using the method of smooth inversion after Lizarralde and Swift (1999). (b) 3D DAS VSP velocity model created using top formation surfaces to build an initial velocity model, which was then checked and optimised according to ray tracing results.

5.4.4 3D imaging

For imaging, a commercial 3D Kirchhoff migration algorithm (VSProwess Ltd.) was used. Calculated via ray tracing, the reflection-point loci for each source-receiver pair are interpolated and used to map each processed sample to its modelled image point coordinate. This is routinely known as VSP common depth point (CDP) mapping (Dillon and Thomson, 1984). Once the reflectivity is mapped approximately to the correct location it can be binned. An efficient surface tracking algorithm is used to find all those bins within the specified aperture angle intersected by the reflection ellipsoid.

For migration, we used a 12.5 m x 12.5 m horizontal and a 5 m depth bin size. After extensive testing, we chose a 12° aperture which allowed to sum the main reflections best and to preserve image details. In addition, the migration operator removed some of the imaging artefacts. A scaled version of each mapped sample is summed into each of these bins (normally cos-squared window). A by-product of migration is a bin count cube. A 3D bin density image along two lines and the depth slice at 4100 m are shown in Figure 5.4. This 3D visualisation discloses holes in the seismic coverage at 4100 m depth. Gaps in coverage are particularly noticeable east of the observation well. To avoid imaging artefacts, bin density information was used first to normalise amplitudes in the 3D DAS VSP volume. Afterwards, the bin density information is utilized to identify high uncertainty areas where the image fold is sparse and to clip the resulting cube in accordance to it. Furthermore, the bin density cube was employed to determine an area with a reasonable coverage (Figure 5.4a, dark blue rectangle) for further clipping of horizon maps.

The suppression of the ringing noise by means of MPD denoising and amplitude normalisation techniques, significantly improved the imaging results. Figure 5.5a shows the result of the migration which excludes denoising from the processing flow. The first problem that can be noticed are inconsistent significant amplitude anomalies, especially clearly visible around borehole Gt GrSk 4/05 (Figure 5.5a) in the reservoir section from 4000 m till 4500 m depth. Apart from that, the "noisy" cube has decreased resolution and horizon continuity in comparison with the "clean" cube (Figure 5.5b).

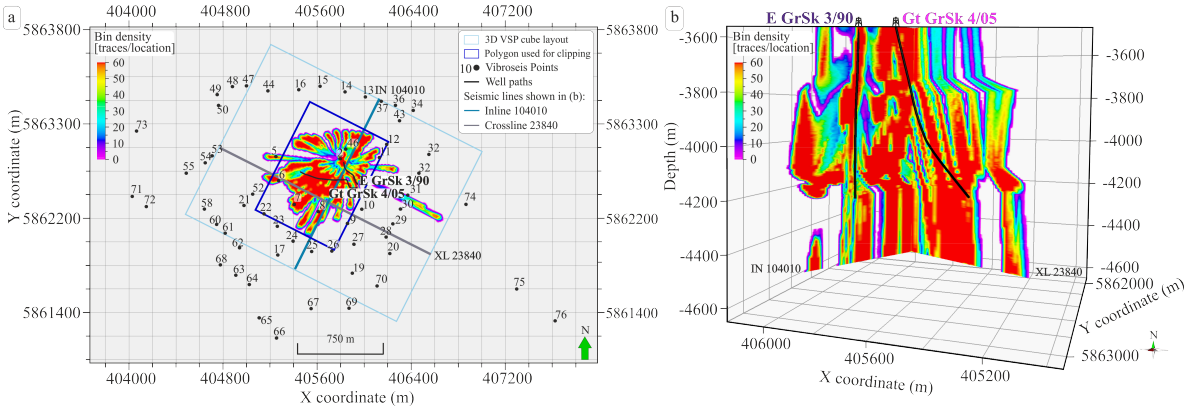

Figure 5.4: Examples of the ray coverage for the study area. Depth slice of a 3D bin density volume at 4100 m depth (a). 3D visualisation of two seismic lines in the 3D bin density cube (b) (for location see a).

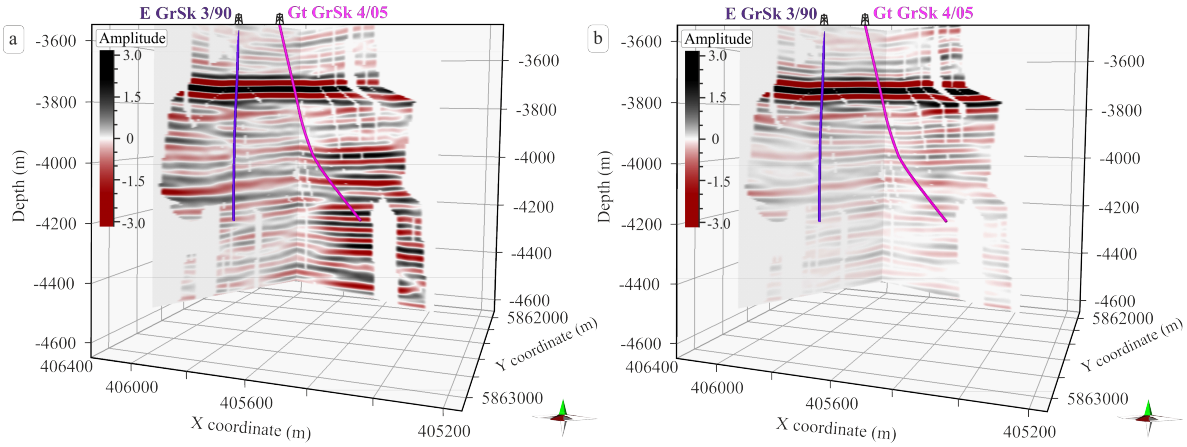

Figure 5.5: A comparison of 3D DAS VSP cubes generated with a model-based Kirchhoff migration algorithm (a) without and (b) with MPD denoising.

5.5 Reservoir imaging

The resulting 3D DAS VSP cube image is 1600 m x 2000 m, which has a relatively limited illumination range with a maximum inline/crossline extent of less than 900 m. The image of the subsurface is the most complete and best around the boreholes. Reflections in the vicinity of the wells reach up to 4500 m depth (Figure 5.6). To interpret the 3D DAS VSP imaging results (Figure 5.6a), we compare it with the 3D surface seismic cube (Krawczyk et al., 2019; Norden et al., in revision) after prestack depth migration (Figure 5.6b). The polarity of the DAS data was changed to match the polarity of the geophones. The 3D surface seismics was restricted according to the 3D DAS VSP cube layout. Bin size for borehole volume is 12.5 m x 12.5 m and for surface seismic volume is 25 m x 25 m. This means that inlines / crosslines of the 3D DAS VSP cube are 2 times denser.

The reservoir section is situated at a depth interval between 4 - 4.5 km and has an average velocity of 4700 m/s; the dominant frequencies in 3D surface seismics are between 20 and 50 Hz. With wireline 3D DAS VSP the frequencies are from 30 to 70 Hz. This gives a vertical resolution estimation of 24 - 47 m for the conventional surface seismic cube and a more favourable 16 - 34 m for the borehole seismic dataset.

Several reflectors can be mapped with high confidence across both volumes. Especially the main marker horizons of the typical stratigraphy in the North German Basin were successfully imaged (Figure 5.6): top Staßfurt-Basalanhydrit Fm (Z_1), top Rotliegend (Z_3), within Mellin-Schlichten (R_1), within Dethlingen Fm (R_3), the top and the bottom of Elbe sandstone reservoir (top ESR, base ESR), and possibly top of the Carboniferous (R_8). Although both cubes have similarities, there are distinct differences related to the higher vertical resolution of the VSP measurements. In the following chapters we will focus on each structural feature separately.

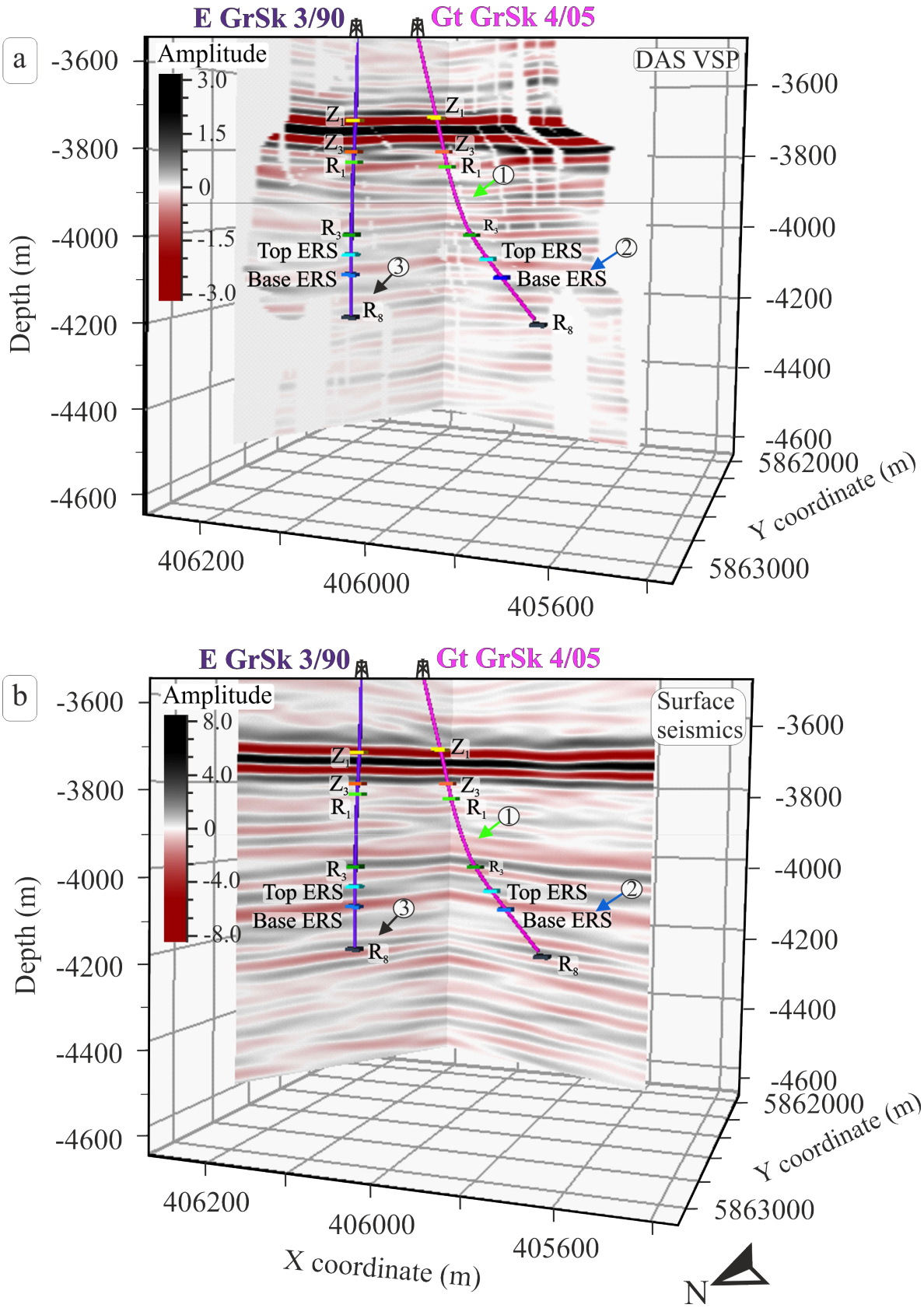

Figure 5.6: A comparison of 3D DAS VSP cube (a) and prestack depth migrated 3D surface seismic cube (b). Arrows with numbers highlight major interpretation features in the 3D DAS VSP and 3D surface seismic cubes. Light green arrows (1) point out the difference in seismic resolution in the upper Rotliegend; dark blue arrows (2) show the position of the Elbe reservoir sandstone horizon. Dark grey arrows (3) mark the location of unconformity in lower Rotliegend formation. Main seismic reflectors labelled on the figures: top Staßfurt-Basalanhydrit Fm (Z_1), top Rotliegend (Z_3), within Mellin-Schlichten (R_1), within Dethlingen Fm (R_3), top ESR - top of Elbe sandstone reservoir, base ESR - base of Elbe sandstone reservoir, R_8 - Base Effusive Rotliegend.

5.5.1 Upper Rotliegend horizons

The most prominent reflections in both seismic cubes are closely situated reflection bands from the transition from salt to anhydrite (Staßfurt-Basalanhydrit Fm (Z_1)), followed by the reflection Z_3 from the base of Zechstein. Together these closely situated seismic responses create a complex wavelet superimposition consisting out of 5 phases. (Figure 5.6). Salt layers are underlayed by upper Rotliegend sediments.

For the first time in the area of the research platform Groß Schönebeck, borehole seismics allows the separation of thin interlaying of siltstone and silty mudstone structures in the upper Rotliegend sediments in the depth range from 3800 m to 4000 m (Figure 5.6a, light green arrow (1)). On the 3D surface seismics (Krawczyk et al., 2019; Norden et al., in revision) a thick unresolved high amplitude continuous layer with visible thickness variations can be observed at approximately 3900 m (Figure 5.6b, light green arrow (1)). In contrast to the 3D surface seismic cube, on the 3D DAS VSP cube, two closely situated thin layers can be traced with a relatively constant thicknesses (Figure 5.6a, light green arrow (1)).

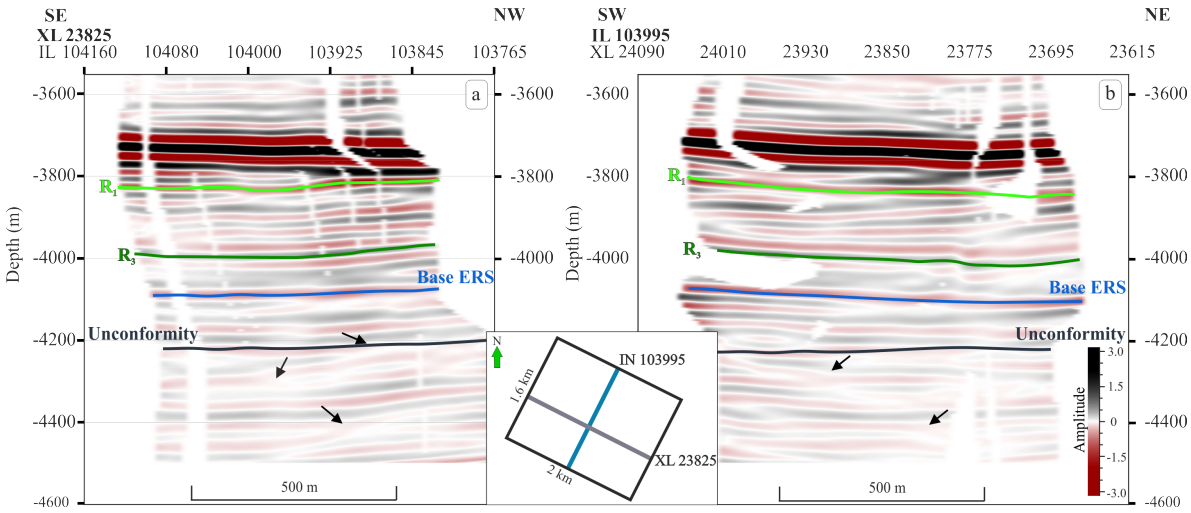

Figure 5.7: Seismic lines extracted from the 3D DAS VSP cube with horizons interpretation. (a) Seismic cross-line and (b) seismic inline, showing thin interlayered horizons in the upper Rotliegend (light green and dark green lines), base of Elbe sandstone reservoir (dark blue line) and the Lower Rotliegend unconformity (dark grey line). Black small arrows point out the locations of the numerous pinch outs.

By comparing the depth sections between 3800 m and 4000 m on both cubes, it can be noted that thin interlaying horizons in the 3D DAS VSP cube have various dipping characteristics, whereas the 3D surface seismic cube shows only thicker horizontal lines, sometimes even not continuous and with amplitudes variations along them. This might be related to the difference in the frequency content of surface and borehole seismic surveys, and as a result with the latter case having a higher resolution. The results of 3D DAS VSP imaging allows to trace a few thin horizons in the upper Rotliegend interval. Figure 5.7 demonstrates an inline and a crossline extracted from the central part of the seismic cube with interpreted horizons corresponding to reflections within Mellin-Schlichten (R_1) and within Dethlingen Fm (R_3). Reflector R_1 can be identified as a negative amplitude event associated with a sandstone interlayer inside siltstone sediments of Hannover Fm around the depth of 3800 m (Moeck et al., 2009). There is a decrease in gamma-ray, neutron porosity and Vp logs at this interval, resulting in decreased

acoustic impedance values. Reflector R_3 is identified as a positive amplitude event at a depth of 4010 m (Henninges et al., 2021a; Norden et al., in revision). It marks the transition from the Dethlingen sandstones to a succession of siltstones, followed by mudstones. A change in lithology can be identified by increased gamma-ray, density, and sonic velocity values, which leads to the increase of acoustic impedance. Depth variations of these horizons are visible already in a small volume around the boreholes. The indication of these variations in lithological sequences is also present in the corridor stacks within this interval (Henninges et al., 2021a).

5.5.2 Elbe reservoir sandstone layer

One of the possible targets for geothermal exploration are sandstones of the Dethlingen formation / Lower Elbe subgroup. In the Brandenburg area the lower part of the Dethlingen formation comprises fine-to-coarse grained sandstone with high quality reservoir properties (porosity 8-10 % and permeability of 10 - 100 mD (Trautwein and Huenges, 2005)). This layer was deposited in aeolian setting and then reworked by aquatic processes. The Elbe reservoir sandstone (ERS) layer is located between 4060 to 4100 m depth in the E GrSk 3/90 well (Bauer et al., 2020). On well logs this interval is characterised by decreased P-wave velocity, caused by an increased porosity of this section (Trautwein and Huenges, 2005). This geological unit was successfully imaged on both 3D images (Figure 5.6, dark blue arrows (2)).

In the conventional surface seismic image (Krawczyk et al., 2019; Norden et al., in revision), the base of ERS horizon can be traced as a continuous negative phase at around 4080 m depth, with increasing thickness toward the southwest direction. Even the theoretical resolution should be between 24 - 47 m. Bauer et al. (2020) showed via finite-difference forward modelling that this complex layer in the reservoir section still won't be adequately resolved since the theoretical resolution cannot be achieved due to challenging geological settings above and below the ERS.

Within the depth range from 4060 to 4100 m the depth section from 4070 to 4090 m shows a low variability in logs values, indicating a "cleaner" part of the sandstone layer. The high resolution of the 3D DAS VSP cube allows to see an internal structure inside this interval and trace depth variations of the base of the intra-reservoir horizon within Elbe sandstone reservoir. It may represent porous parts of a stacked fluvial sandstone body within the sandy Dethlingen Fm. succession. This interval's base is characterised by negative phases (decreased acoustic impedance) on the seismic 3D DAS VSP cube. We picked this horizon through the entire volume and created a depth contour map (Figure 5.8a). The map was clipped using the dark blue polygon shown on Figure 5.4a, to avoid interpolation artefacts in the regions with low coverage. The base ERS horizon lies at 4080 m on the southwest and at approximately 4100 m depth on the northeast. On the seismic section (Figure 5.8b), it is clearly visible that there is a pinch out on the southwest part of the profile, which was not distinguishable on the 3D surface seismics cube and visible as a thickness variation.

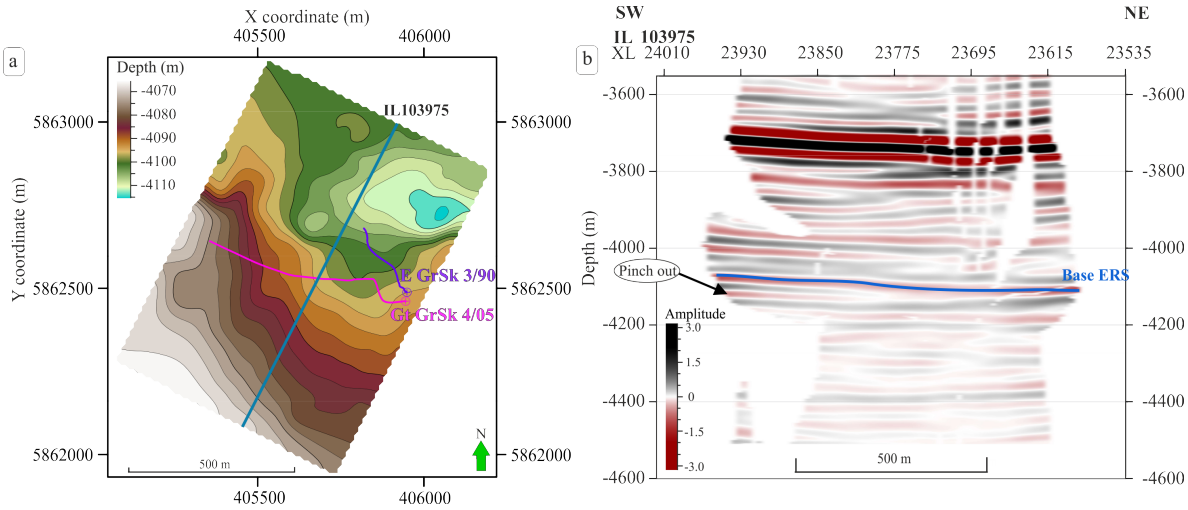

Figure 5.8: Spatial extent of the Elbe reservoir sandstone layer. Depth contour map of the Elbe sandstone reservoir bottom horizon. The dark blue line marks the location of the inline shown in (b): seismic section from the 3D DAS VSP volume with the interpretation of the Elbe reservoir sandstone (ERS) horizon.

The top of the ERS horizon corresponds to positive phase (increased acoustic impedance) on 3D DAS VSP cube. In general it follows similar paleo relief of the base ERS with the deepest values around 4050 m in the southwest and 4080 m in the northeast (Figure 5.9a). However, local depth variations are present, and therefore the thickness of the Elbe reservoir sandstone layer is highly variable in close proximity to the boreholes (Figure 5.9b). It ranges from 20 to 35 m.

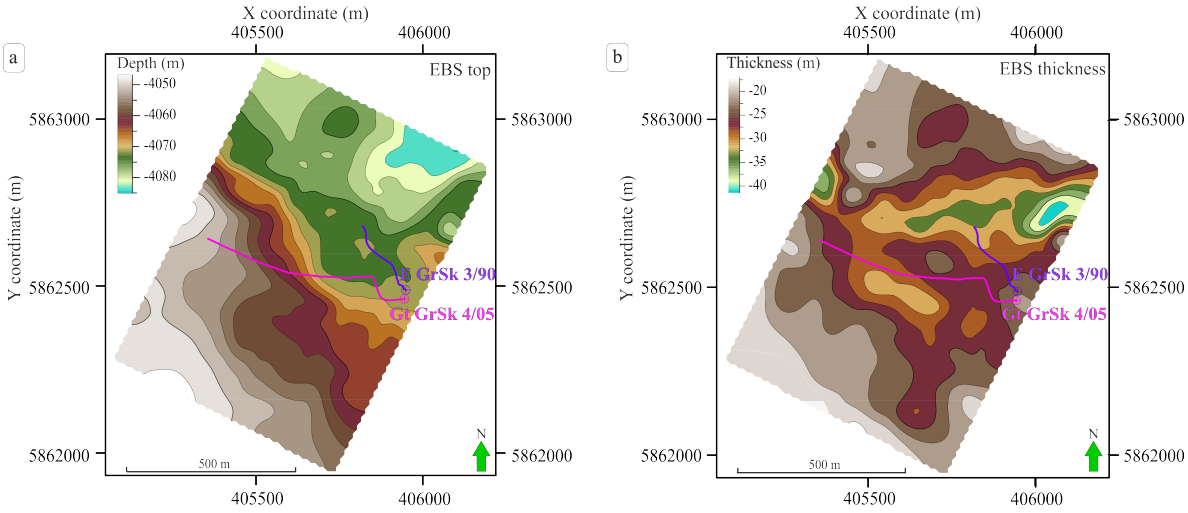

Figure 5.9: Mapping results within the study area: depth contour map of the top Elbe reservoir sandstone layer (a) and the ERS thickness (b).

5.5.3 The lower Rotliegend unconfomity

Another essential feature of the seismic interpretation on the 3D DAS VSP and the 3D surface seismics (Krawczyk et al., 2019; Norden et al., in revision) cubes is the change in seismic reflection pattern (Figure 5.6) at a depth around 4200 m. On the 3D surface seismics, this is visible as a change from horizontal continuous reflectors to layers with inconsistent amplitudes and a lower reflectivity in the lower Rotlieged formation (Figure 5.6b, the dark grey arrow

(3)). On the 3D DAS VSP cube, a change from nearly horizontal to inclined reflectors can be detected (Figure 5.6a, the dark grey arrow (3)). This change of the seismic facies evidences the existence of an unconformity in the area where we expect volcanic rocks. We will refer to it as lower Rotliegend unconfomity.

On the seismic cross-line and inline shown in Figure 5.7 a and b, the possible unconformity boundary is marked by a thick dark grey line. This reflection has weak, uncertain characteristics. Small black arrows indicate numerous exciting pinch outs below this horizon, which were used as indicators of the type change of the layering. Due to reduced reflectivity and gaps in the cubes, tracing this horizon accurately is a pretty challenging task. Therefore the resulting depth contour map might have errors, especially at the edges of the dataset. Nevertheless, in the area between the two boreholes where we have the best coverage, we can see that the depth variation of the lower Rotliegend unconformity is relatively limited to the depth range between 4200 - 4230 m (Figure 5.10).

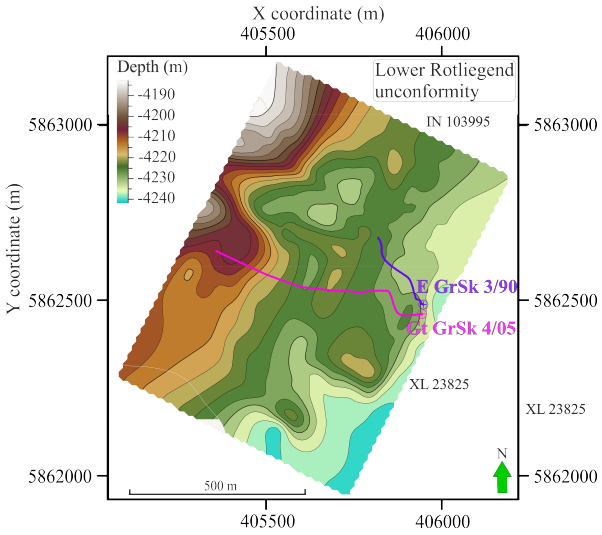

Figure 5.10: Spatial distribution of the unconformity boundary. Depth of the Lower Rotliegend unconformity.

5.6 Discussion & Outlook

5.6.1 The Groß Schönebeck experiment

With this study, we investigated the applicability of the DAS wireline acquisition method for detailed deep geothermal reservoir imaging and the capability to bridge the gap between well logs and 3D surface seismics. 3D DAS VSP provides, on average, a two times better-resolved image than 3D surface seismics and has a significant potentical in the geothermal sector. Data acquisition using constellation fibres or new interrogators with higher signal-to-noise ratio can help notably improve the quality of the wireline DAS data recording and compensate for signal loses in the deep reservoir section. Nethertheless, more research on fibre coupling improvement and location control in the borehole is strongly advised, which could allow wireline DAS acquisition to become a routine for numerous applications.

VSP surveys conducted with distributed sensors permanently installed behind casing or along the tubing provide the advantage of good coupling conditions and the possibility

to perform time-lapse studies. Successfully reported case studies include applications for unconventional exploration in Texas (Shultz and Simmons, 2019) to create a detailed image of the formation around the well. Application of DAS for CO2 monitoring (Correa et al., 2019; Götz et al., 2018) is a well-known routine to provide a reliable method for targeted, detailed imaging and 4D monitoring of the site. 3D DAS VSP surveys in oil and gas exploration reduce exploration risks in regions with a challenging environment, for instance, in the presence of strong production noise (Jiang et al., 2016), in areas with complex salt tectonics (Bartels et al., 2015) etc. In general, all the surveys mentioned above have a better signal-to-noise ratio than data typically recorded with wireline DAS acquisition.

Wireline DAS, however, has a great advantage. It allows to acquire seismic data in already drilled and cemented boreholes. This can be done at a low cost and in a small amount of time. Even though wireline 3D DAS VSP at the Groß Schönebeck site has worse coupling conditions than conventional DAS cemented behind the casing, the resolution of the imaged seismic volume is still in the same range of 20 m.

To the best of the authors knowledge, there are only limited examples of wireline DAS applications with active seismic sources for geothermal exploration. One known example was recorded in 2016 at the geothermal field at Brady Hot Springs, Nevada (Miller et al., 2018). A fibre optical cable was deployed into the accessible 363 m portion of the vertical well 56-1. This dataset has a limited depth range (up to 297 m only), and only two shot points were used for data acquisition. No 3D image was created. Therefore, the experiments conducted at the Groß Schönebeck in-situ laboratory and Brady Hot Springs are quite different and it is problematic to compare these two datasets. Thus, recorded data at the Groß Schönebeck is unique among the experiments conducted for geothermal exploration, with reflection information recorded down to 4.2 km deep.

A spiral survey design at the Groß Schönebeck site led to a ray focusing on the target reservoir area yielding an equably distributed offset and azimuth coverage. Good results were achieved with only 61 VPs. Nevertheless, low to zero ray coverage in some regions of the 3D VSP survey resulted in a lack of data required for a successful migration process without excessive artefacts. Due to budget limitations, the number of vibrator points had to be restricted and quite often positioned in such a way that they don't have overlapping ray penetrating areas. Therefore, petal-shaped footprints, with the highest coverage in the centre, are prominent in bin density slices (Figure 5.4a) revealing a partial illumination problem. Consequently, the resulting migrated depth slices have gaps and are not well suitable for classical attribute analysis. These limitations led to the usage of the 3D DAS VSP cube for structural interpretation only.

A similar experiment to the Groß Schönebeck survey was conducted for hydrocarbons exploration in China's Heibei region (Yu et al., 2016a). DAS walkaway and walkaround VSP with wireline survey consisted of 386 successful shot points, 6 times more than at the Groß Schönebeck experiment. The data acquisition for the in-situ laboratory in the Brandenburg area was probably less time-consuming, effortful and costly than this experiment in China. However, densely regularly placed source positions allowed to get a detailed resolved 3D image for the area of interest in Heibei region without gaps and prominent migration artefacts. The experiment in China showed that with a larger amount of source points a better coverage can

be achieved, however, one should always look for a trade off between a reasonable coverage and acquisition cost already during the planning phase.

5.6.2 Data processing

The experiment at the Groß Schönebeck allowed gaining valuable knowledge on survey planning and data processing. One of the biggest challenges for this dataset was a ringing noise problem. At the early stages of the data processing, an intermediate solution for denoising included Burg adaptive deconvolution combined with careful exclusion of depth intervals with a poor signal-to-noise ratio from the data processing. To further improve imaging results and limit migration artefacts due to sparse coverage, it was necessary to improve the signal-to-noise ratio of the data and include more data into migration calculations. Therefore, an essential part in successful data imaging results played careful denoising using the MPD approach.

Besides the quantity of the data, another important parameter, which will significantly influence the imaging results, is the migration aperture (Schleicher et al., 1997; Sun, 2000). After extensive testing we came to the conclusion that a strict restriction of 5° can lead to an ambiguous and inconsistent summation of the main horizons. On the other hand, a too broad aperture can reduce the resolution of the horizons. Thus, a compromise between these parameters should be found. Additionally, due to its stacking nature, the migration operator will also attenuate to some extent the residual noise in the data.

5.6.3 Future geothermal exploration plans

The results of our 3D DAS VSP experiments prove that this type of measurement can significantly contribute to exploration campaigns. The wireline DAS VSP allows reducing risks and can have a higher resolution compared to the conventional 3D surface seismics interpretation which does not provide enough information due to the limited resolution of the data.

The Elbe reservoir sandstone layer currently represents one of potential targets for the future geothermal exploration. The 3D VSP imaging results clarified the sandstone layer's effective thickness with good reservoir properties. According to our estimations, it varies between 25 to 40 m (Figure 5.9b) near the boreholes locations. The fluvial nature of these deposits is perhaps responsible for this high variability. Previously the thickness of this layer was overestimated to be around 80 m (Zimmermann et al., 2010). Our results are also supported by updated thicknesses from the 3D surface seismic experiment, calculated using wavelet transform-based seismic facies classification (Bauer et al., 2020; Norden et al., in revision).

The observed lower thicknesses may explain why a matrix-dominated exploration approach did not succeed at the Groß Schönebeck as the reservoir volume which is able to contribute to the fluid flow is considerably lower than expected beforehand. However, the mapped variations of the more porous reservoir thickness, representing most likely the variability of facies-related petrophysical properties, should be considered for the design of the fracture-dominated geothermal systems.

At the depth level around 4200 m, we mapped the lower Rotliegend unconformity. There is a hypothesis that deposits of permo-carboniferous volcanic rocks lay below this border, which

represent another possible target for future exploration (Norden et al., in revision). According to literature sources (Guterch et al., 2010), lower Rotliegned volcanics have a significant time-gap in sedimentation and therefore mapped unconformity horizon could indicate a difference in layering caused by erosion. The 3D DAS VSP imaging successfully contributed to the determination of this critical boundary since it was not well characterised on the 3D surface seismics cube. The bottom of permo-carboniferous volcanic rocks is not detectable neither on the 3D DAS VSP nor on the 3D surface seismic cubes. This implies that the thickness of this deposit's sections can be greater than 300 m. Considering this information, the economic profitability is significantly higher for treated volcanic rocks than for the Elbe reservoir sandstone layer. Nevertheless, we believe it is crucial to determine the exact depth by drilling, perform core analysis, and use well logging methods to determine the precise composition of sediments below this border and essential parameters such as porosity and permeability before developing concepts for possible reservoir treatments in volcanites.

The exact development plans of the site are still under discussion. Possible scenarios include implementing a new stimulation concept and possibly drilling a new well (GrSk 5) or deepening the existing borehole E GrSk 3/90.

5.7 Conclusion

We analysed the 3D DAS VSP imaging results acquired with wireline DAS installation at the Groß Schönebeck geothermal research site. Despite the numerous difficulties during the data acquisition campaign, the borehole seismics was able to image the target interval and substantially contribute to the detailed interpretation of the geothermal reservoir.

The 3-dimensional image created using borehole yields:

- Resolution of thin complex upper Rotliegent geological structure;
- Mapping of the Elbe reservoir sandstone;
- Detection of the lower Rotliegend unconformity in the region with possible volcanic rocks.

The interpretation of the 3D DAS VSP cube evidenced the unexpected absence of faults with larger vertical offsets and fractures. Furthermore, no indications for free gas were found in the data. These findings are important for the further development of the Groß Schönebeck in-situ geothermal laboratory.

Wireline DAS is still a relatively new method. It allows for a significantly increase in the number of sensors and a larger recording aperture, which results in imaging over a larger depth interval. Thus, it is cheaper and faster than the application of conventional borehole sensors. Nevertheless, careful survey planning and sophisticated data processing are vital for successful imaging results.

This successful case study at the Groß Schönebeck site can play a crucial role in developing and applying modern, efficient geothermal exploration methods in the Northern German Basin and other regions with comparable lithology.

5.8 Acknowledgements

Funding of the present work was provided by the German Federal Ministry of Economic Affairs and Energy (grant 0324065), and the European Commission, Horizon 2020 Framework Programme (grant nos. DESTRESS (691728) and EPOS IP (676564)). We would like to thank all contractors involved in the acquisition and processing. The authors would like sincerely to acknowledge Ernst Huenges for establishing research activities at the Groß Schönebeck in-situ geothermal laboratory, Manfred Stiller, Jan Henninges and Klaus Bauer for experiment planning, supervision of the fieldwork and data acquisition, as well as constructive discussions on data processing. We also thank all our colleagues from GFZ German Research Centre for Geosciences for their contribution to this work. The authors also acknowledge James Bailey, Mary Humphries and Colin Humphries for providing VSProwess software and sharing their extensive VSP data processing knowledge.

6

Discussion

Growing demand for the exploration of deep geothermal reservoirs (3.5-4 km) dictates a substantial reduction in acquisition time, improved cost efficiency and reliable operation for increasingly complex and harsh environments. It becomes more essential to obtain a comprehensive characterisation of the internal geometry of the reservoir, quantitative estimations of petrophysical properties. In addition, there is a high demand for monitoring reservoir changes over time. Up-scaling and achieving 2570 TWh energy production from geothermal by 2050 (The European Commission, 2021) will be most challenging without improving borehole seismic data acquisition techniques. In my thesis, I demonstrated that vertical seismic profiling data acquired using wireline fibre optic could significantly contribute to the characterisation of the deep geothermal reservoir. To perform an assessment of the wireline DAS-VSP method, I evaluated the acquired data, demonstrated the advantages and disadvantages related to cable installation and, most notably, how this technique can contribute to the characterisation of the reservoir and geothermal exploration.

6.1 DAS performance in comparison with conventional sensors

One of the first questions that needed to be answered is how wireline DAS's performance compares to conventional sensors. As a part of the study, in Chapter 3 DAS recordings were compared to the vertical component of the conventional accelerometer data (VSI) tool acquired at four depth levels 1200, 2400, 3600 and 4207 m in Gt GrSk 4/05 was provided. DAS strain rate data shows good agreement with independent accelerometer traces for first arrivals; however, the reflections have the opposite polarities. This polarity change is one of the well-known features of the DAS data previously demonstrated by Hartog et al. (2014), Mateeva et al. (2014), or Willis et al. (2019). On the other hand, DAS conversion to acceleration via the transfer function after Egorov et al. (2018) corrects the upgoing reflections polarities, such as they now coincide with accelerometer data. I proved that the waveforms acquired using wireline DAS have a good agreement with accelerometer traces in case of sufficient coupling with a borehole wall.

DAS recordings from the experiment at the Groß Schönebeck have a good signal-to-noise ratio. The values vary from different VPs; the depth level around 1000 m has 40-50 dB, dropping down to 4-10 dB at the well bottom around 4200 m. This data quality was reached with 16 vertical stacking rates on average. Similar performance was achieved in the offset VSP survey acquired in May 2017 at the CO2CRC Otway, Australia. Correa et al. (2017) showed a comparison between two Silixa Ltd interrogator units iDAS v2, iDAS v3 (optimised for improved performance with constellation fibre) and a geophone chain. For zero offset position, a signal-to-noise value is around 45 and 48 dB at a depth of 1000 m for iDAS v2 and iDAS v3, respectively. With increasing offset, the signal-to-noise for iDAS v2 around 1000 m drops significantly to the range of 20-30 dB, for iDAS v3 unit values stays at around 40-50 dB. However, it should be noticed that these results were obtained after stacking 50 shots for each offset point. In our experiment, similar signal-to-noise values were achieved with 16 vertical stacking rates on average. This demonstrates the performance discrepancy for interrogator units of different manufacturers, which should be taken into account during the experiment planning stage.

During earlier stages of the DAS method development, fibre optic seismic data used to have a significantly lower signal-to-noise ratio than conventional sensors (Hartog et al., 2014). The signal-to-noise ratio of the DAS data compared to geophone is approximately 10-20 dB lower, as demonstrated in Correa et al. 2017. However, DAS interrogators have been improving significantly over the years. Previously, DAS interrogators mainly used coherent light sources (Lindsey et al., 2020). These interrogators are limited in spatial resolution by their pulse length and limited in dynamic range by their pulse energy. Recent developments include chirped compression techniques that use an optical sweep rather than a coherent light source, allowing to probe much longer fibres. Low noise measurements have been reported up to 171 km using optical sweeps (Waagaard et al., 2021). In addition, it is essential to note that seismic data measurement with DAS has, in principle different physical nature and therefore cannot be considered an extended geophone chain equivalent (Correa, 2018). Thus, the comparisons of the sensor's performances are a complex topic, which requires a good understanding of the DAS measurement principles and parameters. Most recently Titov et al. (2022) proposed using log-based metrics to quantify and qualify VSP data products.

6.2 DAS-VSP acquisition advantages

Seismic data acquisition using DAS has comparative advantages over conventional borehole seismic tools. Application of the interrogator units allows utilising a fibre optic cable to create a dense array of receivers with spatial sampling up to a few meters.

At the Groß Schönebeck site, for the first time in the history of the application of VSP surveys for geothermal exploration data were simultaneously acquired in two 4.2 km, which remains the deepest recorded datasets up to this date with the application of DAS technology. VSP datasets presented in Chapters 3 and 4 were recorded at two boreholes simultaneously for the whole trajectory of the well, with 840 and 873 (before the cable failure event) recording points for borehole E GrSk 3/90 and Gt GrSk 4/05, respectively. Installed fibre optic cable allowed measuring unaliased seismic waveforms with a spatial sampling of 5 meters. Thus, DAS

seismic measurements provide dense recordings without interfering with any other operational activity in a borehole. This significantly reduced both time and acquisition costs.

Two popular tools currently used for recording VSPs, Sercel SlimWave (used in the study Reiser et al., 2020) and Avalon ASR gimbal (used in the study Guglielmetti et al., 2020), use 3-C geophone chains, which had 17 and 24 levels, respectively. Although some manufacturers have tools with up to 100 levels, they are not commonly applied in geothermal exploration due to increased difficulties in operations and costs. This limitation in a number of channels implies that the maximum surveying depth range that can be covered per shot is 170 m for the Sercel system and 240 m for the Avalon ASR tool, respectively, in the case of 10 m channel spacing. Therefore, to survey a deep well with these conventional tools, it is necessary to repeatedly move the wireline geophone chain tools and perform another shot with the source.

Thus, to survey a deep well (up to 4.2 km like in Groß Schönebeck site) with these conventional tools, it is necessary to move the wireline geophone chain at least 25 times for the Sercel tool and 18 times for the Avalon ASR. This implies that each vibrator source position has to be repeated 18 to 25 times for our case. Furthermore, Reiser et al. (2020) report that Sercel SlimWave used for the VSP study in Iceland had only six calliper arms, which led to proper coupling only for six geophones out of 17 and dramatically limited the recordable depth range.

VSP surveys with dense spacing are very expensive and often cost prohibited for geothermal applications. The efficient use of resources for the geothermal exploration survey means that tools movements inside the borehole should be minimised. Unfortunately, with conventional geophone chains, this is a major challenge. That is why the demand for innovation is high.

Furthermore, conventional geophones can usually function in temperatures up to 135°C (150°C peak), can corrode, making them unreliable for geothermal applications in general and are especially unsuitable for long term monitoring. The temperature at the Groß Schönebeck site inside the reservoir is around 140° C, which is on the temperature limit of geophone's applications. Although some seismic amplitudes variations with a time were noticed (Chapter 3), the data acquired using the fibre optics cable remained reliable. Kasahara et al. (2021) demonstrated a dataset recorded in extreme temperatures up to 240° C, supporting the idea that DAS can be used in harsh geothermal settings.

6.3 Limitations of the wireline DAS-VSP method

Although wireline DAS technology offers a convenient and reliable method for seismic data acquisition, it has certain limitations as any geophysical method. Unlike conventional geophones, fibre optical cables have directional sensitivity patterns (Hartog, 2017; Wu et al., 2017; Martin et al., 2021). In practice, this means that the response function of the fibre for P-waves is described by $\cos^2(\theta)$ of the angle of incidence and $\sin 2\theta$ for S-waves (Wu et al., 2017). Helically wounded cables (HWCs) were designed to address these limitations and to improve the broadband sensitivity of P-wave arrivals (Kuvshinov, 2016; Baird, 2020).

In the experiment at the Groß Schönebeck in-situ laboratory in both boreholes, we acquired the data using straight fibres (Chapter 3). To restrain the DAS method limitations related to a dependence on the angle of incidence during the experiment planning stage, a sophisticated

ray tracing was performed to optimise VPs positions and, as a result, the data quality for deep geothermal reservoir imaging. Thus, the influence of this method's limitation was significantly restricted. However, as it was discussed in Chapter 3 most shallow 500 meters for larger offsets have an absent P wave arrival. This happened because an angle of incidence for a seismic wave exceeds the critical angle for these shallow depths.

Another DAS specific is related to the nature of the recorded measurement. Stain or strain rate values are averaged over the interval called gauge length. As shown by Dean et al. (2017) careful optimisation of this parameter is needed to guarantee optimal signal-to-noise ratio and resolution. In Chapter 3, I showed that for average velocities (around 4500 m/s) profile inside the reservoir section and frequencies which we expect to record, the optimal gauge length value is equal to 40 m.

One of the scientific objections for this detailed imaging using vertical seismic profiling was to study local discontinuities elements in the reservoir section. As a result, neither borehole seismic cube nor surface seismic cube detected apparent faults or fractures. Nevertheless, this result might be connected to several limitations of the seismic method and the specifics related to DAS technology.

First, the created fracture by the hydrofracturing cannot be imaged unless there is a distinct acoustic contrast or offset detectable by seismic methods. For 3D DAS VSP imaging, gauge lengths of 20 and 40 m were used (Chapter 3). These values might be too high to detect small scale features, such as fractures. Theoretically, a smaller gauge length is necessary for small scale details imaging, such as fractures, but it comes at the expense of having a lower signal-to-noise ratio.

To achieve a sharper and more detailed image at the Groß Schönebeck, it is necessary to further improve the velocity model used for migration. Sophisticated anisotropy study and inclusion of the heterogeneities into the existing layered velocity model will allow to further improve the reservoir image. This might be especially important for the potential fracture mapping in the case of data acquisition with active seismic methods.

To better understand the expected response from the fractures, it is essential to perform finite-difference modelling to predict the wave propagation in the fractured reservoir. It could be possible to estimate the size, contrast required to image a fracture, characterise, and interpret the individual response with such modelling. Further modelling studies are necessary to evaluate necessary acquisition parameters.

6.4 Coupling noise problem in wireline operations

Distributed acoustic sensing data recorded during wireline operations is subject to ringing noise. This problem was previously reported by Hartog et al. (2014), Dean et al. (2015), Yu et al. (2016a). In Chapter 4 it was explained that loosened uncoupled intervals of the fibre optics cable act like a guitar string and create a series of peaks and notches in the amplitude spectra. This notably reduces the signal to noise ratio of the data since the energy from the vibrator causes cable vibrations, which obscures later arrivals. Moreover, the velocity of the standing waves travelling along the cable is similar to the formation velocity in the reservoir section. Therefore, coupling noise after the correlation process has a similar dip,

which obscures actual reflections. Thus, coupling noise issues should be taken into account already at the stage of survey planning, since the effect that cable vibrations have on the seismic data, can be mitigated.

Chapter 4 contains information on a developed denoising method to tackle this type of the noise in the data. The suggested approach is based on matching pursuit decomposition, which is relatively widely applied for signal processing in various fields such as geophysics, neuroscience and astrophysics.

Despite the broad range of applications, the suggested methodology based on MPD was not yet applied for a coupling noise problem in wireline DAS data. The proposed denoising method passed through extensive testing and successfully cleaned all recorded seismic data. Hense, this approach is shown to be a robust and relatively computationally fast method.

6.5 Wireline DAS-VSP experiment at the Groß Schönebeck in-situ laboratory

The experiment at the Groß Schönebeck in-situ laboratory has a unique target-oriented survey design. A total of 61 and 18 vibrator points were recorded using the wireline DAS acquisition method in well E GrSk 3/90 and well Gt GrSk 4/05, respectively. The source points had various offsets from 200 to 2000 meters with a layout organised as a spiral pattern around the target area to ensure a proper azimuth distribution. Nevertheless, due to cable failure inside the Gt GrSk 4, described in Chapter 3 the resulting coverage in the reservoir section has significant gaps. This is why the seismic data interpretation shown in Chapter 5 was challenging.

The survey design strongly depends on research objectives and local geology. For oil and gas exploration, similar spiral source positioning is commonly used (Yu et al., 2016a; Lim et al., 2020. Yu et al. (2016a) showed one of the first imaging results from a 3D DAS VSP walkaway acquired using wireline cable deployed in a 4 km deep vertical well in the north-eastern of China. Overall, 386 shot points were placed on different offsets around the borehole, creating a radial pattern similar to source positioning at the Groß Schönebeck. This allowed to create a 3D cube borehole seismic cube with a higher vertical and lateral resolution than the surface seismic in the study area. (Lim et al., 2020) recorded one of the most extensive onshore VSP surveys consisting of 1701 VP arranged in a spiral around the borehole and using permanently installed fibre optic cable in methane hydrate research test well in North Slope, Alaska, USA. Phenomenal dataset quality of the 3D DAS VSP data revealed indications of the sub-fault system that are not presented in the surface seismic data. As a result, VSP data reveals more detailed geological structures information and lowers the exploration risks.

Using zero-offset data processing recorded at the Groß Schönebeck geothermal research platform, accurate time-depth relationships and interval velocities profiles, and corridor stack, which represents reflectivity profile at the borehole location with high precision, were created. A corridor stack is especially valuable for comparison with a surface seismic. It helps to identify reflections and correlate them with surface seismic results. In addition, since vertical seismic profiling records the downgoing wavefield as well as the upgoing wavefield, it can significantly

contribute to the understanding of the wave propagation process, which is beneficial for the processing and interpretation of surface seismic data.

Using sophisticated data analysis and processing workflows tailored for VSP offset data specifics, a detailed image of the subsurface in the vicinity of the boreholes was created. Advanced imaging techniques allowed to limit migration artefacts that are typical for sparse VSP surveys, as in Reiser et al. (2020); Kasahara et al. (2021), and therefore presented results do not suffer from so-called "migration smiles". Thus, characteristics of the subsurface are clearly visible and not disturbed due to migration aperture summation problems.

In our case, the reflections in the 3D VSP cube reach 4.5 km depth. The known typical geological elements of the North German basin are successfully imaged. According to Göthel (2016) seismic horizons in lower Rotliegend are referred to as "Phantom horizons" and do not have a reliable definition. For the first time at the Groß Schönebeck geothermal research platform development, vertical seismic profiling allowed a detailed characterisation of structural settings in a depth section below a thick salt layer. Chapter 5 shows complex interlaying of the upper Rotliegend. Reflectors within Mellin-Schlichten (R_1) correspond to thin sandstone interlayering inside siltstone sediments of Hannover Fm., and within Dethlingen Fm (R_3), which marks the transition from Dethlingen sandstones to siltstone-mudstone succession, were traced and interpreted on a seismic cube. A higher vertical resolution of the borehole seismic allowed to trace thickness variations of the Elbe sandstone layer, representing one of the possible exploration targets. In addition, a change of type of the layering indicated the presence of lower Rotliegend unconformity, which was hardly identified in the 3D surface seismic cube.

Overall, the created image agrees with existing concepts of the geological settings of the site and interpretation results obtained using an independent 3D surface seismic experiment. Thus, the interpretation of the imaging results provides vital information for the further development of deep geothermal resources at the Groß Schönebeck facilities. Consequently, the results of our field studies show that the DAS seismic method is effective for geothermal exploration.

VSP surveys for geothermal are still rarely acquired. Even though some of the mentioned borehole seismic measurements with conventional geophones had similar or even better spatial sampling between the receivers, almost all studies performed analysis using only 2D seismic gathers for subsurface analysis (Guglielmetti et al., 2020; Kasahara et al., 2021; Lorenzo et al., 2015; Reiser et al., 2020). Due to time-cost constraints, these measurements had a very limited number of source positions, which restricted imaging results. Hyperbola-shaped reflections often dominate these imaging results, making the interpretation quite challenging. In the case of the 3D imaging results presented from the Brady geothermal field, the major difference is in depth, which is limited to 600 m in this case study (Trainor-Guitton et al., 2018).

In general, VSP surveys and DAS VSP surveys, in particular, are beneficial for imaging improvement in complex geological settings. M.F. Rahim et al. (2018) demonstrated improved reflector continuity and faults detection below the gas clouds in DAS VSP imaging results compared to the image created using OBN data. Zhan and Nahm (2020) presented a 3D DAS VSP result which allowed to fill in the gaps between multiple wells in the Mars field, deepwater Gulf of Mexico.

6.6 The place of wireline DAS-VSP in the geothermal exploration process

The geothermal project passes several development stages, including resources assessment, development, and operation, which requires risk minimisation procedures for safe and sustainable operations.

The first phase is exploration. The input from several disciplines such as geophysical methods, geochemistry, hydrology, geothermal engineering, reservoir engineering, and material science is used to assess the economic value and design a power plant for heat exploitation.

Evaluation of the geothermal resources is performed based on a combined analysis of the site's geological settings and thermal and hydraulic properties. The main objectives of geothermal exploration are determining the depth of resources, temperature, productivity, and sustainability of specific targets. All necessary parameters must be estimated for the target interval. Furthermore, uncertainties must be evaluated to guarantee risk minimisation for exploration and production.

Evaluation of the thermal energy stored in the reservoir could be performed following the volumetric heat in place model (Garg and Combs, 2015; Muffler and Cataldi, 1978), which uses temperature, thickness, area, and heat capacity of hosting rocks:

$$q_r = V\bar{\rho}\bar{c}(T_R - T_r), \tag{6.1}$$

where c_l, c_g, c_r = heat capacity of liquid water, steam, and rock grains; A = reservoir area; H = reservoir thickness; S_l, S_g = liquid water and steam saturation in pores ($S_l + S_g = 1$); T_r =reference temperature; T_R = average reservoir temperature; V = reservoir volume ($=AH$); ϕ = porosity; $\bar{\rho}\bar{c}$ =volumetric heat capacity of fluid-saturated rock [$=\phi S_l \rho_l c_l + \phi S_g \rho_g c_g + (1 - \phi)\rho_r c_r$]; ρ_l, ρ_g, ρ_r= density of liquid water, steam, and rock grains.

It should be noted that this formula describes energy stored and available In the reservoir (Garg and Combs, 2015; Muffler and Cataldi, 1978), but does not include recovered energy. It is essential to consider parameters such as the heat recovery factor to get estimations of the economic value of the reservoir. I will focus mainly on the formula for initially available heat for simplicity reasons.

3D DAS VSP surveys can be utilised to obtain detailed knowledge of the geologic setting in the proximity of the boreholes. The higher resolution of the borehole data provides essential input for 3D geological models of the exploration sites. The range of potential applications includes stratigraphic models, structural information, mapping of existing discontinuities, which is crucial for locating the drilling site, and drill path optimisation.

In addition, the 3D DAS VSP cube can be used as an input for inversion to derive acoustic impedance and delineate petrophysical reservoir properties. Unlike point measurement with well logging methods, the borehole seismic cube provides the spatial distribution of the investigated parameters. Reservoir parameters such as density, porosity and permeability are essential for geothermal potential assessment. Therefore, these calculations are considered as a basis for numerical reservoir models.

Thus, for the heat in place analysis, the essential parameters such as reservoir size and depth estimations (V), and petrophysical properties estimations calculated via inversion process can be provided by 3D DAS VSP surveys.

High upfront costs of geothermal exploration require the application of more cost-effective methods for data acquisition. Compared with conventional 3D VSP surveys, DAS 3D VSP has incontestable advantages in terms of cost efficiency and data collection simplicity. A temporarily deployed fibre optic cable stays in the borehole during the whole acquisition and allows to collect the data from the entire length at once. This considerably minimises acquisition time and, consequently, reduces the financial costs required for data recordings. Thus, DAS 3D VSP acquired with the wireline cable method could potentially provide valuable input and become a regular part of the geothermal exploration process.

6.7 DAS for monitoring purposes

One of the key objectives for the application of wireline DAS data acquisition could be monitoring. However, this task is very challenging. DAS VSP data quality is affected by the influence of several factors: geological formation-specific, borehole-completion/condition specific, DAS cable design specific, DAS cable coupling, and DAS acquisition electronics system specifics (Verdel et al., 2018). To be able to separate effects related to changes in geological formation conditions, such as increased permeability after fracturing, one has to understand and be able to control other parts of this DAS transfer function chain.

Permanently installed distributed sensors provide the advantage of a well-controlled acquisition environment. Fibre optic cable has extended exploitation live and can stay in a borehole for decades without degrading and provides good coupling conditions. Therefore, this allows for a cost-effective and reliable method for targeted, detailed imaging and continuous site monitoring.

DAS technology is globally used for monitoring during hydraulic testing measurements. Fibre optic cables installed in borehole conditions can be used for micro-seismicity analysis to provide information about active discontinuities locations (Verdon et al., 2020). The results from the paper Wamriew et al. (2021) indicate that the trained network can detect and locate microseismic events from DAS data and simultaneously update the velocity model to a high degree of precision. This then can create a tool that can be used to fast track the decision-making process in the field and safety traffic light systems. Borodin and Segal (2020) evaluated the high-frequency DAS signal for the purpose of continuous monitoring of acoustic energy at depth levels and identification of different stages of fracturing in the data. The authors proved that this method is more effective than microseismic event monitoring methods since it provides accurate (3-8 m) real-time fracturing monitoring. The analysis of the low-frequency signals recorded at the Mirror Lake Fractured Rock Hydrology site successfully indicated fracture growth locations, allowing a better understanding of the hydraulic connectivity of the reservoir (Becker et al., 2020).

The application of the wireline DAS for monitoring is still limited. Chang and Nakata (2022) demonstrated a method based on cable reverberation signals analysis recorded at the Brady Geothermal Field, USA, which allowed to correlate the velocity changes with injection

intensity. Consequently, this method can be applied for borehole conditions monitoring and reservoir properties changes. The Dataset discussed by Lipus et al. (2022) also indicates a possible correlation between the loose part of the cable vibrations and changes in injection rates at the geothermal site Schäftlarnstraße in Munich, Germany. At the Groß Schönebeck, the analysis of the frequency changes of the coupling noise over the depth can be potentially used for injection rates monitoring. Therefore, additional studies are needed to prove the applicability of this method.

Another important application of the seismic data recorded using fibre-optic cables is time-lapse (4D) seismic surveys. The DAS with permanently installed cable provides seismic data suitable for identifying the changes in the reservoir, such as the CO2 plume migration, petrophysical quantification of the CO2 distribution in the reservoir, and geomechanical modelling. These installations allow on-demand data acquisition and consequently permit near real-time subsurface deformation risk models updates based on real-time data. Such measurements can serve as input data for subsurface stress and, as a result, storage containment risk management models. Hence, detailed risk quantification becomes possible. Successful case studies include onshore projects in Ketzin, Germany (Götz et al., 2018), CO2CRC Otway Project in Victoria, Australia (Correa et al., 2019), and offshore application (Tiwari et al., 2021; Wilson et al., 2021). Consequently, monitoring CCS facilities with fibre optics can ensure that caprock's integrity meets operational and regulatory objectives. Apart from CCS, some attempts are made to use permanently installed fibre optic cable in the oil and gas sector to monitor the changes in the reservoir, for instance, in the Culzean field, UK (Merry et al., 2021).

Typically, geothermal power plants are designed for a life span of at least 30 years. Therefore, to guarantee consistent and reliable functioning of the plant facilities during the production phase, it is crucial to have a reliable tool for monitoring. For instance, high salinity can lead to problems with heat extraction due to the precipitation of solid fractions and, as a result, significantly limit the life span of the created heat extraction loop. The characterisation of the geothermal fluid's chemical composition can show indications of adverse chemical effects such as increases in dissolved gas levels or changes in reservoir conditions leading to scaling. These processes can be monitored with seismic methods. By implementing state of the art monitoring techniques, such as DAS-VSP, combined with numerical models, potential risks could be identified and resolved, mitigating significant losses and resource degradation.

DAS VSP data collected at the Groß Schönebeck geothermal research platform was acquired using wireline cable, which was freely suspended inside two boreholes (Chapter 3). This creates not well controllable coupling conditions, which can cause coupling noise described in detail in Chapter 4. In addition, DAS channel depth allocation has certain ambiguity due to the geometry interpolation between a point close to the well head and well bottom. Combined with the current state of the wireline DAS technology development, all these factors create many challenges for understanding and controlling the coupling conditions of the wireline cable inside the borehole. More research is needed to understand the feasibility and constraints better for monitoring the geothermal reservoir using wireline DAS VSP techniques. After the reservoir treatment, a repeated DAS-VSP experiment can significantly contribute to expansion of the method application boundaries. Nevertheless, detailed studies on coupling conditions

of the cable inside the well casing and sophisticated analysis of the recorded waveforms are needed before applying well-established workflows for 4D processing.

Thus, the wireline DAS VSP method, individually adapted for each specific geothermal project, is a valuable method to achieve successful exploration of geothermal resources and, consequently, extraction and sustainable exploitation.

7

Conclusions

Wireline DAS VSP allows to create a detailed 3D subsurface image of the Gross Schönebeck deep geothermal reservoir. Structural interpretation of the 3D borehole cube revealed critical geological aspects which may play a key role in the further development of this in-situ geothermal laboratory.

Experiment design

Measurements with a fibre-optic cable freely suspended into the borehole can be quickly and cost-effectively applied for seismic data acquisition for geothermal exploration. A dense receiver array permits recording unaliased seismic data with a spatial sampling of a few meters continuously over the whole depth range of the borehole. Acquisition parameters, such as cable slack, vibroseis sweep parameters, source repetitions per VP, and gauge length, need to be optimised to record high-quality data. Vertical seismic profiling using wireline cable provides the advantage of a cost-effective and reliable method for targeted, detailed imaging of the studied reservoir area. Known survey planning techniques, such as ray tracing, allow to successfully avoid limitations related to the dependency on the angle of incidence during the experiment planning stage.

Data processing

Generally, a standard VSP processing workflow can be applied to the wireline DAS VSP data. However, certain data specifics should be considered, such as signal-to-noise ratio, resolution dependency on the gauge length, differences in polarities for reflections, etc.

The wireline DAS method has a well-known drawback related to limited controllable coupling conditions, which create coherent noise patterns in the data, and the directionality sensitivity. The cable can freely move inside the borehole at specific depth regions and create specific stripy or zig-zag noise patterns. Moreover, in some cases, the influence of the noise significantly disturbs the P-wave arrivals, making these parts of the data less reliable. The coupling noise problem can be treated by means of data processing. Different techniques can be used to tackle the coupling noise problem. However, some of them, like MPD with Gabor

atoms, can be relatively computationally intensive. Providing additional slack to the cable was tested as a method to reduce the coupling noise. This allowed decreasing the cable ringing at the expense of the general amplitude levels. Therefore, this problem is a cornerstone for the further development of the wireline acquisition method. It is beneficial to continue developing the acquisition method and find a solution for improved coupling.

Apart from inconsistent amplitude problems caused by noise and other unknown reasons, the acquired dataset at Groß Schönebeck has gaps in coverage. By testing, it was shown that the Kirchhoff migration algorithm with restricted aperture reduces migration artefacts. In combination with clipping of unreliable parts of the data cube, this imaging technique reduces the ambiguity of the imaging results. As a result of processing the 3D DAS VSP dataset, a detailed image of the subsurface can be created. Since VSP techniques allow recording acoustic data in-depth with one way travel time, the frequency content of the data is usually broader in comparison with 3D surface seismics.

Reservoir characterisation

Since the DAS VSP contains higher frequency components, it allows for more precise geological boundaries and primary reflectors tracking than a 3D surface seismic. At the Groß Schönebeck site, the mapped internal structure inside the Elbe reservoir sandstone layer can correspond to variations of the more porous reservoir thickness, which is currently considered a target for further reservoir treatment and heat extraction. Therefore, this new information on internal reservoir structure can help explain why a matrix-dominated approach did not succeed during the first attempts of the geothermal exploration of the site since the effective reservoir volume is significantly lower than expected. This type of data proved to be very valuable for input data for geological modelling, leading to a refinement of the geothermal/economic exploration models.

In addition, 3D DAS VSP shed light on complex interlayers inside the Upper Rotliegend interval, which previously stayed beyond detailed exploration due to previous seismic campaigns limitations. A Lower Rotliegend unconformity feature was tracked, providing more information on the volcanic rocks, which are considered as secondary exploration target after the Elbe reservoir sandstone layer.

Thus, VSP DAS data helps in reducing the uncertainty and exploration risks by providing valuable information for the geological characterisation of a site. Since the benefits from the application of the method also include a reduction in costs, and operational risks, 3D DAS VSP acquired with wireline cable may become a standard method for geothermal exploration. Due to the further development of DAS interrogators, it is also expected that their cost will decrease so that more high-quality data will be gained, helping develop subsurface use in the future.

References

Ahmed, F. Y.: Gas Detection Using Matching Pursuit Spectral Decomposition Seismic Attribute, in: Conference Proceedings, 74th EAGE Conference and Exhibition incorporating EUROPEC, Copenhagen, Denmark, 4-7 June 2012, p. P155, https://doi.org/10.3997/2214-4609.20148530, 2012.

Ahmed, K. A., Schwarz, B., and Gajewski, D.: Application of the 3D common-reflection-surface stack workflow in a crystalline rock environment, Geophysical Prospecting, 63, 990–998, https://doi.org/10.1111/1365-2478.12282, 2015.

Al-Mashhor, A. A., Al-Shuhail, A. A., Hanafy, S. M., and Mousa, W. A.: First Arrival Picking of Seismic Data Based on Trace Envelope, IEEE Access, 7, 128 806–128 815, https://doi.org/10.1109/ACCESS.2019.2939320, 2019.

Backus, M. M.: Water reverberations - their nature and elimination, Geophysics, 24, 233–261, https://doi.org/10.1190/1.1438579, 1959.

Baird, A.: Modelling the Response of Helically Wound DAS Cables to Microseismic Arrivals, in: Conference Proceedings, First EAGE Workshop on Fibre Optic Sensing, Amsterdam, the Netherlands, 9-11 March 2020, pp. 1–5, https://doi.org/10.3997/2214-4609.202030019, 2020.

Bakku, S. K., Fehler, M., Wills, P., Mestayer, J., Mateeva, A., and Lopez, J.: Vertical seismic profiling using distributed acoustic sensing in a hydrofrac treatment well, in: Expanded Abstracts, 84th SEG Annual Meeting, Denver, Colorado, USA, 26-31 October 2014, pp. 5024–5028, https://doi.org/10.1190/segam2014-1559.1, 2014.

Ballesteros, M.: Applying Petroleum Exploration Data to Identify Geothermal Targets in the North Perth Basin, Australia, in: Expanded Abstracts, AAPG European Region, Geothermal Cross Over Technology Workshop, Part II, Utrecht, The Netherlands, 18-19 April 2018, p. 80701, https://doi.org/10.1306/80701Ballesteros2019, 2018.

Barberan, C., Allanic, C., Avila, D., Hy-Billiot, J., Hartog, A., Frignet, B., and Lees, G.: Multi-offset Seismic Acquisition Using Optical Fiber Behind Tubing, in: Conference Proceedings, 74th EAGE Conference and Exhibition incorporating EUROPEC, Copenhagen, Denmark, 4-7 June 2012, pp. cp–293–00 802, https://doi.org/10.3997/2214-4609.20148798, 2012.

Barbier, E.: Geothermal energy technology and current status: an overview, Renewable and Sustainable Energy Reviews, 6, 3–65, https://doi.org/10.1016/S1364-0321(02)00002-3, 2002.

Bartels, T., Gelhaus, M., and Humphries, M.: VSP Measurements Used as a Tool for Sub Salt Near Field Development, in: Conference Proceedings, 77th EAGE Annual Meeting, Madrid, Spain, 1-4 June 2015, p. We N104 15, https://doi.org/10.3997/2214-4609.201412918, 2015.

Bauer, K., Moeck, I., Norden, B., Schulze, A., Weber, M., and Wirth, H.: Tomographic P wave velocity and vertical velocity gradient structure across the geothermal site Groß Schönebeck (NE German Basin): Relationship to lithology, salt tectonics, and thermal regime, Journal of Geophysical Research: Solid Earth, 115, https://doi.org/10.1029/2009JB006895, 2010.

Bauer, K., Norden, B., Ivanova, A., Stiller, M., and Krawczyk, C. M.: Wavelet transform-based seismic facies classification and modelling: application to a geothermal target horizon in the NE German Basin, Geophysical Prospecting, 68, 466–482, https://doi.org/10.1111/1365-2478.12853, 2020.

Becker, M. W., Coleman, T. I., and Ciervo, C. C.: Distributed Acoustic Sensing as a Distributed Hydraulic Sensor in Fractured Bedrock, Water Resources Research, 56, e2020WR028 140, https://doi.org/https://doi.org/10.1029/2020WR028140, 2020.

Bellefleur, G., Schetselaar, E., Wade, D., White, D., Enkin, R., and Schmitt, D. R.: Vertical seismic profiling using distributed acoustic sensing with scatter-enhanced fibre-optic cable at the Cu–Au New Afton porphyry deposit, British Columbia, Canada, Geophysical Prospecting, 68, 313–333, https://doi.org/10.1111/1365-2478.12828, 2020.

BJV Design Inc webpage, Vertical seismic profiles: URL `https://www.bjv-3ddesign.com/seismic-acquisition-geometries/vsp/`, (last access: 1 April 2022), 2022.

Blackburn, J., Daniels, J., Dingwall, S., Hampden-Smith, G., Leaney, S., Le Calvez, J., Nutt, L., Menkiti, H., Sanchez, A., and Schinelli, M.: Borehole seismic surveys: Beyond the vertical profile, Oilfield Review, 19, 20–35, URL `https://www.researchgate.net/publication/288369522_Borehole_seismic_surveys_Beyond_the_vertical_profile`, (last access: 1 April 2022), 2007.

Blöcher, G., Cacace, M., Reinsch, T., and Watanabe, N.: Evaluation of three exploitation concepts for a deep geothermal system in the North German Basin, Computers & Geosciences, 82, 120–129, https://doi.org/10.1016/j.cageo.2015.06.005, 2015.

Blöcher, G., Reinsch, T., Henninges, J., Milsch, H., Regenspurg, S., Kummerow, J., Francke, H., Kranz, S., Saadat, A., Zimmermann, G., and Huenges, E.: Hydraulic history and current state of the deep geothermal reservoir Groß Schönebeck, Geothermics, 63, 27–43, https://doi.org/10.1016/j.geothermics.2015.07.008, 2016.

Booth, A. D., Christoffersen, P., Schoonman, C., Clarke, A., Hubbard, B., Law, R., Doyle, S. H., Chudley, T. R., and Chalari, A.: Distributed Acoustic Sensing of Seismic Properties in a Borehole Drilled on a Fast-Flowing Greenlandic Outlet Glacier, Geophysical Research Letters, 47, e2020GL088 148, https://doi.org/10.1029/2020GL088148, 2020.

Borland, W., Hearn, R., and Sayed, A.: Improving the acquisition efficiency of acquiring borehole seismic data by recording optical distributed acoustic data on a wireline hybrid electrooptical cable, in: Expanded Abstracts, 86th SEG Annual Meeting, Dallas, Texas, USA, 6-21 October 2016, pp. 800–804, https://doi.org/10.1190/segam2016-13951115.1, 2016.

Borodin, I. and Segal, A.: Real-Time Hydraulic Fracturing Monitoring via Distributed Acoustic Sensing (DAS) Acquisition of Pumping Noise, in: Conference Proceedings, First EAGE Workshop on Fibre Optic Sensing, Amsterdam, the Netherlands, 9-11 March 2020, pp. 1–5, European Association of Geoscientists & Engineers, https://doi.org/10.3997/2214-4609.202030007, 2020.

Braile, L.: A Short Course in Seismic Reflection Profiling. Theory, Wave Propagation in Layered Media, Data Acquisition, Processing, Interpretation., Earth, Atmospheric, and Planetary Sciences Purdue University, West Lafayette, Indiana, USA, June, URL `http://citeseerx.ist.psu.edu/viewdoc/download?doi=10.1.1.601.7125&rep=rep1&type=pdf`, (last access: 1 April 2022), 2016.

Brauner, W., Dürschner, H., Koopmann, B., Marschall, R., and Peters, K.: Moving source profiling (MVP), Geophysical Prospecting, 36, 6–21, https://doi.org/10.1111/j.1365-2478.1988.tb02148.x, 1988.

Brisbourne, A. M., Kendall, M., Kufner, S.-K., Hudson, T. S., and Smith, A. M.: Downhole distributed acoustic seismic profiling at Skytrain Ice Rise, West Antarctica, The Cryosphere Discussions, 2021, 1–18, https://doi.org/10.5194/tc-2021-1, 2021.

Buness, H. A., von Hartmann, H., Rumpel, H.-M., Krawczyk, C. M., and Schulz, R.: Fault imaging in sparsely sampled 3D seismic data using common-reflection-surface processing and attribute analysis – a study in the Upper Rhine Graben, Geophysical Prospecting, 62, 443–452, https://doi.org/10.1111/1365-2478.12099, 2014.

Burg, J.: Maximum Energy Spectral Analysis, Ph.D. thesis, Stanford University, URL http://sepwww.stanford.edu/data/media/public/oldreports/sep06/06_01.pdf, (last access: 1 April 2022), 1975.

Burg, J. P.: The relationship between maximum entropy spectra and maximum likelihood spectra, Geophysics, 37, 375–376, https://doi.org/10.1190/1.1440265, 1972.

Cai, Z., Wang, Y., Liu, C., Zhang, Q., and Xu, X.: Cable noise analysis and suppression in DAS-VSP data, in: Expended abstracts, AAPG | SEG 2016 International Conference & Exhibition, Barcelona, Spain, 3-6 April 2016, pp. 170–170, https://doi.org/10.1190/ice2016-6501714.1, 2016.

Carrara, S., Shortall, R., and Uihlein, A.: Geothermal Energy - Technology Development Report 2020, Publications Office of the European Union, https://doi.org/10.2760/16847, 2020.

Casini, M., Ciuffi, S., Fiordelisi, A., Mazzotti, A., and Stucchi, E.: Results of a 3D seismic survey at the Travale (Italy) test site, Geothermics, 39, 4–12, https://doi.org/10.1016/j.geothermics.2009.11.003, 2010.

Chamorro, C. R., García-Cuesta, J. L., Mondéjar, M. E., and Pérez-Madrazo, A.: Enhanced geothermal systems in Europe: An estimation and comparison of the technical and sustainable potentials, Energy, 65, 250–263, https://doi.org/10.1016/j.energy.2013.11.078, 2014.

Chang, H. and Nakata, N.: Investigation of the time-lapse changes with the DAS borehole data at the Brady geothermal field using deconvolution interferometry, in: Expanded abstracts, 90th SEG Annual Meeting, online, 11-16 October 2020, pp. 3417–3421, https://doi.org/10.1190/segam2020-3426023.1, 2020.

Chang, H. and Nakata, N.: Investigation of Time-Lapse Changes with DAS Borehole Data at the Brady Geothermal Field Using Deconvolution Interferometry, Remote Sensing, 14, https://doi.org/10.3390/rs14010185, 2022.

Chen, J., Ning, J., Chen, W., Wang, X., Wang, W., and Zhang, G.: Distributed acoustic sensing coupling noise removal based on sparse optimization, Interpretation, 7, T373–T382, https://doi.org/10.1190/INT-2018-0080.1, 2019.

Chen, S., Li, Y., and Cheng, J.: Ground Roll Attenuation Applying Matching Pursuit Algorithm, in: Conference Proceedings, 80th EAGE Conference and Exhibition, Copenhagen, Denmark, 11-14 June 2018, p. TuP702, https://doi.org/10.3997/2214-4609.201800934, 2018.

Constantinou, A., Farahani, A., Cuny, T., and Hartog, A.: Improving DAS acquisition by real-time monitoring of wireline cable coupling, in: Expanded Abstracts, 86th SEG Annual Meeting, Dallas, Texas, USA, 16-21 October 2016, pp. 5603–5607, https://doi.org/10.1190/segam2016-13950092.1, 2016.

Correa, J.: Distributed Acoustic Sensing for Seismic Imaging and Reservoir Monitoring Applied to CO2 Geosequestration, Ph.D. thesis, Curtin University, URL http://hdl.handle.net/20.500.11937/75668, (last access: 1 April 2022), 2018.

Correa, J., Egorov, A., Tertyshnikov, K., Bona, A., Pevzner, R., Dean, T., Freifeld, B., and Marshall, S.: Analysis of signal to noise and directivity characteristics of DAS VSP at near and far offsets — A CO2CRC Otway Project data example, The Leading Edge, 36, 994a1–994a7, https://doi.org/10.1190/tle36120994a1.1, 2017.

Correa, J., Pevzner, R., Bona, A., Tertyshnikov, K., Freifeld, B., Robertson, M., and Daley, T.: 3D vertical seismic profile acquired with distributed acoustic sensing on tubing installation: A case study from the CO2CRC Otway Project, Interpretation, 7, SA11–SA19, https://doi.org/10.1190/INT-2018-0086.1, 2019.

Cosma, C., Heikkinen, P., and Keskinen, J.: Multiazimuth VSP for Rock Characterization of Deep Nuclear Waste Disposal Sites in Finland, In Book: Hardrock Seismic Exploration, chap. 14, pp. 207–226, Society of Exploration Geophysicists, https://doi.org/10.1190/1.9781560802396.ch14, 2012.

Crucelis, C. L. and Aldana, M.: Automatic first break picking in VSP data using fuzzy logic systems, in: Expanded Abstracts, 79th SEG Annual Meeting, Expanded Abstracts, pp. 4189–4193, https://doi.org/10.1190/1.3255747, 2009.

Daley, T., Miller, D., Dodds, K., Cook, P., and Freifeld, B.: Field testing of modular borehole monitoring with simultaneous distributed acoustic sensing and geophone vertical seismic profiles at Citronelle, Alabama, Geophysical Prospecting, 64, 1318–1334, https://doi.org/10.1111/1365-2478.12324, 2016.

Daley, T. M., Freifeld, B. M., Ajo-Franklin, J., Dou, S., Pevzner, R., Shulakova, V., Kashikar, S., Miller, D. E., Goetz, J., Henninges, J., and Lueth, S.: Field testing of fiber-optic distributed acoustic sensing (DAS) for subsurface seismic monitoring, The Leading Edge, 32, 699–706, https://doi.org/10.1190/tle32060699.1, 2013.

Dean, T., Constantinou, A., Cuny, T., Frignet, B., Hartog, A., Kimura, T., Kolesar, R., Lane, D., and Lees, G.: Vertical seismic profiles: Now just another log?, in: Expanded Abstracts, 85th SEG Annual Meeting, New Orleans, Louisiana, 18–23 October 2015, pp. 5544–5548, https://doi.org/10.1190/segam2015-5804007.1, 2015.

Dean, T., Cuny, T., and Hartog, A. H.: The effect of gauge length on axially incident P-waves measured using fibre optic distributed vibration sensing, Geophysical Prospecting, 65, 184–193, https://doi.org/10.1111/1365-2478.12419, 2017.

Didraga, C.: DAS VSP Recorded Simultaneously in Cemented and Tubing Installed Fiber Optic Cables, in: Conference Proceedings, 77th EAGE Conference and Exhibition, Madrid, Spain, 1-4 June 2015, p. Tu N118 14, https://doi.org/10.3997/2214-4609.201412738, 2015.

Dillon, P. B.: A comparison between Kirchhoff and GRT migration on VSP data, Geophysical Prospecting, 38, 757–777, https://doi.org/10.1111/j.1365-2478.1990.tb01873.x, 1990.

Dillon, P. B. and Thomson, R. C.: Offset source VSP surveys and their image reconstruction, Geophysical Prospecting, 32, 790–811, https://doi.org/10.1111/j.1365-2478.1984.tb00739.x, 1984.

Doornenbal, J., Abbink, O., Duin, E., Dusar, M., Hoth, P., Jasionowski, M., Lott, G., Mathiesen, A., Papiernik, B., Peryt, T., Veldkamp, J., and Wirth, H.: Introduction, stratigraphic framework and mapping, In book: Petroleum Geological Atlas of the Southern Permian Basin Area, Chapter 1, ISBN: 978-90-73781-61-0, EAGE Publications b.v., Houten, The Netherlands, 2010.

Dou, S., Lindsey, N., Wagner, A. M., Daley, T. M., Freifeld, B., Robertson, M., Peterson, J., Ulrich, C., Martin, E. R., and Ajo-Franklin, J. B.: Distributed Acoustic Sensing for Seismic Monitoring of The Near Surface: A Traffic-Noise Interferometry Case Study, Scientific Reports, 7, 11 620, https://doi.org/10.1038/s41598-017-11986-4, 2017.

Durka, P., Malinowska, U., Zieleniewska, M., O'Reilly, C., Różański, P., and Żygierewicz, J.: Spindles in Svarog: Framework and software for parametrization of EEG transients, Frontiers in Human Neuroscience, 9, 258, https://doi.org/https://dx.doi.org/10.3389/fnhum.2015.00258, 2015.

Egorov, A., Correa, J., Bóna, A., Pevzner, R., Tertyshnikov, K., Glubokovskikh, S., Puzyrev, V., and Gurevich, B.: Elastic full-waveform inversion of vertical seismic profile data acquired with distributed acoustic sensors, Geophysics, 83, R273–R281, https://doi.org/10.1190/geo2017-0718.1, 2018.

Elboth, T., Geoteam, F., Qaisrani, H. H., and Hertweck, T.: De-noising seismic data in the time-frequency domain, in: Expanded Abstracts, 78th SEG Annual Meeting, Las Vegas,Nevada, USA, 9-14 November 2008, pp. 2622–2626, https://doi.org/10.1190/1.3063887, 2008.

Every, M. J., King, R., and Weaver, D. S.: Vortex-excited vibrations of cylinders and cables and their suppression, Ocean Engineering, 9, 135–157, https://doi.org/10.1016/0029-8018(82)90010-5, 1982.

Frignet, B. and Hartog, A.: Optical vertical seismic profile on wireline cable, in: Conference Proceedings, SPWLA 55th Annual Logging Symposium, Abu Dhabi, UAE, 18–22 May 2014, pp. SPWLA–2014–FFFF, URL `https://onepetro.org/SPWLAALS/proceedings-pdf/SPWLA14/All-SPWLA14/SPWLA-2014-FFFF/1568971/spwla-2014-ffff.pdf`, (last access: 1 April 2022), 2014.

Friðleifsson, G. O., Elders, W. A., Zierenberg, R. A., Stefánsson, A., Fowler, A. P. G., Weisenberger, T. B., Harðarson, B. S., and Mesfin, K. G.: The Iceland Deep Drilling Project 4.5 km deep well, IDDP-2, in the seawater-recharged Reykjanes geothermal field in SW Iceland has successfully reached its supercritical target, Scientific Drilling, 23, 1–12, https://doi.org/10.5194/sd-23-1-2017, 2017.

Friðleifsson, G. Ó., Albertsson, A., Stefánsson, A., Þórólfsson, G., Mesfin, K. G., Sigurðsson, K., Sigurðsson, Ó., and Þór Gíslason: The Reykjanes DEEPEGS Demonstration Well - IDDP-2, in: Proceedings, European Geothermal Congress, The Hague, The Netherlands, 11-14 June 2019, URL http://europeangeothermalcongress.eu/wp-content/uploads/2019/07/51.pdf, (last access: 1 April 2022), 2019.

Galperin, E., Samokhvalov, M., and Kennett, P.: Vertical seismic profiling and its exploration potential, Modern Approaches in Geophysics, Springer Netherlands, ISBN: 9789027714503, 1985.

Garg, S. and Combs, J.: A reformulation of USGS volumetric "heat in place" resource estimation method, Geothermics, 55, 150–158, https://doi.org/10.1016/j.geothermics.2015.02.004, 2015.

Garrison, G. H., Þór Guðlaugsson, S., Ádám, L., Ingimundarson, A., Cladouhos, T. T., , and Petty, S.: Valhall dual-well 3D DAS VSP field trial and imaging for active wells, in: Proceedings, Geothermal Resources Council Annual Meeting, Geothermal Energy Here and Now: Sustainable, Clean, Flexible, Geothermal Resources Council Transactions Volume 40, Sacramento, California, USA, 23-26 October 2016, ISBN: 9781510837072, pp. 5582–5586, 2016.

Gast, R., Pasternak, M., Piske, J., , and Rasch, H.-J.: Rotliegend in Northeastern Germany: Regional Overview, Stratigraphy, Facies and Diagenesis, in Book: Results of hydrocarbon exploration in in Permian Rocks (Zechstein and Rotliegend) of the State of Brandenburg, Germany and in the Thuringian Basin between 1991 and 1996, Geologisches Jahrbuch, Schweizerbart, Stuttgart, Germany, ISBN 978-3-510-96347-8, 1998.

Gelchinsky, B. and Shtivelman, V.: Automatic picking of first arrivals and parameterization of traveltime curves, Geophysical Prospecting, 31, 915–928, https://doi.org/10.1111/j.1365-2478.1983.tb01097.x, 1983.

Genter, A., Evans, K., Cuenot, N., Fritsch, D., and Sanjuan, B.: Contribution of the exploration of deep crystalline fractured reservoir of Soultz to the knowledge of enhanced geothermal systems (EGS), Comptes Rendus Geoscience, 342, 502–516, https://doi.org/10.1016/j.crte.2010.01.006, 2010.

Grandi, S., Dean, M., and Tucker, O.: Efficient Containment Monitoring with Distributed Acoustic Sensing: Feasibility Studies for the Former Peterhead CCS Project, Energy Procedia, 114, 3889–3904, https://doi.org/10.1016/j.egypro.2017.03.1521, 2017.

Griffiths, L. J., Smolka, F. R., and Trembly, L. D.: Adaptive deconvolution: a new technique for processing time-varying seismic data, Geophysics, 42, 742–759, https://doi.org/10.1190/1.1440743, 1977.

Guglielmetti, L., Poletto, F., Corubolo, P., Bitri, A., Dezayes, C., Farina, B., Martin, F., Meneghini, F., Moscariello, A., Nawratil de Bono, C., and Schleifer, A.: Results of a walk-above vertical seismic profiling survey acquired at the Thônex-01 geothermal well (Switzerland) to delineate fractured carbonate formations for geothermal development, Geophysical Prospecting, 68, 1139–1153, https://doi.org/10.1111/1365-2478.12912, 2020.

Guterch, A., Wybraniec, S., Grad, M., Chadwick, A., Krawczyk, C., Ziegler, P., Thybo, H., and De Vos, W.: Crustal structure and structural framework, In Book: Petroleum Geological Atlas of the Southern Permian Basin Area, EAGE Publications b.v., Houten, The Netherlands, ISBN: 978-90-73781-61-0, 2010.

Gutiérrez-Negrín, L., Félix, I., Romo-Jones, J., and León, J.: Geothermal energy in Mexico: update and perspectives, in: Proceedings World Geothermal Congress 2020+1, Reykjavik, Iceland, April - October 2021, URL https://www.geothermal-energy.org/pdf/IGAstandard/WGC/2020/01004.pdf, (last access: 1 April 2022), 2021.

Göthel, M.: Lithologische Interpretation und stratigraphisches Niveau der reflexionsseismischen Horizonte im Untergrund Brandenburgs einschließlich Berlins, Brandenburgische Geowiss. Beiträge, 23, 85–90, URL https://lbgr.brandenburg.de/sixcms/media.php/9/BGB-1-2_16_Goethel_85-90.pdf, (last access: 1 April 2022), 2016.

Götz, J., Lüth, S., Henninges, J., and Reinsch, T.: Vertical seismic profiling using a daisy-chained deployment of fibre-optic cables in four wells simultaneously – Case study at the Ketzin carbon dioxide storage site, Geophysical Prospecting, 66, 1201–1214, https://doi.org/10.1111/1365-2478.12638, 2018.

Hardage, B.: Vertical Seismic Profiling: Principles, no. v. 14 in Handbook of geophysical exploration, Pergamon, ISBN: 9780080435183, 2000.

Hartog, A.: An Introduction to Distributed Optical Fibre Sensors, CRC Press, Boca Raton, Florida, USA, https://doi.org/10.1201/9781315119014, 2017.

Hartog, A., Frignet, B., Mackie, D., and Clark, M.: Vertical seismic optical profiling on wireline logging cable, Geophysical Prospecting, 62, 693–701, https://doi.org/10.1111/1365-2478.12141, 2014.

Hartog, A. H., Kotov, O., and Liokumovich, L.: The Optics of Distributed Vibration Sensing, in: Conference Proceedings, Second EAGE Workshop on Permanent Reservoir Monitoring 2013 – Current and Future Trends, Stavanger, Norway, 2-5 July 2013, pp. Th–01–04, https://doi.org/10.3997/2214-4609.20131301, 2013.

Henninges, J., Baumann, G., Brandt, W., Cunow, C., Poser, M., Schrötter, J., and Huenges, E.: A Novel Hybrid Wireline Logging System for Downhole Monitoring of Fluid Injection and Production in Deep Reservoirs, in: Conference Proceedings, 73rd EAGE Conference & Exhibition, Vienna, Austria, 23-27 May 2011, https://doi.org/10.3997/2214-4609.20149727, 2011.

Henninges, J., Götz, J., Jousset, P., Lüth, S., and Reinsch, T.: New Methods in Geophysical Exploration and Monitoring with DTS and DAS, in: Conference Proceedings, EAGE/DGG Workshop on Fibre Optic Technology in Geophysics, Potsdam, Germany, 31 March 2017, p. FrSR07, https://doi.org/10.3997/2214-4609.201700156, 2017.

Henninges, J., Martuganova, E., Stiller, M., Norden, B., and Krawczyk, C. M.: Wireline distributed acoustic sensing allows 4.2 km deep vertical seismic profiling of the Rotliegend 150°C geothermal reservoir in the North German Basin, Solid Earth, 12, 521–537, https://doi.org/10.5194/se-12-521-2021, 2021a.

Henninges, J., Martuganova, E., Stiller, M., Norden, B., and Krawczyk, C. M.: DAS-VSP Data from the Feb. 2017 Survey at the Groß Schönebeck Site, Germany, GFZ Data Services, https://doi.org/10.5880/GFZ.4.8.2021.001, 2021b.

Hernández-Ochoa, A., Iglesias, E., López-Blanco, S., Martínez Estrella, J., Paredes Soberanes, A., Torres Rodríguez, R., Reyes Picasso, N., González Reyes, I., Lira Argüello, R., Prol Ledesma, R., and Espinoza Ojeda, O.: Assessment of the Technical Potential for Enhanced Geothermal Systems in Mexico, in: Proceedings World Geothermal Congress 2020+1, Reykjavik, Iceland, March-October 2021, URL `https://www.geothermal-energy.org/explore/our-databases/conference-paper-database/`, (last access: 1 April 2022), 2021.

Hinds, R. C., Anderson, N. L., Kuzmiski, R. D., and Hardage, B. A.: VSP Interpretive Processing: Theory and Practice, Society of Exploration Geophysicists, https://doi.org/10.1190/1.9781560801894, 1996.

Hloušek, F., Hellwig, O., and Buske, S.: Three-dimensional focused seismic imaging for geothermal exploration in crystalline rock near Schneeberg, Germany, Geophysical Prospecting, 63, 999–1014, https://doi.org/10.1111/1365-2478.12239, 2015.

Hogarth, R. and Holl, H.-G.: Lessons learned from the Habanero EGS project., in: Conference Proceedings, Geothermal Resources Council Annual Meeting, Geothermal Energy: Power to Do More, Geothermal Resources Council Transactions Volume 41, Salt Lake City, UT, USA, 1 - 4 October, pp. 865–877, ISSN: 0193–5933, 2017.

Hu, K., Brent, T., Issler, D., and Chen, Z.: Synthetic seismograms from borehole seismic data and well logs, Beaufort-Mackenzie Basin., URL `https://emrlibrary.gov.yk.ca/gsc/open_files/6056.pdf`, (last access: 1 April 2022), 2015.

Huang, Y., Zhang, M., Gao, K., Sabin, A., and Huang, L.: Imaging Complex Subsurface Structures for Geothermal Exploration at Pirouette Mountain and Eleven-Mile Canyon in Nevada, Frontiers in Earth Science, 9, 1–13, https://doi.org/10.3389/feart.2021.782901, 2021.

Hudson, T., Baird, A., Kendall, J., Kufner, S., Brisbourne, A., Smith, A., Butcher, A., Chalari, A., and Clarke, A.: Distributed Acoustic Sensing in Antarctica: What we can learn for studying microseismicity elsewhere, in: Conference Proceedings, EAGE GeoTech 2021 Second EAGE Workshop on Distributed Fibre Optic Sensing, no. 1 in Online, 1-2 March 2021, pp. 1–5, https://doi.org/10.3997/2214-4609.202131037, 2021.

Huenges, E., Trautwein-Bruns, U., Legarth, B., and Zimmermann, G.: Fluid Pressure Variation in a Sedimentary Geothermal Reservoir in the North German Basin: Case Study Groß Schönebeck, Pure and Applied Geophysics, 163, 2141–2152, https://doi.org/10.1007/s00024-006-0122-2, 2006.

Humphries, M., Vidal, J., and de Dios, J.: VSP Monitoring for CO2 Migration Tracking in Fractured Rock Massifs, in: Conference Proceedings, 77th EAGE Conference and Exhibition, no. 1 in Madrid, Spain, 1-4 June 2015, pp. 1–5, European Association of Geoscientists & Engineers, https://doi.org/10.3997/2214-4609.201412672, 2015.

IEA Geothermal: The 2019 Annual Report, IEA Geothermal, URL `https://iea-gia.org/publications-2/annual-reports/`, (last access: 1 April 2022), 2020.

Jia, Y. and Ma, J.: What can machine learning do for seismic data processing? An interpolation application, Geophysics, 82, V163–V177, https://doi.org/10.1190/geo2016-0300.1, 2017.

Jiang, T., Zhan, G., Hance, T., Sugianto, S., Soulas, S., and Kjos, E.: Valhall dual-well 3D DAS VSP field trial and imaging for active wells, in: Expanded Abstracts, 86th SEG Annual Meeting, Dallas, Texas, USA, 16-21 October 2016, pp. 5582–5586, https://doi.org/10.1190/segam2016-13871754., 2016.

Jousset, P., Reinsch, T., Ryberg, T., Blanck, H., Clarke, A., Aghayev, R., Hersir, G., Henninges, J., Weber, M., and Krawczyk, C. M.: Dynamic strain determination using fibre-optic cables allows imaging of seismological and structural features, Nature Communications, 9, 2509, https://doi.org/10.1038/s41467-018-04860-y, 2018.

Kamal, A.: Waves, Springer, Berlin, Heidelberg, https://doi.org/10.1007/978-3-642-11943-9_8, 2011.

Karray, M. and Lefebvre, G.: Modal Analysis of Surface Waves (MMASW)Technique for Hazard Studies, In book: Shear Wave Velocity Measurement Guidelines for Canadian Seismic Site Characterization in Soil and Rock, pp. Open File 7078, 67–76, Geological Survey of Canada, https://doi.org/10.4095/291760, 2012.

Karrenbach, M., Kahn, D., Cole, S., Ridge, A., Boone, K., Rich, J., Silver, K., and Langton, D.: Hydraulic-fracturing-induced strain and microseismic using in situ distributed fiber-optic sensing, The Leading Edge, 36, 837–844, https://doi.org/10.1190/tle36100837.1, 2017.

Kasahara, J., Hasada, Y., Haruyasu, K., Mikada, H., and Fujise, Y.: A DAS-VSP Study Around the Geothermal Field of the Ohnuma Geothermal Power Plant in Northern Honshu, Japan, in: Proceedings, 46th Workshop on Geothermal Reservoir Engineering, Stanford University, Stanford, California, USA, 15-17 February 2021, pp. SGP–TR–218, URL `https://pangea.stanford.edu/ERE/db/GeoConf/papers/SGW/2021/Kasahara.pdf`, (last access: 1 April 2022), 2021.

Konietzky, H.: Deep geothermal energy, TU Bergakademie Freiberg, URL `https://tu-freiberg.de/sites/default/files/media/professur-felsmechanik-32204/E-book/49_deep_geothermal_energy_0.pdf`, (last access: 1 April 2022), 2020.

Krawczyk, C. M.: Wie Glasfaserkabel als Geosensoren zur Erkundung und Überwachung des Untergrunds genutzt werden können – Anwendungen und Potenzial von ortsverteilten faseroptischen Messungen (How fibre optic cables can be used as geosensors to explore and monitor the subsurface – Applications and Potential of distributed acoustic sensing)., Brandenburgische Geowiss. Beiträge, 28 (1/2), 15–28, URL `https://lbgr.brandenburg.de/sixcms/media.php/9/BGB%201_2_2021_Krawczyk_dl.pdf`, (last access: 1 April 2022), 2021.

Krawczyk, C. M., Stiller, M., Bauer, K., Norden, B., Henninges, J., Ivanova, A., and Huenges, E.: 3-D seismic exploration across the deep geothermal research platform Groß Schönebeck north of Berlin/Germany, Geothermal Energy, 7, 15, https://doi.org/10.1186/s40517-019-0131-x, 2019.

Krischer, L., Megies, T., Barsch, R., Beyreuther, M., Lecocq, T., Caudron, C., and Wassermann, J.: ObsPy: A bridge for seismology into the scientific Python ecosystem, Computational Science & Discovery, 8, 014 003, https://doi.org/10.1088/1749-4699/8/1/014003, 2015.

Kuvshinov, B.: Interaction of helically wound fibre-optic cables with plane seismic waves, Geophysical Prospecting, 64, 671–688, https://doi.org/10.1111/1365-2478.12303, 2016.

Kuś, R., Różański, P. T., and Durka, P. J.: Multivariate matching pursuit in optimal Gabor dictionaries: theory and software with interface for EEG/MEG via Svarog, BioMedical Engineering OnLine, 12, 94, https://doi.org/10.1186/1475-925X-12-94, 2013.

Kästner, F., Giese, R., Planke, S., Millett, J. M., and Ólafur G. Flóvenz: Seismic imaging in the Krafla high-temperature geothermal field, NE Iceland, using zero- and far-offset vertical seismic profiling (VSP) data, Journal of Volcanology and Geothermal Research, 391, 106 315, https://doi.org/10.1016/j.jvolgeores.2018.02.016, 2020.

Lellouch, A., Lindsey, N. J., Ellsworth, W. L., and Biondi, B. L.: Comparison between Distributed Acoustic Sensing and Geophones: Downhole Microseismic Monitoring of the FORGE Geothermal Experiment, Seismological Research Letters, 91, 3256–3268, https://doi.org/10.1785/0220200149, 2020.

Lellouch, A., Schultz, R., Lindsey, N., Biondi, B., and Ellsworth, W.: Low-Magnitude Seismicity With a Downhole Distributed Acoustic Sensing Array—Examples From the FORGE Geothermal Experiment, Journal of Geophysical Research: Solid Earth, 126, e2020JB020 462, https://doi.org/10.1029/2020JB020462, 2021.

Li, Z. and Zhan, Z.: Pushing the limit of earthquake detection with distributed acoustic sensing and template matching: a case study at the Brady geothermal field, Geophysical Journal International, 215, 1583–1593, https://doi.org/10.1093/gji/ggy359, 2018.

Liang, S., Hu, T., Cui, D., and Ding, P.: Weak signal enhancement using adaptive local similarity and neighboring super-virtual trace for first arrival picking, Journal of Geophysics and Engineering, 17, 1005–1015, https://doi.org/10.1093/jge/gxaa059, 2020.

Lim, T., Fujimoto, A., Kobayashi, T., and Mondanos, M.: DAS 3DVSP Data Acquisition for Methane Hydrate Research, in: Conference Proceedings, EAGE Workshop on Fiber Optic Sensing for Energy Applications in Asia Pacific, Kuala Lumpur, Malaysia, 9-11 November 2020, pp. 1–5, https://doi.org/10.3997/2214-4609.202070014, 2020.

Lindsey, N. J., Rademacher, H., and Ajo-Franklin, J. B.: On the Broadband Instrument Response of Fiber-Optic DAS Arrays, Journal of Geophysical Research: Solid Earth, 125, e2019JB018 145, https://doi.org/10.1029/2019JB018145, e2019JB018145 10.1029/2019JB018145, 2020.

Lior, I., Sladen, A., Rivet, D., Ampuero, J.-P., Hello, Y., Becerril, C., Martins, H. F., Lamare, P., Jestin, C., Tsagkli, S., and Markou, C.: On the Detection Capabilities of Underwater Distributed Acoustic Sensing, Journal of Geophysical Research: Solid Earth, 126, e2020JB020 925, https://doi.org/10.1029/2020JB020925, 2021.

Lipus, M. P., Schölderle, F., Reinsch, T., Wollin, C., Krawczyk, C., Pfrang, D., and Zosseder, K.: Dynamic motion monitoring of a 3.6 km long steel rod in a borehole during cold-water injection with distributed fiber-optic sensing, Solid Earth, 13, 161–176, https://doi.org/10.5194/se-13-161-2022, 2022.

Lizarralde, D. and Swift, S.: Smooth inversion of VSP traveltime data, Geophysics, 64, 659–661, https://doi.org/10.1190/1.1444574, 1999.

Lorenzo, C., Soto, J., Palma, H., Diez, H., and Pérez, H.: Vertical Seismic Profile (VSP) in Injection Well AZ-03, Los Azufres Geothermal Field, México, in: Proceedings, World Geothermal Congress, Melbourne, Australia, 19-25 April 2015, URL https://www.geothermal-energy.org/pdf/IGAstandard/WGC/2015/11009.pdf, (last access: 1 April 2022), 2015.

Luo, F., Feng, B., and Wang, H.: Automatic first-arrival picking method via intelligent Markov optimal decision processes, Journal of Geophysics and Engineering, 18, 406–417, https://doi.org/10.1093/jge/gxab026, 2021.

Lüschen, E., Wolfgramm, M., Fritzer, T., Dussel, M., Thomas, R., and Schulz, R.: 3D seismic survey explores geothermal targets for reservoir characterization at Unterhaching, Munich, Germany, Geothermics, 50, 167–179, https://doi.org/10.1016/j.geothermics.2013.09.007, 2014.

Maćkowski, T., Sowi|e|bB, A., and Wachowicz-Pyzik, A.: Seismic Methods in Geothermal Water Resource Exploration: Case Study from Łódź Trough, Central Part of Poland, Geofluids, 2019, 3052 806, https://doi.org/10.1155/2019/3052806, 2019.

Mallat, S. G. and Zhang, Z.: Matching pursuits with time-frequency dictionaries, IEEE Transactions on Signal Processing, 41, 3397–3415, https://doi.org/10.1109/78.258082, 1993.

Martin, E. R., Lindsey, N. J., Ajo-Franklin, J. B., and Biondi, B. L.: Introduction to Interferometry of Fiber-Optic Strain Measurements, in Book: Distributed Acoustic Sensing in Geophysics, chap. 9, pp. 111–129, American Geophysical Union (AGU), https://doi.org/10.1002/9781119521808.ch9, 2021.

Martuganova, E., Stiller, M., Bauer, K., Henninges, J., and Krawczyk, C. M.: Cable reverberations during wireline distributed acoustic sensing measurements: their nature and methods for elimination, Geophysical Prospecting, 69, 1034–1054, https://doi.org/10.1111/1365-2478.13090, 2021.

Martuganova, E., Stiller, M., Henninges, J., and Krawczyk, C. M.: 3D deep geothermal reservoir imaging with wireline distributed acoustic sensing in two boreholes, Solid Earth Discussions, https://doi.org/10.5194/se-2021-138, In review.

Mateeva, A., Lopez, J., Potters, H., Mestayer, J., Cox, B., Kiyashchenko, D., Wills, P., Grandi, S., Hornman, K., Kuvshinov, B., Berlang, W., Yang, Z., and Detomo, R.: Distributed acoustic sensing for reservoir monitoring with vertical seismic profiling, Geophysical Prospecting, 62, 679–692, https://doi.org/10.1111/1365-2478.12116, 2014.

Merry, A., Lesnikov, V., Jones, R., Mitra, A., and Rennison, P.: A DAS VSP Pilot Survey for 3D Imaging and 4D Monitoring at the Culzean Field, UKCS, in: Conference Proceedings, 82nd EAGE Annual Conference & Exhibition, no. 1 in Amsterdam, The Netherlands, 18-21 October 2021, pp. 1–5, https://doi.org/10.3997/2214-4609.202112653, 2021.

Mestayer, J., Cox, B., Wills, P., Kiyashchenko, D., Lopez, J., Costello, M., Bourne, S., Ugueto, G., Lupton, R., Solano, G., Hill, D., and Lewis, A.: Field trials of distributed acoustic sensing for geophysical monitoring, in: Expanded Abstracts, 81st SEG Annual Meeting, San Antonio, Texas, USA, 18-23 September 2011, pp. 4253–4257, https://doi.org/10.1190/1.3628095, 2011.

Miller, D., Parker, T., Kashikar, S., Todorov, M., and Bostick, T.: Vertical Seismic Profiling Using a Fibre-optic Cable as a Distributed Acoustic Sensor, in: Conference Proceedings, 74th EAGE Conference and Exhibition incorporating EUROPEC, Copenhagen, Denmark, 4-7 June 2012, p. Y004, https://doi.org/10.3997/2214-4609.20148799, 2012.

Miller, D., Coleman, T., Zeng, X., Patterson, J., Reinisch, E., Wang, H., Fratta, D., Trainor-Guitton, W., Thurber, C., Robertson, M., Feigl, K., and Team, T.: DAS and DTS at Brady Hot Springs: Observations about Coupling and Coupled Interpretations, in: Proceedings, 43rd Workshop on Geothermal Reservoir Engineering, Stanford University, Stanford, California, USA, 12–14 February 2018, URL https://pangea.stanford.edu/ERE/pdf/IGAstandard/SGW/2018/Miller.pdf, (last access: 1 April 2022), 2018.

Moeck, I., Schandelmeier, H., and Holl, H.-G.: The stress regime in a Rotliegend reservoir of the Northeast German Basin, International Journal of Earth Sciences, 98, 1643–1654, https://doi.org/10.1007/s00531-008-0316-1, 2009.

Molteni, D., Williams, M. J., and Wilson, C.: Detecting microseismicity using distributed vibration, First Break, 35, 51–55, https://doi.org/10.3997/1365-2397.35.4.87841, 2017.

Mondanos, M. and Coleman, T.: Application of distributed fibre-optic sensing to geothermal reservoir characterization and monitoring, First Break, 37, 51–56, https://doi.org/10.3997/1365-2397.n0040, 2019.

Muffler, P. and Cataldi, R.: Methods for regional assessment of geothermal resources, Geothermics, 7, 53–89, https://doi.org/10.1016/0375-6505(78)90002-0, 1978.

Müller, G.: Theory of Elastic Waves, (Scientific Technical Report STR; 07/03, Deutsches GeoForschungsZentrum GFZ, Potsdam, Germany, https://doi.org/10.2312/GFZ.b103-07037, 2007.

Munn, J., Coleman, T., Parker, B., Mondanos, M., and Chalari, A.: Novel cable coupling technique for improved shallow distributed acoustic sensor VSPs, Journal of Applied Geophysics, 138, 72–79, https://doi.org/10.1016/j.jappgeo.2017.01.007, 2017.

Naldrett, G., Parker, T., Shatalin, S., Mondanos, M., and Farhadiroushan, M.: High-resolution Carina distributed acoustic fibreoptic sensor for permanent reservoir monitoring and extending the reach into subsea fields, First Break, 38, 71–76, https://doi.org/10.3997/1365-2397.fb2020012, 2020.

Niedzwecki, J. and Fang, S. M.: Suppression of flow-induced vibrations using ribbon fairings, International Journal of Computational Methods and Experimental Measurements, 1, 395–405, https://doi.org/10.2495/CMEM-V1-N4-395-405, 2013.

Nishimura, T., Emoto, K., Nakahara, H., Miura, S., Yamamoto, M., Sugimura, S., Ishikawa, A., and Kimura, T.: Source location of volcanic earthquakes and subsurface characterization using fiber-optic cable and distributed acoustic sensing system, Scientific Reports, 11, 6319, https://doi.org/10.1038/s41598-021-85621-8, 2021.

Norden, B., Bauer, K., and Krawczyk, C. M.: From pilot site knowledge via integrated reservoir characterization to utilization perspectives of a deep geothermal reservoir: 3D geological model at the research platform Groß Schönebeck in the Northeast German Basin., Geothermal Energy, https://doi.org/10.21203/rs.3.rs-1660889/v1, in revision.

Ozbek, A., Özdemir, A., and Vassallo, M.: Interpolation of Irregularly Sampled Data by Matching Pursuit, in: Conference Proceedings, 70th EAGE Conference and Exhibition incorporating SPE EUROPEC, Rome, Italy, 9-12 June 2008, p. G025, https://doi.org/10.3997/2214-4609.20147734, 2008.

Parker, T., Shatalin, S., and Farhadiroushan, M.: Distributed Acoustic Sensing – a new tool for seismic applications, First Break, 32, https://doi.org/10.3997/1365-2397.2013034, 2014.

Place, J., Sausse, J., Marthelot, J.-M., Diraison, M., Géraud, Y., and Naville, C.: 3-D mapping of permeable structures affecting a deep granite basement using isotropic 3C VSP data, Geophysical Journal International, 186, 245–263, https://doi.org/10.1111/j.1365-246X.2011.05012.x, 2011.

Pussak, M., Bauer, K., Stiller, M., and Bujakowski, W.: Improved 3D seismic attribute mapping by CRS stacking instead of NMO stacking: Application to a geothermal reservoir in the Polish Basin, Journal of Applied Geophysics, 103, 186–198, https://doi.org/10.1016/j.jappgeo.2014.01.020, 2014.

Rahim, M. A., Ghazali, A., and Davis, M.: Joint Imaging Of 3D Fiber Optic Das Vsp And Obn To Solve Shallow Gas Cloud Problem In Bokor Field Malaysia, in: Conference Proceedings, EAGE Conference on Reservoir Geoscience, no. 1 in Kuala Lumpur, Malaysia, 3-5 December 2018, pp. 1–6, European Association of Geoscientists & Engineers, https://doi.org/10.3997/2214-4609.201803225, 2018.

Raisutis, R., Kazys, R., Mazeika, L., Samaitis, V., and Zukauskas, E.: Propagation of Ultrasonic Guided Waves in Composite Multi-Wire Ropes, Materials, 9, 451, https://doi.org/10.3390/ma9060451, 2016.

Rehling, J., Siemerink, E., Borgh, M. T., and Zaalberg-Metselaar, G.: The Dutch Scan Geothermal Seismic Exploration Program – Current Status and Future Plans, in: Conference Proceedings, 82nd EAGE Annual Conference & Exhibition, no. 1 in Amsterdam, The Netherlands, 18-21 October 2021, pp. 1–5, https://doi.org/10.3997/2214-4609.202010751, 2021.

Reinhardt, H.: Structure of Northeast Germany: Regional Depth and Thickness Maps of Permian to Tertiary Intervals Compiled from Seismic Reflection Data, in Book: Generation, Accumulation and Production of Europe's Hydrocarbons III. Special Publication of the European Association of Petroleum Geoscientists No. 3, pp. 155–165, Springer, Berlin, Heidelberg, https://doi.org/10.1007/978-3-642-77859-9_13, 1993.

Reinsch, T., Henninges, J., Götz, J., Jousset, P., Bruhn, D., and Lüth, S.: Distributed Acoustic Sensing Technology for Seismic Exploration in Magmatic Geothermal Areas, in: Proceedings, World Geothermal Congress, Melbourne, Australia, 16–24 April 2015, URL `https://gfzpublic.gfz-potsdam.de/rest/items/item_1182900_4/component/file_1182899/content`, (last access: 1 April 2022), 2015.

Reiser, F., Schmelzbach, C., Sollberger, D., Maurer, H., Greenhalgh, S., Planke, S., Kästner, F., Ólafur Flóvenz, Giese, R., Halldórsdóttir, S., and Hersir, G. P.: Imaging the high-temperature geothermal field at Krafla using vertical seismic profiling, Journal of Volcanology and Geothermal Research, 391, 106 474, https://doi.org/10.1016/j.jvolgeores.2018.10.019, 2020.

Richards, A.: Quantitative Seismology: Theory and Methods, Geological Magazine, Volumes I and II, 208–208, https://doi.org/10.1017/S0016756800034439, 1981.

Robein, E.: Seismic Imaging: A Review of the Techniques, Their Principles, Merits and Limitations, Education tour series, ISBN: 9789073781788, EAGE Publications, URL `https://books.google.de/books?id=QbDySAAACAAJ`, 2010.

Ryberg, T. and Haberland, C.: Bayesian inversion of refraction seismic traveltime data, Geophysical Journal International, 212, 1645–1656, https://doi.org/10.1093/gji/ggx500, 2018.

Sabbione, J. I. and Velis, D.: Automatic first-breaks picking: New strategies and algorithms, Geophysics, 75, V67–V76, https://doi.org/10.1190/1.3463703, 2010.

Salaun, N., Toubiana, H., Mitschler, J.-B., Gigou, G., Carriere, X., Maurer, V., and Richard, A.: High-resolution 3D seismic imaging and refined velocity model building improve the image of a deep geothermal reservoir in the Upper Rhine Graben, The Leading Edge, 39, 857–863, https://doi.org/10.1190/tle39120857.1, 2020.

Salisbury, M. H., Harvey, C. W., and Matthews, L.: The Acoustic Properties of Ores and Host Rocks in Hardrock Terranes, In Book: Hardrock Seismic Exploration, chap. 1, pp. 9–19, Society of Exploration Geophysicists, https://doi.org/10.1190/1.9781560802396.ch1, 2012.

Sallas, J. J.: Seismic vibrator control and the downgoing P-wave, Geophysics, 49, 732–740, https://doi.org/10.1190/1.1441701, 1984.

Sausse, J., Dezayes, C., Dorbath, L., Genter, A., and Place, J.: 3D model of fracture zones at Soultz-sous-Forêts based on geological data, image logs, induced microseismicity and vertical seismic profiles, Comptes Rendus Geoscience, 342, 531–545, https://doi.org/10.1016/j.crte.2010.01.011, 2010.

Schilke, S., Donno, D., Chauris, H., Hartog, A., Farahani, A., and Pico, Y.: Numerical evaluation of sensor coupling of distributed acoustic sensing systems in vertical seismic profiling, in: Expanded Abstracts, 86th SEG Annual Meeting, Dallas, Texas, USA, 16-21 October 2016, pp. 677–681, https://doi.org/10.1190/segam2016-13527500.1, 2016.

Schilke, S., Donno, D., Hartog, A., and Chauris, H.: DAS and its Coupling for VSP Applications Using Wireline Cable, in: Conference Proceedings, EAGE/DGG Workshop on Fibre Optic Technology in Geophysics, Potsdam, Germany, 31 March 2017, p. FrSR09, https://doi.org/10.3997/2214-4609.201700158, 2017.

Schleicher, J., Hubral, P., Tygel, M., and Jaya, M. S.: Minimum apertures and Fresnel zones in migration and demigration, Geophysics, 62, 183–194, https://doi.org/10.1190/1.1444118, 1997.

Schmelzbach, C., Greenhalgh, S., Reiser, F., Girard, J.-F., Bretaudeau, F., Capar, L., and Bitri, A.: Advanced seismic processing/imaging techniques and their potential for geothermal exploration, Interpretation, 4, SR1–SR18, https://doi.org/10.1190/INT-2016-0017.1, 2016.

Semnani, A., Wang, L., Ostadhassan, M., Nabi-Bidhendi, M., and Araabi, B. N.: Time-frequency decomposition of seismic signals via quantum swarm evolutionary matching pursuit, Geophysical Prospecting, 67, 1701–1719, https://doi.org/10.1111/1365-2478.12767, 2019.

Sheriff, R. E. and Geldart, L. P.: Exploration Seismology, Cambridge University Press, 2 edn., https://doi.org/10.1017/CBO9781139168359, 1995.

Shultz, W. and Simmons, J.: 3D DAS VSP in unconventionals: A case study, in: Expanded Abstracts, 89th SEG Annual Meeting, San Antonio, Texas, USA, 15-20 September 2019, pp. 979–983, https://doi.org/10.1190/segam2019-3214518.1, 2019.

Siler, D. L. and Pepin, J. D.: 3-D Geologic Controls of Hydrothermal Fluid Flow at Brady geothermal field, Nevada, USA, Geothermics, 94, 102 112, https://doi.org/10.1016/j.geothermics.2021.102112, 2021.

Simm, R. and White, R.: Phase, polarity and the interpreter's wavelet, First Break, 20, 277–281, https://doi.org/10.1046/j.1365-2397.2002.00277.x, 2002.

Song, J.-G., Gong, Y.-L., and Li, S.: High-resolution frequency-domain Radon transform and variable-depth streamer data deghosting, Applied Geophysics, 12, 564–572, https://doi.org/10.1007/s11770-015-0525-x, 2015.

Spagnolini, U.: Adaptive picking of refracted first arrivals, Geophysical Prospecting, 39, 293–312, https://doi.org/10.1111/j.1365-2478.1991.tb00314.x, 1991.

Spica, Z. J., Nishida, K., Akuhara, T., Pétrélis, F., Shinohara, M., and Yamada, T.: Marine Sediment Characterized by Ocean-Bottom Fiber-Optic Seismology, Geophysical Research Letters, 47, e2020GL088 360, https://doi.org/10.1029/2020GL088360, 2020a.

Spica, Z. J., Perton, M., Martin, E. R., Beroza, G. C., and Biondi, B.: Urban Seismic Site Characterization by Fiber-Optic Seismology, Journal of Geophysical Research: Solid Earth, 125, e2019JB018 656, https://doi.org/10.1029/2019JB018656, 2020b.

Stiller, M., Krawczyk, C. M., Bauer, K., Henninges, J., Norden, B., Huenges, E., and Spalek, A.: 3D-Seismik am Geothermieforschungsstandort Groß Schönebeck, BBR - Fachmagazin für Brunnen- und Leitungsbau, 1, 84—91, (last access: 1 April 2022), 2018.

Sun, J.: Limited-aperture migration, Geophysics, 65, 584–595, https://doi.org/10.1190/1.1444754, 2000.

The European Commission: Report from the commission to the European parliament and the council. Progress on competitiveness of clean energy technologies. Part 4/5, Publications Office of the European Union, Brussels (Belgium), URL `https://eur-lex.europa.eu/resource.html?uri=cellar:871975a1-0e05-11eb-bc07-01aa75ed71a1.0001.02/DOC_4&format=PDF`, (last access: 1 April 2022), 2021.

The ObsPy Development Team: ObsPy 1.1.0, https://doi.org/10.5281/ZENODO.165135, 2017.

The Svarog developers team: BrainTech/matching-pursuit, URL `https://github.com/BrainTech/matching-pursuit`, 2014.

The Svarog developers team: BrainTech/svarog, URL `https://github.com/BrainTech/svarog`, 2016.

Thomsen, L.: Weak elastic anisotropy, Geophysics, 51, 1954–1966, https://doi.org/10.1190/1.1442051, 1986.

Titov, A., Kazei, V., AlDawood, A., Alfataierge, E., Bakulin, A., and Osypov, K.: Quantification of DAS VSP Quality: SNR vs. Log-Based Metrics, Sensors, 22, 1–13, https://doi.org/10.3390/s22031027, 2022.

Tiwari, P. K., Das, D. P., Patil, P. A., Chidambaram, P., Low, Z., Chandran, P. K., Abdul Hamid, M. K., and Tewari, R. D.: Offshore MMV Planning for Sustainability of CO2 Storage in a Depleted Carbonate Reservoir, Malaysia, in: Conference Proceedings, The SPE/IATMI Asia Pacific Oil & Gas Conference and Exhibition, Online, 12–14 October 2021, https://doi.org/10.2118/205692-MS, 2021.

Trainor-Guitton, W., Guitton, A., Jreij, S., Powers, H., Sullivan, C. B., Simmons, J., and Porotomo Team: 3D Imaging from vertical DAS fiber at Brady's Natural Laboratory, in: Proceedings, 43rd Workshop on Geothermal Reservoir Engineering, Stanford University, Stanford, California, USA, 12–14 February 2018, URL `https://pangea.stanford.edu/ERE/pdf/IGAstandard/SGW/2018/Trainorguitton.pdf`, (last access: 1 April 2022), 2018.

Trautwein, U. and Huenges, E.: Poroelastic behaviour of physical properties in Rotliegend sandstones under uniaxial strain, International Journal of Rock Mechanics and Mining Sciences, 42, 924–932, https://doi.org/10.1016/j.ijrmms.2005.05.016, rock Physics and Geomechanics, 2005.

Tsuji, T., Hino, R., Sanada, Y., Yamamoto, K., Park, J.-O., No, T., Araki, E., Bangs, N., Huene, R., Moore, G., and Kinoshita, M.: In situ stress state from walkaround VSP anisotropy in the Kumano basin southeast of the Kii Peninsula, Japan, Geochemistry Geophysics Geosystems, 12, Q0AD19, https://doi.org/10.1029/2011GC003583, 2011.

Tsuru, T., No, T., and Fujie, G.: Geophysical imaging of subsurface structures in volcanic area by seismic attenuation profiling, Earth, Planets and Space, 69, 5, https://doi.org/10.1186/s40623-016-0592-0, 2017.

Verdel, A., Paap, B., and Carpentier, S.: TNO report DESTRESS WP6.3. Distributed Acoustic Sensing (DAS) performance monitoring for validation and control, 2018.

Verdon, J. P., Horne, S. A., Clarke, A., Stork, A. L., Baird, A. F., and Kendall, J.-M.: Microseismic monitoring using a fiber-optic distributed acoustic sensor array, Geophysics, 85, KS89–KS99, https://doi.org/10.1190/geo2019-0752.1, 2020.

Von Hartmann, H., Buness, H., Krawczyk, C. M., and Schulz, R.: 3-D seismic analysis of a carbonate platform in the Molasse Basin - reef distribution and internal separation with seismic attributes, Tectonophysics, 572-573, 16–25, https://doi.org/10.1016/j.tecto.2012.06.033, seismic imaging of continents and their margins: New research at the confluence of active and passive seismology, 2012.

VSProwess Ltd Final report: 3D DAS-VSP survey Gross Schoeneck., 2018.

Waagaard, O. H., Rønnekleiv, E., Haukanes, A., Stabo-Eeg, F., Thingbø, D., Forbord, S., Aasen, S. E., and Brenne, J. K.: Real-time low noise distributed acoustic sensing in 171 km low loss fiber, OSA Continuum, 4, 688–701, https://doi.org/10.1364/OSAC.408761, 2021.

Wamriew, D., Pevzner, R., Maltsev, E., and Pissarenko, D.: Deep Neural Networks for Detection and Location of Microseismic Events and Velocity Model Inversion from Microseismic Data Acquired by Distributed Acoustic Sensing Array, Sensors (Basel, Switzerland), 21, 6627, https://doi.org/10.3390/s21196627, 2021.

Wang, Y.: Multichannel Matching Pursuit for Seismic Trace Decomposition, Geophysics, 75, V61–V66, https://doi.org/10.1190/1.3462015, 2010.

Waskom, M., Botvinnik, O., O'Kane, D., Hobson, P., Lukauskas, S., Gemperline, D. C., Augspurger, T., Halchenko, Y., Cole, J. B., Warmenhoven, J., de Ruiter, J., Pye, C., Hoyer, S., Vanderplas, J., Villalba, S., Kunter, G., Quintero, E., Bachant, P., Martin, M., Meyer, K., Miles, A., Ram, Y., Yarkoni, T., Williams, M. L., Evans, C., Fitzgerald, C., Brian, Fonnesbeck, C., Lee, A., and Qalieh, A.: Mwaskom/seaborn: v0.8.1, https://doi.org/10.5281/ZENODO.883859, 2017.

Wawrzyniak, K.: Analysis of Acoustic Full Waveforms Based on Matching Pursuit Parameterization, in: Conference Proceedings, 68th EAGE Conference and Exhibition incorporating SPE EUROPEC, Vienna, Austria, 12-15 June 2006, p. P206, https://doi.org/10.3997/2214-4609.201402445, 2006.

Widrow, B. and Stearns, S.: Adaptive signal processing, Prentice-Hall, Englewood Cliffs, NJ, USA, ISBN: 0-13-004029-0, 1985.

Willis, M. E., Wu, X., Palacios, W., and Ellmauthaler, A.: Understanding cable coupling artifacts in wireline-deployed DAS VSP data, in: Expanded Abstracts, 89th SEG Annual Meeting, San Antonio, Texas, USA, 15-20 September 2019, pp. 5310–5314, https://doi.org/10.1190/segam2019-3208294.1, 2019.

Willis, M. E., Palacios, W., Ellmauthaler, A., and Zhao, X.: Mitigation of Zigzag Noise on DAS VSP Records Acquired in Vertical Wells, in: Conference Proceedings, 82nd EAGE Conference and Exhibition, Online, 8-11 December 2020, pp. 1–5,Th_Dome3_11, https://doi.org/10.3997/2214-4609.202011089, 2020.

Wilson, G. A., Willis, M. E., and Ellmauthaler, A.: Evaluating 3D and 4D DAS VSP image quality of subsea carbon storage, The Leading Edge, 40, 261–266, https://doi.org/10.1190/tle40040261.1, 2021.

Wu, X., Willis, M. E., Palacios, W., Ellmauthaler, A., Barrios, O., Shaw, S., and Quinn, D.: Compressional- and shear-wave studies of distributed acoustic sensing acquired vertical seismic profile data, The Leading Edge, 36, 987–993, https://doi.org/10.1190/tle36120987.1, 2017.

Yilmaz, O.: Seismic Data Analysis: Processing, Inversion, and Interpretation of Seismic Data, Nummer 10, Volume 1, Society of Exploration Geophysicists, https://doi.org/10.1190/1.9781560801580, 2001.

Yu, G., Cai, Z., Chen, Y., Wang, X., Zhang, Q., Li, Y., Wang, Y., Liu, C., Zhao, B., and Greer, J.: Walkaway VSP using multimode optical fibers in a hybrid wireline, The Leading Edge, 35, 615–619, https://doi.org/10.1190/tle35070615.1, 2016a.

Yu, G., Chen, Y., Wang, X., Zhang, Q., Li, Y., Zhao, B., Wu, J., and Greer, J.: Walkaway VSP Using Multimode Optical Fibres in a Hybrid Wireline, in: Conference Proceedings, 78th EAGE Conference and Exhibition, Vienna, Austria, May 30 - June 2 2016, p. Th_STZ2_05, https://doi.org/10.3997/2214-4609.201601602, 2016b.

Yuan, S., Lellouch, A., Clapp, R. G., and Biondi, B.: Near-surface characterization using a roadside distributed acoustic sensing array, The Leading Edge, 39, 646–653, https://doi.org/10.1190/tle39090646.1, 2020.

Zhan, G. and Nahm, J.: Multi-well 3D DAS VSPs: Illumination and imaging beyond the wellbores, in: Expanded Abstracts, 90th SEG Annual Meeting, Online, 11-16 October 2020, pp. 3798–3802, https://doi.org/10.1190/segam2020-3426032.1, 2020.

Zhan, Z.: Distributed Acoustic Sensing Turns Fiber-Optic Cables into Sensitive Seismic Antennas, Seismological Research Letters, 91, 1–15, https://doi.org/10.1785/0220190112, 2019.

Zimmermann, G., Moeck, I., and Blöcher, G.: Cyclic waterfrac stimulation to develop an Enhanced Geothermal System (EGS)—Conceptual design and experimental results, Geothermics, 39, 59–69, https://doi.org/10.1016/j.geothermics.2009.10.003, the European I-GET Project: Integrated Geophysical Exploration Technologies for Deep Geothermal Reservoirs, 2010.

A

Tested approaches

Among described techniques in Chapters 3,4, and 5, several other tests were performed, which were not included in final publication texts. This appendix contains supplementary material, supporting the studied findings and reassuring that suggested data processing approaches were optimal for the studied dataset recorded at the Groß Schönebeck in-situ laboratory.

A.1 Numerical modeling of the standing waves

Zig-zag patterns in the data can be explained with a synthetic model calculated for the first four harmonics for a fixed end case, using a classical formula for displacement (Kamal, 2011):

$$U = 2A \sin \frac{n\pi x}{L} \cos \omega t, \tag{A.1}$$

where A is the displacement amplitude, n is an integer mode number, x is a spatial coordinate, L is the length of the string, ω in an angular frequency, and t is time.

The theoretical description of the fundamental mode and overtones for the displacement in the case of fixed cable ends is shown in Figure A.1a. One should consider that the measuring physical quantity of the hDVS unit is strain. The differentiation of the displacement calculated over spatial coordinate converts the data to strain. This mathematical procedure will swap the positions of nodes and antinodes (Figure A.1b). Therefore, standing wave for closed-ends strain recording will look as displacement for the free-ends case. In the case of an odd number of the harmonic, the strain at the ends of the string is out of phase and for an even number, it is in-phase (Figure A.1b). The transition of the mode from odd to even will change the phase of the one end of the string. This disproportion in phases at the string ends will create the zigzag pattern after correlation with different up and down velocities (Figure A.1c). Figure A.1d shows field data affected by the ringing noise and the seismic section after the correlation (Figure A.1e) with a similar zigzag pattern.

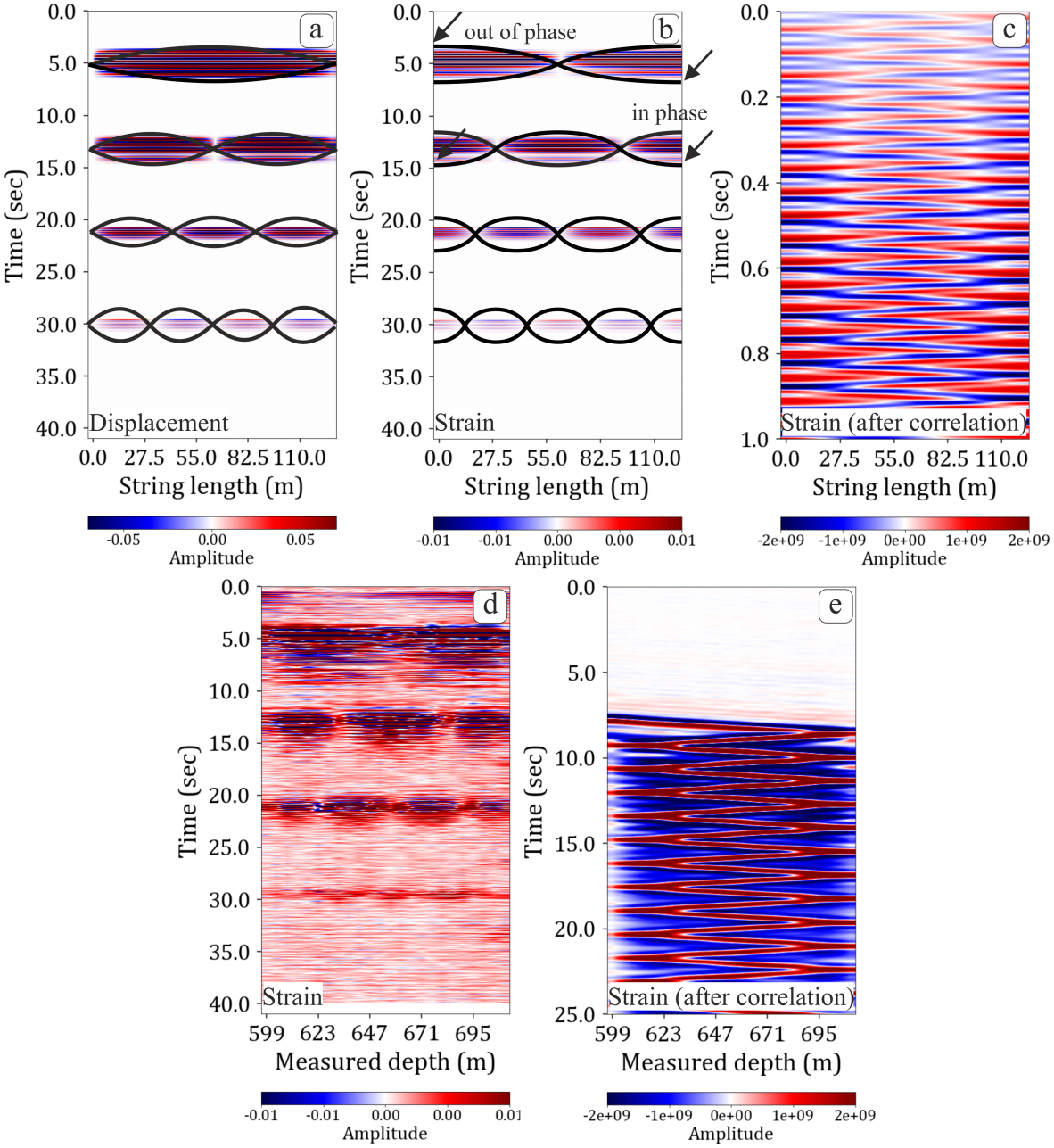

Figure A.1: Standing wave modes for fixed-end cable vibrations for one the main tone and three overtones. (a) Modelled displacement, the bold black line shows theoretical cable movement for the corresponding frequency mode. (b) Modelled strain, the bold black line shows theoretical cable movement for the corresponding frequency mode. (c) Modelled strain after correlation with a sweep signal. (d) Field strain data recording. (e) Field strain data recording after correlation.

A.2 Data processing

Before applying advanced processing techniques, a relatively standard and computationally non-intensive processing flow was applied to the data to get the initial migrated image. Results of imaging with active seismic methods strongly depend on the following processing components: the denoising, velocity model selection and migration algorithm. Figure A.2a shows a simplified scheme of the processing flow used for initial tests.

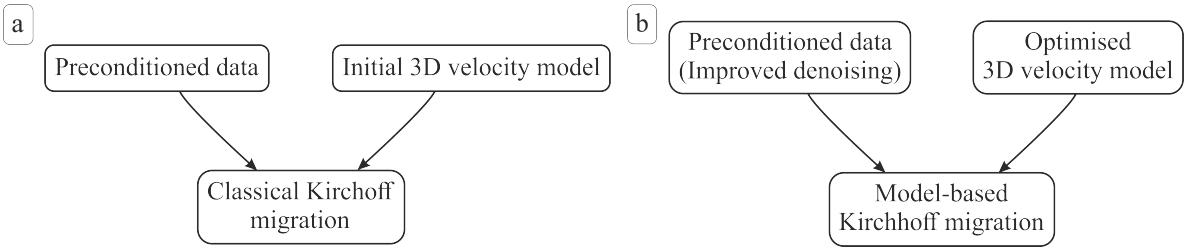

Figure A.2: Simplified processing flow used for data processing. An initial trial processing flow for the first imaging results (a). Optimised processing flow (b).

The main challenge in the data preconditioning step, as it was already mentioned in Chapter 4 and 5, was the coupling noise suppression. Initially, a relatively successful noise suppression was achieved using Burg adaptive deconvolution. An initial 3D velocity model was constructed using 3D surface seismic post-stack time migration velocities, which then was modified using a percentual modification function at a single well location (E GrSk 3/90). Preconditioned data was migrated using the classical Kirchhoff migration, which has been achieved using a commercial algorithm (RadExPro, Deco Geophysical). The results of these processing efforts are presented in Figure A.3a.

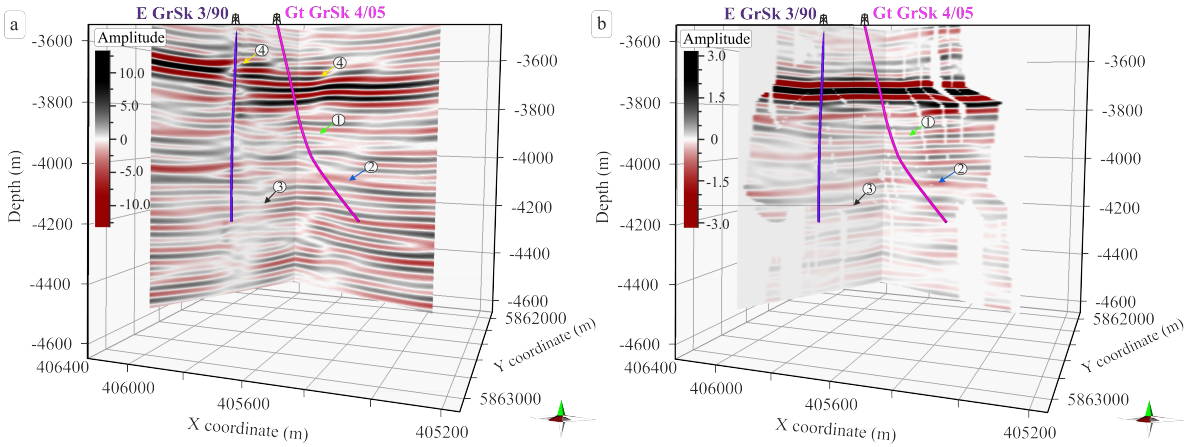

Figure A.3: 3D DAS VSP cube: calculated using initial testing (a) and optimised (b) flows.

Although the earlier version of the cube resolved the thin interlaying in the upper Rotliegend reservoir section (Figure A.3a, light green arrow (1)), as well as inclined horizons structures in lower Rotliegend/ precarboniferous (Figure A.3a, light green arrow (3)), the image, in general, has a lot of migration artefacts. The target Elbe basis sandstone layer was not correctly imaged and can hardly be traced in the vicinity of the boreholes. In addition, the resulting image contains artefacts related to incorrect interpolation in the regions where coverage gaps are expected. Yellow arrows (Figure A.3a, (4)) highlight areas containing improperly stacked reflection horizon, which give a misleading impression of faults/fractures caused by insufficient data coverage for a reliable 3D migration result. Furthermore, in the vicinity of Gt GrSk 4, we see inconsistently high amplitudes zones related to the residual coupling noise in the data.

Therefore, based on analysis of initial imaging tests, it became evident that a better denoising method, improved velocity model, and optimised migration algorithm (Figure A.2b), which can provide ray density information for final imaging clipping, are needed. Extensive testing of state-of-the-art processing techniques was performed before finding the optimum

processing steps for the dataset acquired at the Groß Schönebeck described in Chapter 5. The results of optimised data processing are shown in Figure A.3b.

A.2.1 Velocity model

The velocity model described in Chapter 5 was constructed using the existing geological model (marker horizons) and the initial velocity model based on 3D surface seismic stacking velocities. Then it was optimised using robust 3D ray tracing to minimise the square error between the first break peaks and the modelled arrivals. Since migration results are strongly dependant on the velocity model, it was decided to calculate a velocity model independent of the input data in an attempt to improve the velocity model. To create such velocity estimations - Bayesian formulation was used. This approach represents the solution to an inverse problem in terms of probability distribution of the geophysical model parameters, i.e the posterior probability density (PPD) of the P-wave velocity structure. Velocity averages and uncertainties were computed using a Markov-chain Monte Carlo (McMC) method with the implementation of Metropolis-Hastings sampling to obtain an unbiased sample from the posterior probability density (PPD). Furthermore, a transdimensional and hierarchical version of the McMC method (Ryberg and Haberland, 2018) was used to provide additional estimates of data error statistics (data noise) and appropriate model parametrisation (i.e., number of layers/Voronoi cells). A wide set of velocity models fitting the observations was derived from the broad priors, including initially uninformative models with physically unrealistic velocities, which is useful in the case of no prior knowledge about the subsurface velocities. This allowed to acquire the inference of the PPD simply by averaging a large number of well-fitted models obtained during evolution of Markov chains. The inversion results, which assumes a full 3D model (described by Voronoi cells), is shown in Figure A.4a.

A comparison of the 1D velocity curves extracted along the boreholes from the final 3D VSP model (used in Chapter 5) and the 3D McMC tomography is shown in Figure A.5. The two presented models are noticeably different. The 3D VSP model has stepwise boundaries with some smaller gradients in-between, for instance, for Keuper and Muschelkalk layers. The 3D McMC tomography, in contrast to the 3D VSP velocity model, is represented by a smooth curve. In general, these two curves have close velocity ranges and especially similar values in the depth region below 2400m.

Nevertheless, the 3D McMC tomographic inversion cube (Figure A.4a, black arrows) has features, which do not fit into known geological structures. These structures are a mathematically valid solution of the ill-posed tomographic problem and obviously do not represent rocks velocities. This problem occurs due to the non-optimal rays distribution of the 3D DAS VSP survey. Therefore, the distribution of the Vp velocities of the fitted tomographic inversion models is not Gaussian and averaging of these models gives rise to many non-unique solutions, that can produce misleading results.

Several attempts to combine two models were also made. However, neither clipping of the 3D McMC tomographic inversion cube using uncertainties cube, nor different kind of blending with the 3D VSP velocity model produced any satisfactory results in terms of least square root error for the forward ray-tracing estimations. Therefore, the 3D VSP velocity model was chosen for the final migration calculation.

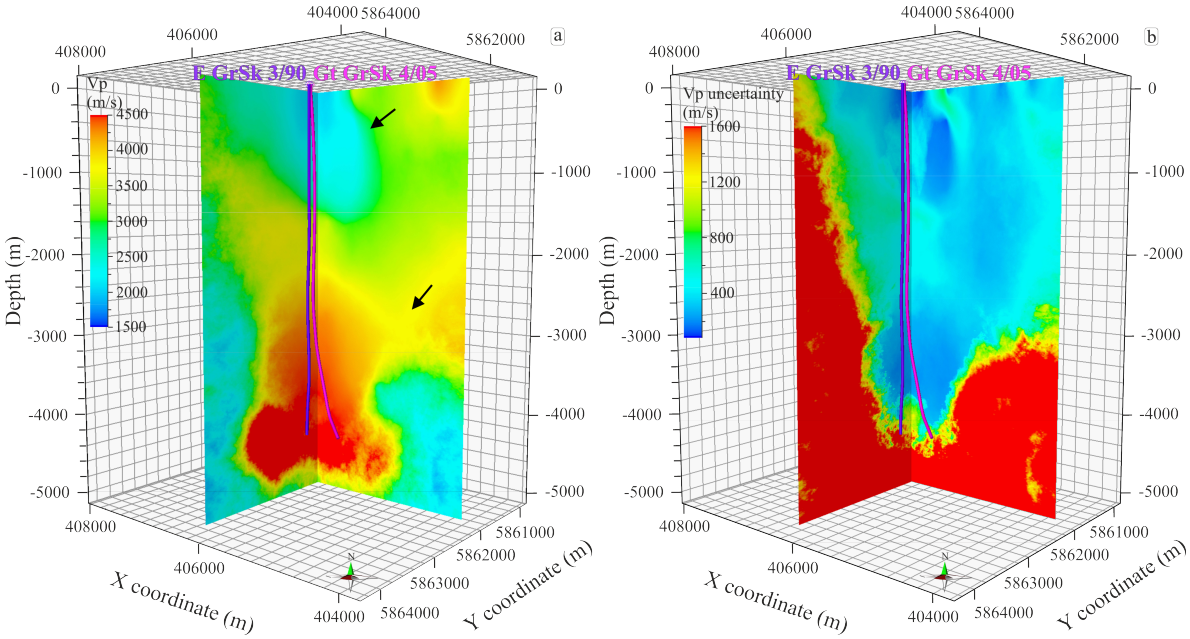

Figure A.4: Results of a transdimensional and hierarchical version of the McMC method inversion: 3D distribution of the Vp velocities (a), 3D uncertainties cube (b).

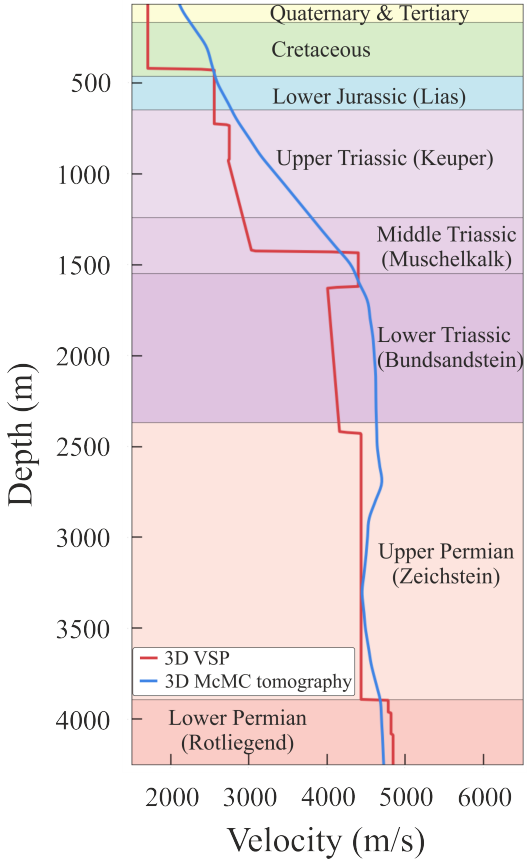

Figure A.5: Velocity profiles along the trajectory of the borehole E GrSk 3/90. Curve extracted from the 3D VSP (a) and 3D McMC tomography velocity cube (b), respectively.

A.2.2 Migration algorithm

Due to different reasons, the 3D VSP data coverage is limited and has profound gaps. Therefore, it was essential to find a migration method that has additional modifications to the classical approach to get reliable results even in the case of a limited amount of data. As shown in Figure A.3a, without clipping of the low coverage zones, the non-existent fault structure can be easily interpreted on the image. Figure A.3b does not provide this misleading information. In addition, a powerful ray-tracing and model-based approach contribute to the correct summation of the thin inclined horizons. Therefore, a careful 3D image post-processing by clipping using bin density information calculated using ray-tracing analysis is beneficial.

B

Contributions to the publications

This works is a cumulative thesis. It is structured and formatted according to the guidance for cumulative dissertations of the Faculty VI of the Technical University of Berlin. Presented papers are published in pear review journals or under review. The following text specifies contributions of each author to each publications.

Chapter 3

Henninges, J., **Martuganova, E.**, Stiller, M., Norden, B. and Krawczyk, C.M. 2021. Wireline distributed acoustic sensing allows 4.2 km deep vertical seismic profiling of the Rotliegend 150°C geothermal reservoir in the North German Basin. Solid Earth 12, 521–537, https://doi.org/10.5194/se-12-521-2021.

I programmed a script for optimal gauge determination and calculated the required value for the Groß Schönebeck site specifics. Then, I performed the seismic data processing and analysis under supervision of authors 1, 3 and 5. Author 1 performed data interpretation under discussion with all co-authors and with input from Author 4 on geological well data. Author 1 and I prepared the manuscript and figures with contributions from all co-authors. Author 1 and Author 5 conceptualized the project. Finally, Author 1 and Author 3 planned and supervised fieldwork and data acquisition.

Chapter 4

Martuganova, E., Stiller, M., Bauer, K., Henninges, J. and Krawczyk, C.M. 2021. Cable reverberations during wireline distributed acoustic sensing measurements: their nature and methods for elimination. Geophysical Prospecting 69, 1034-1054, https://doi.org/10.1111/1365-2478.13090.

I performed coupling noise analysis and found a physical explanation of this phenomena under

discussion with all co-authors. Then, I tested existing state-of-the-art denoising techniques and applied them to the data under supervision of Authors 2 and 3. Based on the MP code from the MP5 and Svarog projects (Kuś, Różański, and Durka (2013); The Svarog developers team (2014); Durka et al. (2015); The Svarog developers team (2016)) I developed the MPD denoising method and applied it to the Groß Schönebeck testing dataset, under supervision of Author 2. Figures and manuscript were prepared by me with a guidance and discussion with all co-authors.

Chapter 5

Martuganova, E. Stiller, M., Norden, B., Henninges, J., and Krawczyk, C.M. In review. 3D deep geothermal reservoir imaging with wireline distributed acoustic sensing in two boreholes. Article is under review in *Solid Earth*.

I developed and adapted the seismic processing flow for the 3D DAS VSP data. I carried out the seismic processing and analysis under supervision of Authors 2 and 5. The interpretation was performed under discussion with all co-authors. I wrote the manuscript and prepared the graphics. Authors 2, 3, 4, 5 and I contributed to the final version of the manuscript. Author 4 and 5 supervised the project.

C

Statutory declaration

I declare that I have written the submitted dissertation independently. The work contained herein is my own except where explicitly stated otherwise in the text. All of the literature material and the other sources I employed when producing this academic work, either literally or in content, are clearly marked and separately listed.

....

Date (Signature)

ISSN 2190-7110